ADVANCED MASTERS IN STRUCTURAL ANALYSIS
OF MONUMENTS AND HISTORICAL CONSTRUCTIONS

Master's Thesis

Mir Abdul Kuddus

Numerical Simulation on Buckling Failure of the Masonry Load Bearing Walls

UNIVERSITAT POLITÈCNICA DE CATALUNYA

University of Minho

Education and Culture

Erasmus Mundus

ADVANCED MASTERS IN STRUCTURAL ANALYSIS
OF MONUMENTS AND HISTORICAL CONSTRUCTIONS

Master's Thesis

Mir Abdul Kuddus

Numerical Simulation on Buckling Failure of the Masonry Load Bearing Walls

This Masters Course has been funded with support from the European Commission. This publication reflects the views only of the author and the Commission cannot be held responsible for any use which may be made of the information contained therein.

SPAIN | 2010

DECLARATION

Name: Mir Abdul Kuddus

Email: mintu_ce_m@yahoo.com

Title of the Msc Dissertation: Numerical Simulation on Buckling Failure of the Masonry Load Bearing Walls

Supervisor(s): Professor Pere Roca Fabregat

Year: 2010

I hereby declare that all information in this document has been obtained and presented in accordance with academic rules and ethical conduct. I also declare that, as required by these rules and conduct, I have fully cited and referenced all material and results that are not original to this work.

I hereby declare that the MSc Consortium responsible for the Advanced Masters in Structural Analysis of Monuments and Historical Constructions is allowed to store and make available electronically the present MSc Dissertation.

University: Technical University of Catalonia, Spain

Date: July 21, 2010

Signature: _____

This page is left blank on purpose

This thesis is dedicated
to my beloved parents, wife and to those who do good deeds
for the sake of ALLAH

ACKNOWLEDGEMENTS

In completing this Master's dissertation, I would like to express my gratefully appreciation to the tremendous help from many professors, fellow students and other friends.

I am highly appreciative and thankful to my supervisor Professor Pere Roca Fabregat for his invaluable advice and guidance during the thesis. I would also like to express my gratitude and thanks to the PhD student Cristian Sandoval, for nice cooperation, frequent attention and encouragement during numerical analysis as well as whole thesis period. Special thanks to Professor Paulo Lourenco for his hospitality and help during the course work in Portugal at University of Minho. I am obliged and grateful to Professor Enrico Garbin for giving me important papers relevant with my study.

A financial support from European Commission by Erasmus Mundus Scholarship is gratefully acknowledged. Also I want to give special thanks to Dora Coelho, Master's Secretariat, for help by solving visa, accommodation, payment and other official issues.

Finally, I would like to express my special thanks and gratitude to my family, for their love, pray and persistent support during my study.

ABSTRACT

Masonry load bearing wall subjected to vertical concentric and eccentric loading may collapse through instability. The buckling behavior of masonry load bearing wall of different slenderness ratio were investigated via testing a series of scale masonry wall subjected to concentric and eccentric vertical loading. A total of thirty six masonry walls were tested in the Laboratory of Technical University of Catalonia (UPC), which was the basis of this numerical study, and results such as the vertical load capacity, vertical deformation, horizontal deflection and type of failure were investigated. In this research, for better understanding of buckling failure of the masonry load bearing wall and to simulate the response of walls tested in laboratory, a numerical finite element model was developed based on the simplified micro model approach. The numerical model was calibrated by using those results found from experimental study. The numerical model was developed, which takes into account both geometrical and material nonlinearities. However, a series of analytical studies were conducted in order to access the accuracy and performance of formulations provided by EUROCODE 6 and ACI-530 for vertical capacity of masonry wall. The influence of tensile strength of units, nonlinear behavior of interface element, slenderness ratio and various end conditions have been investigated together with the effect of different end eccentricity of vertical load.

RESUMEN

(Simulación numérica del fallo por pandeo de paredes de carga de obra de fábrica)

Paredes de carga de obra de fábrica sometidos a carga vertical y excéntrica podrían presentar colapso por pandeo o inestabilidad geométrica. El comportamiento al pandeo de paredes de carga de obra de fábrica con diferentes razones de esbeltez fue estudiado experimentalmente a través de una serie de ensayos en laboratorio con modelos a escala reducida sometidos a carga vertical centrada y excéntrica. Los resultados de 36 paredes ensayadas en el Laboratorio de Tecnología de Estructuras de la Universidad Politécnica de Catalunya (UPC) han servido como base para este estudio numérico. En esta investigación, se preparó un modelo de elementos finitos basado en la técnica de la micromodelización simplificada, con el objeto de lograr una mejor compresión del fallo por pandeo de paredes de carga de obra de fábrica. El modelo numérico fue desarrollado tomando en cuenta nolinealidad geométrica y material. Además, una serie de estudios analíticos también fueron estudiados con el objeto de comprender y evaluar la presición de las formulaciones propuestas por el Eurocódigo 6 y ACI-530 para estimar la capacidad vertical de paredes de carga de obra de fábrica. La influencia de la resistencia a tracción de las unidades, el comportamiento nolineal de los elementos de interfase, la relación de esbeltez y varias condiciones de apoyo han sido investigadas junto con el efecto de diferentes excentricidades de la carga vertical.

CONTENTS

LIST OF FIGURES

LIST OF TABLES

1. INTRODUCTION

Slender masonry load bearing wall subjected to vertical centric and eccentric loading may collapse through instability. This takes place if the compressive strength of the material is not reached any cross-section of the member. Otherwise, the failure occurs of the masonry wall due to crushing of the material itself. The prediction of the collapse load and mode of failure is greatly affected by the model used to analyze the masonry wall. In order to better understanding the buckling characteristic of the masonry wall, it is very important to study the constitutive laws of the components of masonry such as brick and mortar and their interaction. Nevertheless, a significant simplification is possible by assuming masonry to be a continuum medium. An average stress strain relationship between brick and mortar is then considered.

Simplicity and availability is the most important characteristics of masonry construction materials. Load bearing masonry walls in structures are normally designed to act in compression. The wall carries vertical load from above and may also subjected to additional bending moments resulting from the continuity between floors and walls and due to eccentricity of vertical loading. In most load bearing masonry structures, the walls are aligned vertically throughout the height of the structure so that the vertical loads may be transmitted directly to the footing and the soil foundation. The vertical loads effectively pre-stress the masonry work and increase its resistance to cracking on the bed planes. For most load bearing walls, the effects of lateral wind loads are significant only in walls which carry relatively small vertical loads. However, slender masonry walls may be especially sensitive to the combined effects of vertical and lateral loads with different load eccentricity because of possibility of failure due to lateral instability. For this reason, the analysis of masonry load bearing walls requires consideration of the fundamental behavior of the units and mortar components under combination of axial compression and flexure with load eccentricity. So, it is important to have a reasonable design formula of the walls for the carrying capacity under vertical loads. This formula should include the slenderness ratio of walls and the possible variations of the eccentricity of the vertical load.

1.1 Background and need for Research

The failure mechanisms of masonry walls subjected to vertical loads are well documented, but a review of research carried out on masonry walls shows that due to the scarcity of test data there is no comprehensive method has been available for analyzing the complete load deformation relationships for slender walls of any chosen geometric configuration, material properties and load combination up to the collapse. Such an analysis requires consideration of the effects of both geometric and material nonlinearity. Chapman and Slatford (1957) obtained closed form solutions for the load deformation behavior of brittle elastic wall by assuming that masonry material has no tensile strength and that cracking occurs whenever a tensile stress would develop.

Shalin (1978) reviewed the results of analysis carried out by a number of authors and presented experimental evidence in support of the calculations. Further work was carried out by Sawko and Towler (1982) who proposed a numerical procedure for calculating the failure load of a no-tension material wall. Some analytical solutions also have been worked out for linear elastic material with or without tensile strength. More recently, an analytical solution has been carried out by Romano et al. (1993), considering no tension bearing masonry with a monomial stress–strain relationship in compression. However, all this models neglect some features of the masonry material which became significant especially in the prediction of failure load. First experimental results of tests on masonry panels under axial compression have shown nonlinear stress-strain relationships with a descending branch beyond the compressive strength (compressive softening). When the compressive strength is reached, a splitting failure of some units occurs. That is the tensile stresses induced by mortar produce in the unit cracks parallel to the direction of the load.

Practically, load bearing masonry wall has tensile strength and the actual stiffness of a partially cracked wall is influenced by the tension stress field in the units which remain intact between the cracks at the unit-mortar interfaces. As a result, analyses which assume a no-tension material are imprecise for some forms of structural masonry work. Parland et al. (1982) proposed a method for determining buckling failure load of a slender wall, taking into account the effect of tension stress field which exists between the cracked joints. However, the linear elastic materials were used in this analysis. To predict accurately the behavior of

slender masonry walls subjected to vertical loads, the method of analysis should include the effects of discrete cracking at the mortar joints and the behavior caused by a of non-linear mortar, Parland et al. (1982). The method should also take into account the influence of end condition and eccentricity of loads which may, in some circumstances, significantly affect the buckling characteristic of a wall under vertical load. However, although a large amount of research has been conducted to understand the buckling behavior of the masonry load bearing walls, the knowledge obtained from previous research is difficult to synthesize. In experimental research, this is due primarily to the lack of uniformity in test protocols and difficulties associated with testing stiff brittle systems. In analytical research, this is due primarily to the difficulties in tracking cracking in a heterogeneous medium, numerical stability associated with contact problems and stiff system behavior, and the large models needed to track the buckling behavior properly.

These problems have their origin, again, on our inability to properly model the problem at the three required scales: material, component, and structure levels. At the material level, although many tests have been conducted on the compressive strength of masonry, the buckling behavior of masonry wall is still unclear because it is a quite complex racking problem at the interface between masonry units and mortar. In addition, there is still no conclusive knowledge about the relationship among several critical strength parameters: the bed-joint tensile strength and the shear friction factor along the cracked bed joint surface. The lack of this knowledge does not permit a complete understanding of the nonlinear behavior of masonry wall.

A similar problem exists at the component level. For instance, even though numerous experiments have been conducted on the strength and the failure modes of individual masonry wall under vertical loads, and several formulas have been proposed for the strength of a masonry wall corresponding to certain failure mode based on these experimental research results, no comprehensive theory is available to explain the interactions of different failure modes and the corresponding load-displacement relationship of masonry load bearing wall with effects of slenderness ratio and eccentricity of vertical loads, Payne et al. (1990). The lack of such theory makes it difficult to extrapolate the knowledge obtained from walls with a given configuration to other walls with different configurations, and from the isolated walls to the walls existing in a perforated wall. At the structure level, the problem is more

daunting. Due to the large demands on the experimental facilities and funding, tests of entire unreinforced masonry structures, especially of full-scale masonry structures, are seldom conducted. As a result, little knowledge is available on the structural behavior of masonry buildings at the 3D structural level. These issues include the governing mechanisms for a slender wall, the effects of flexible and rigid diaphragms on the performance of the entire masonry building, the coupling effects between perpendicular walls, and the building torsion.
In this research, experimental, numerical and analytical investigation were carried out to make a clear understanding of the capacity and buckling characteristic of masonry load bearing wall by considering combined effects of the following factors which influence the load carrying capacity of real masonry structures:

influence of tensile strength of masonry;

- non-linear stress-strain characteristics of the mortar;
- geometrical and material non-linearity;
- variations in the end support condition and vertical load eccentricity;
- different slenderness ratio.

Test results from a series of scale laboratory case studies are compared with the numerical and analytical predictions. Results obtained in the parametric studies are compared with failure loads calculated by using different codes which do not include all the factors described above. Conclusions are drawn on the relative importance of tensile strength, non-linear geometrical and material properties with different end eccentricity.

1.2 Objectives of this Study

This study focuses on the experimental, analytical and numerical finite element analysis of unreinforced masonry load bearing wall. The numerical finite element model was developed, which can be approximated as being in a state of plane stress, such as panels. The walls under consideration are subjected to the vertical loads with various end condition and load eccentricity. The primary aim of this study is the evaluation of the strength and characterizes the buckling behavior of the masonry load bearing wall. The objectives of this study are:

- a review on theoretical, experimental and numerical investigations of bucking failure of masonry walls subjected to vertical loading;
- to characterize the buckling failure, develop a series of experiments of masonry load bearing walls of different slenderness ratio, concentric and eccentric vertical loading;
- to select and validate a constitutive micro-model for simulating the response of the walls tested in laboratory;
- to verify the developed model by comparing the predicted behavior with the behavior observed in experiments on different types of walls. The developed model should be able to predict the failure mode and the ultimate load with reasonable agreement with the experimental values;
- to observe the response of wall by changing different parameters and sensitivity analysis;
- to assess the accuracy and performance of available analytical formulations from masonry standards for vertical capacity of masonry walls;
- to compare the experimental results with the values obtained from numerical and analytical study;
- to draw a conclusion on the performance of the model, accuracy of the current standards and effects of different parameters on buckling failure of the masonry load bearing wall.

2. LITERATURE REVIEW

2.1 General

Load bearing masonry is among the most ancient architectural technologies, yet continues to provide boundless opportunities for both traditional and modern design. Historically, the structural design of masonry buildings was based on the empirical requirements of building codes for minimum wall thickness and maximum height. Bearing wall construction for buildings higher than three to five stories was uneconomical and other methods of support (steel or concrete skeleton frame) were generally used. In 1965, there was a renewed interest on the part of the design professional, architect and engineer, in modern bearing wall construction, wherein the design is based on a rational structural analysis rather than on outmoded arbitrary requirements. Many research projects have been conducted on the properties of the three basic components and the overall unreinforced masonry wall with vertical load and load eccentricities. Section 2.2 gives a brief introduction on the properties of masonry materials. Sections 2.3 to 2.7 discuss the influence of slenderness ratio, end eccentricity and tensile strength on the stability and capacity of masonry load bearing wall under vertical load.

2.2 Masonry Materials and Properties

A close-up view of a typical masonry wall is shown in Figure 1. Masonry is a composite construction material consisting of masonry units and mortars built following certain pattern. The mechanical properties of masonry vary considerably due to variable material properties of units and mortars. For example, mortar is typically composed of cement, lime, sand and enough water to produce a plastic, workable mixture. Several different types of mortars have been widely used in the construction, as shown in Table 1 (ASTM 1958).

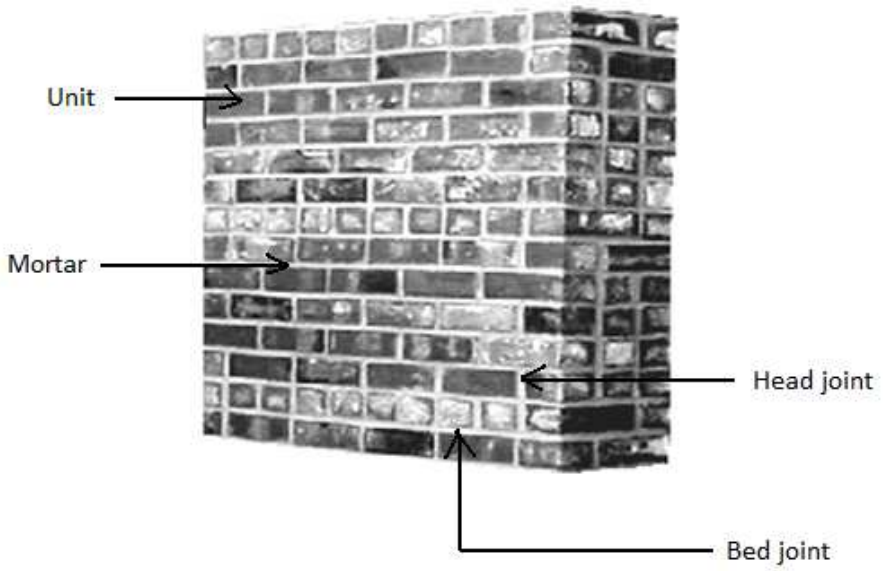

Figure 1: Typical masonry wall.

Table 1: Mortar compositions by volumes.

Type	Ratio (cement: lime: sand)	Compressive strength(psi)
M	1:0:3	2500
S	0.5-1:0.25-0.5:4.5	1800
N	1:0.5-1.25:6	750
O	1:2:9	350
K*	0.5:2:7.5	75

*No longer used in construction after 1960's

Brick, concrete masonry units, clay tile, and stone have all been used for the masonry units in previous practice. Brick masonry is the focus of this research, because it makes up majority of the existing unreinforced masonry buildings.

The mechanical properties of masonry as a composite material are functions primarily of the mechanical properties of the individual masonry units, mortars, and the bond characteristics between units and mortar. Strictly speaking, unreinforced masonry construction results in an anisotropic material. However, for a simplified design approach, the elastic properties of masonry materials are usually considered as isotropic. These elastic, isotropic properties are

taken as those determined from tests on masonry prisms perpendicular to the bed joints. The elastic modulus of masonry is controlled by the combined elastic modulus of masonry units and mortar (Hamid et al. 1987). Previous research indicates a large scatter in the measured elastic modulus of masonry. Two reasons explain the large scatter. First, the material properties of masonry units and mortar vary significantly by themselves. Second, different workmanship factors may contribute to the variation as well. The European code (EC6 1995) gives the following formulae for calculating Young's modulus E and shear modulus G of masonry material for a design purpose:

$$E = 1000 f_m \; ; G = 0.4E \tag{1}$$

Where, f_m is the characteristic compressive strength of masonry. Some other researchers recognized that masonry is actually a nonlinear material and thus its elastic modulus varies with different stress level. Experimental stress-strain relationship of mortar, brick, masonry prism and masonry panel is shown in the Figure 2. Usually the compressive strength of the masonry falls in between compressive strength of bricks and mortar.

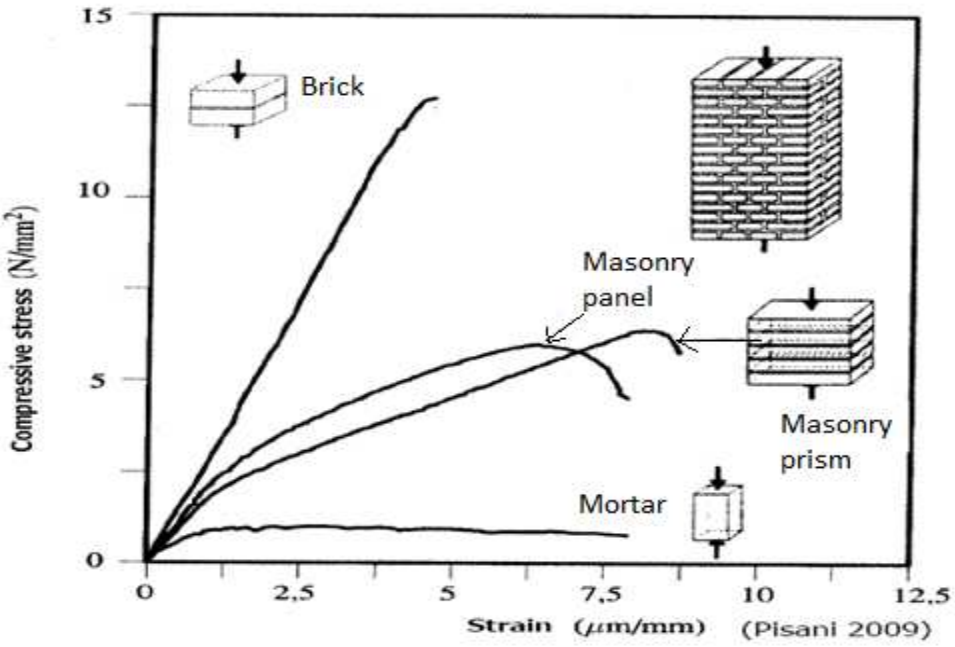

Figure 2: Typical stress-strain diagram of masonry components.

Compressive strength tests are easy to perform and give a good indication of the general quality of materials used. The CEN Eurocode 6 (1995) uses the compressive strength of the components to determine the strength of masonry even if a true indication of those values is not simple. For masonry units, standard tests with solid platens result in an artificial compressive strength due to the restraint effect of the platens. The CEN Eurocode 6 (1995) minimizes this effect by considering a normalized compressive strength f_b, that result from the standard compressive strength in the relevant direction of loading multiplied by an appropriate size or shape factor. The normalized compressive strength refers to a cube specimen with 100 x 100 x 100 (mm^3) and cannot be considered representative of the true strength. The normalized compressive strength of unit is calculated according to Eurocode 6: $f_b = f_{b,m}*\delta$, where δ=shape coefficient. The compressive strength test for masonry unit is shown in Figure 3.

(a) (b) ©

Figure 3: Test of masonry units (da Porto 2003) (a) test setup (b) and (c) specimen after test.

It is difficult to relate the tensile strength of the masonry unit to its compressive strength due to the different shapes, materials, manufacture processes and volume of perforations. For the longitudinal tensile strength of clay, calcium-silicate and concrete units, Schubert (1988a) carried out an extensive testing program and obtained a ratio between the tensile and compressive strength that ranges from 0.03 to 0.10. For the fracture energy G_f of solid clay and calcium-silicate units, both in the longitudinal and normal directions, Van der Pluijm (1992) found values ranging from 0.06 to 0.13 (Nmm/mm^2) for tensile strength values ranging from 1.5 to 3.5 (N/mm^2).

Experiments on the biaxial behavior of bricks and blocks are also lacking in the literature. This aspect gains relevance due to the usual orthotropy of the units due to perforations. As a

consequence, the biaxial behavior of a brick or block with a given shape is likely to be unknown, even if the behavior of the material from which the unit is made, e.g. concrete or clay, is known. For the mortar, the compressive strength f_m is obtained from standard tests carried out in the two halves of the 40 × 40 × 160 (mm^3) prisms used for the flexural test. The specimens are casted in steel molds and the water absorption effect of the unit is ignored, being thus non-representative of the mortar inside the composite. Currently, investigations in mortar disks extracted from the masonry joints are being carried out to fully characterize the mortar behavior, Schubert and Hoffman (1994). Nevertheless, there is still a lack of knowledge about the complete mortar uniaxial behavior, both in compression and tension.

The nonlinear properties of masonry, such as ultimate strength and ductility, are also direction-depended. Specifically, several critical strength values, such as the compressive strength perpendicular to the bed joints, the tensile strength perpendicular to the bed joints are generally utilized to describe the nonlinear properties of masonry. Extensive research has been conducted on this topic. Detailed description of the experimental research which was the basis of numerical simulation can be found in Chapter 4. A new model, which can illustrate the relationship of these ultimate strength values with the lateral deformation and slenderness ratio, will also be presented in Chapter 5 and 6.

2.3 Buckling and Material Overstressing

Any compression member usually fails both due to the buckling and material overstressing. The more slender the member the greater the possibility to buckling failure; the more squat the member the greater propensity to material overstressing. The combination of buckling failure mode with the mode of ultimate material failure is shown in the Figure 4. The figure shows that with the increasing of both slenderness ratio and reduction factor the paossibility of buckling failure increases. The material failure occurs in the case of low slenderness ratio with high reduction factor. In addition, buckling failure connect with material failure where the members may fail due to combination of both mechanisms. High slenderness ratio andlow reduction factors indicate general buckling when low slenderness ratio and high reduction factors produce Euler buckling.

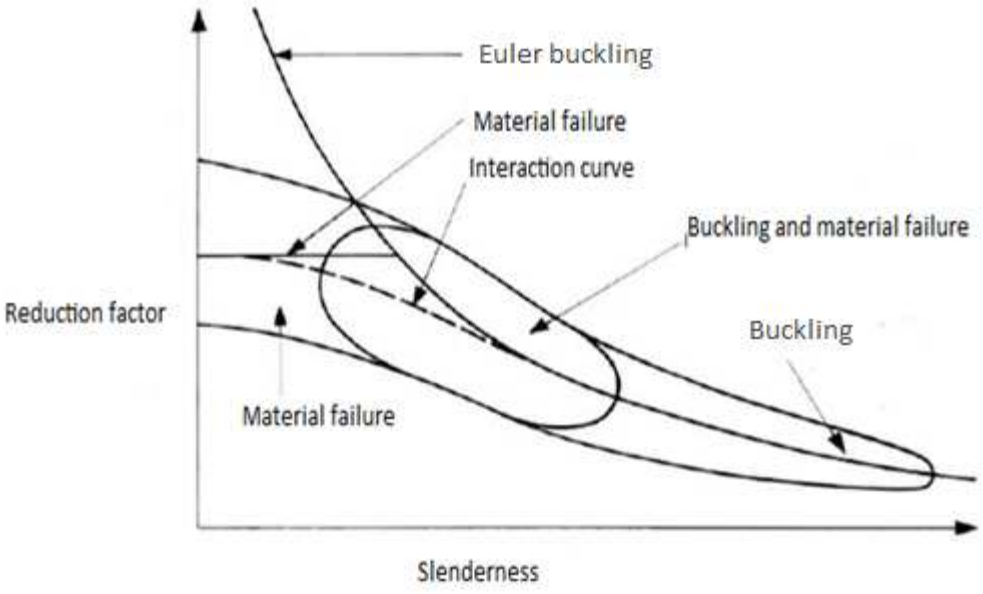

Figure 4: Buckling and material overstressing interaction curve (Morton, 1990).

The mathematical solution for the differential equation describing a perfectly idealized strut was proposed by Euler as:

$$P_c = \pi^2 \frac{EI}{{L_e}^2} \tag{2}$$

Writing this formula in terms of critical stress:

$$\sigma_E = \frac{P_c}{A} = \frac{\pi^2}{A} \frac{EI}{{L_e}^2} \tag{3}$$

or

$$\sigma_E = \pi^2 E/(L_e/r)^2 \tag{4}$$

Where,

r radius of gyration;

P_c Euler critical load;

L_e effective length (or height) of member;

E elastic modulus of masonry;

I second moment of area of section;

A area of section.

The material strength properties have been rigoriously investigated and BS 5628 contains table of characteristic strength f_k for the various masonry formats. In general:

$$P_{ult} = \sigma_{ult} \tag{5}$$

and for wall construction the maximum stress:

$$\sigma_{ult} = f_k \tag{6}$$

The above model is based on the basic Rankine approach of having a straight line joining the two axes(see Figure 5):

$$\frac{1}{P} = \frac{1}{P_{material\ failure}} \frac{1}{P_{\ buckling\ failure}} \tag{7}$$

Presenting this in terms of stresses:

$$\frac{\sigma}{\sigma_{ult}} = 1 - \frac{\sigma}{\sigma_E} \tag{8}$$

Where,

P_{ult} ultimate load for material strength failure;

σ_{ult} ultimate stress for material strength failure;

σ_E Euler critical stress.

This is a emperical relationship between the elastic modulus of masonry, E and the compressive strength of the masonry. This is incorporated in BS 5628: part 2 as 900 f_k (MPa) for the short term modulus of elasticity of clay, calcium silicate and concrete masonry. Again, according to Eurocode 6, this relation is consideed as 1000 f_k (MPa).

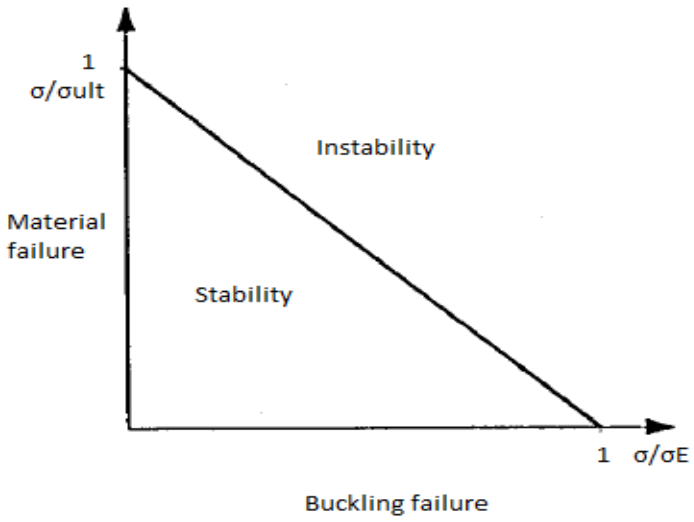

Figure 5: Combining buckling with material overstressing of masonry.

2.4 Concentric Loading Wall

The brickwork has a number of peculiarities that make the different development. This exposed several problems and observations. In this section Masonry walls with vertical load which applied without any eccentricity is described. Previous sections have presented the expression for the Euler critical buckling load in wall under centered load. This expression is valid in the case of composite parts of a material elastic follow the Hooke's law.

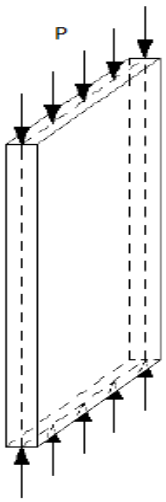

Figure 6: Concentrically loaded wall.

In this case, the stresses are evenly distributed, with the stress instability:

$$\sigma_{cr} = \frac{P_{cr}}{A} = E\left(\pi.\frac{i}{h}\right)^2 \tag{9}$$

Where,

A cross sectional area;

E modulus of elasticity;

i = $\sqrt{\frac{I}{A}}$ radius of gyration;

h height of the wall.

In the case of brickwork, this expression becomes invalid because the material not satisfies Hooke's law, means no linear proportionality between stress and strain. For this situation the formula derived by Ritter (quoted by Knutsson, 1991) is introduces:

$$E = E_0 \left(1 - \frac{\sigma}{f_c}\right) \tag{10}$$

With,

E tangent modulus of elasticity for small strains;

f_c compressive strength.

Introducing this value of E in the expression 9 gives:

$$\sigma_{cr} = E_0 \left(1 - \frac{\sigma_{cr}}{f_c}\right)\left(\pi . \frac{i}{h}\right)^2 \tag{11}$$

Can be expressed as:

$$\sigma_{cr} = \frac{P_{cr}}{A} = \frac{f_c}{1 + \frac{f_c}{\pi^2 . E_0}\left(\frac{h}{i}\right)^2} \tag{12}$$

This expression is commonly known as Ritter's formula, is used as the Rankine, Grashof, Engesser Winkler or have been associated with it (Knutsson, 1991).

2.5 Eccentric Loading Wall

Ritter's formula shown above is valid for masonry walls subjected to centered load. In a real case, it is common to find situations where the loads are applied eccentric.

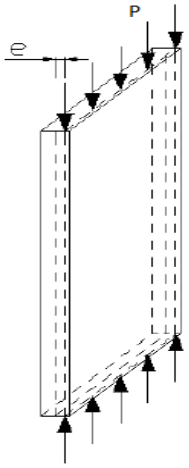

Figure 7: Eccentrically loaded wall.

In these cases, a simplification can make by assuming a symmetrical stress distribution around the load and neglecting the part of the section outside of the distribution. With this simplification, the bearing capacity of the structure can be calculated as a structure with load centered and with a thickness equal to (Figure 8):

$$2\left(\frac{t}{2}-e\right)=(t-2e) \tag{13}$$

Where,

t total thickness of the wall; and

e eccentricity with which the load is applied.

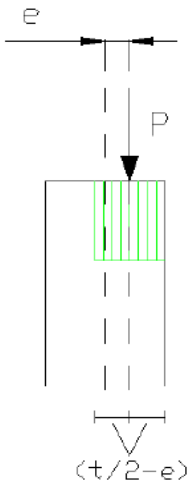

Figure 8: Simplification consists in assuming a symmetrical stress distribution around load.

Therefore, the critical stress can be calculated as:

$$\sigma_{cr}=\frac{P_{cr}}{A_c}=\frac{f_c}{1+\frac{f_c}{\pi^2.E_0}\left(\frac{h}{i_c}\right)^2} \tag{14}$$

Where,

A_c compressed cross-sectional area considering the new equivalent thickness;

$I_c=\sqrt{\frac{I}{A_c}}$, radius of gyration of the compressed section.

The latter term is more general and applies to both load cases centered (in which eccentricity is null and the compressed area is the total area of the section) and the case of load eccentrically applied.

Resistance may be affected by the fact that on the surface of the masonry mortar is not confined, being the weaker joints near the surface. This may be especially critical for walls with a reduced thickness. In order to consider this effect, Knutsson (1991) proposed the stress reduction by a coefficient k_t.

$K_t = 0.8$ for walls with $90 < t \leq 125$ mm

$K_t = 0.9$ for walls with $125 < t \leq 175$ mm

$K_t = 1$ for walls with $t > 175$ mm

As explained above, the critical load is determined as:

$$P_{cr} = K_t \sigma_{cr} A_c = K_t \frac{f_c}{1 + \frac{f_c}{\pi^2 E_0}\left(\frac{h}{i_c}\right)^2} A_c \quad (15)$$

Can be expressed in abbreviated form as:

$$P_{cr} = K_t K_s A_c f_c \quad (16)$$

Where,

$$K_s = \frac{1}{1 + \frac{1}{\pi^2 K_r}\left(\frac{h}{i_c}\right)^2};$$

$K_r = \frac{E_0}{f_c}$ Ritter constant for the material.

The expression obtained can be particularized for the case of rectangular sections, which is:

$$P_{cr} = K_t K_s (t - 2e) l f_c \quad (17)$$

With,

$$K_s = \frac{1}{1 + \frac{12}{\pi^2 K_r}\left(\frac{h}{t - 2e}\right)^2};$$

l total width of the wall;

t thickness of the wall;and

e eccentricity of load application.

When the load is applied on a solid wall with an eccentricity greater than t/6, the wall develops tension within a certain zone. The zone is shown in Figure 9. It is assumed that this portion of the wall cracks slightly at each joint, in compliance with the assumption of a no tension material. The geometry of the cracked section changes for different values of

eccentricity of load application. It is therefore necessary to apply the principles of the basic approach to the remaining uncracked portion of the wall.

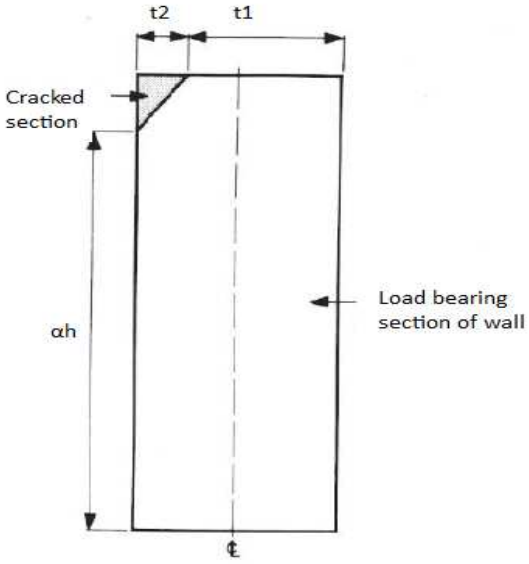

Figure 9: Tension zone in a solid eccentrically loaded wall.

Figure 10 shows, schematically, the effect of increasing eccentricity ratio on the size of the wedge shaped cracked section. The position of the maximum deflection rises progressively above the mid-height of the wall. In addition, the critical load of the wall is progressively reduced as the area of the tapered portion of the wall becomes smaller.

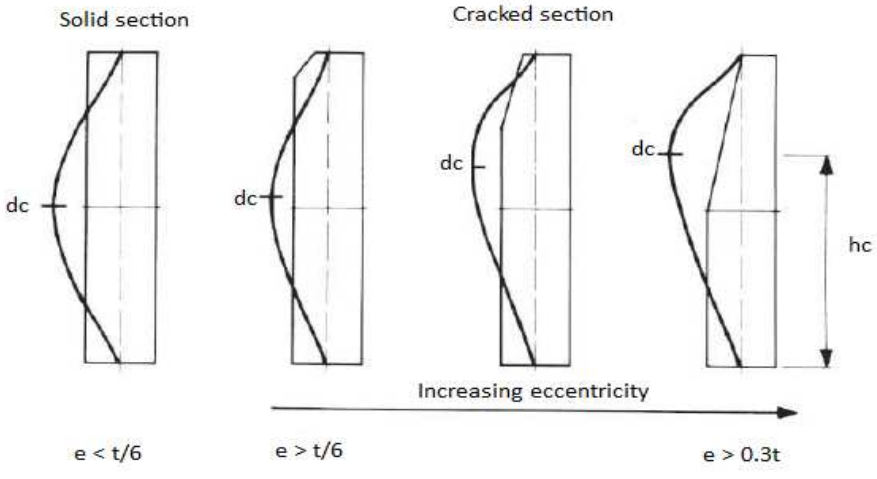

Figure 10: Effect of increasing eccentricity on the size of cracked section.

An important aspect is that for the range of applied eccentricity (at the top of the wall) $t/6 < e \leq 0.3t$ the width of the section at a critical section remains t. When $e > 0.3t$ the size of the wedge shaped cracked section intrudes through the critical section and its thickness is less than wall thickness, t.

2.6 Effects of Slenderness Ratio and Eccentricity of Loading

The modern masonry wall constructions allow slenderness of the wall and the eccentricity of vertical loading by the application of a reduction factor to the masonry strength. In traditional construction usually the load bearing walls are relatively thick and if the ratio of height to thickness is no more than about 10, the effect of slenderness will be negligible. DIN 1053 limits the slenderness ratio to 20 and permits only the two better quality grades between 10 and 20. In this range the material strength is to be reduced by a factor (25-h/t)/15 and only light loading is permitted on walls having a slenderness ratio over 14. On the other hand, the Eurocode-6 limits the slenderness ratio for masonry wall to 27. Within this constraint Hendry (1976) calculated maximum stresses due to eccentric loading by using conventional linear theory. The maximum compressive should not exceed the material strength divided by an appropriate safety factor. No tensile strength is assumed in this case.

The effect of slenderness ratio and eccentricity on the compressive strength of walls was investigated by Hasan and Hendry (1976), to determine whether reduction factors prescribed in various codes are conservatives. One third scale model has been tested with axial and eccentric loading and with various end conditions.

The results were compared with various national codes. Twenty five specimens were tested in different end conditions such as flat ended, reinforced concrete slab and hinged with different load eccentricity. The walls were constructed by using stretcher course and English bond. Results found in this test shows decrease in strength of walls of flat ended with the increase in slenderness ratio except of wall of slenderness ratio 12. In all walls except hinge supported series, the first hairline crack appeared between 50-60% of failure load and enlarged with further increase of load. The general mode of failure of the walls was vertical splitting accompanied by crushing and splitting of various courses of bricks. However, in walls of slenderness ratio 25 and all walls of vertical load eccentricity t/3 group failure occurred at

mortar brick interface due to breakdown of bond between the mortar and the brick at the time of maximum deflection.

2.7 Influence of Tensile strength on Masonry Wall Stability

The influence of tensile strength on the stability of masonry wall was investigated by Schultz and Bean, a sample cantilever masonry wall is used to demonstrate the sensitivity of critical axial loads on masonry tensile strength. The wall, the profile of which is shown in Figure 11, is subjected to a concentrated eccentric vertical load *P*, a concentrated horizontal top load *Q*, a distributed horizontal load *q*, and weight *W*, distributed along wall height. The wall is subdivided into *N* elements of equal length.

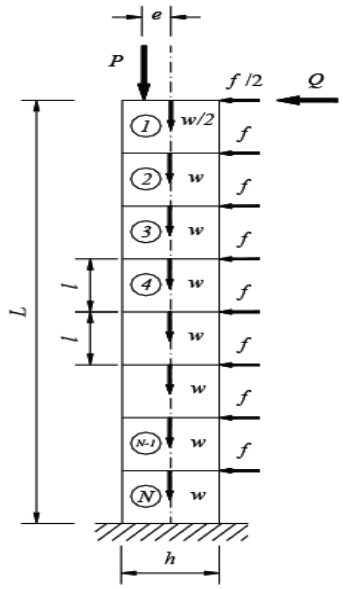

Figure 11: Idealized masonry wall (Schultz et al, 2009).

The distributed loads, namely weight *W* and lateral load *q* are converted to concentrated nodal loads (i.e., $w = W/N$ and $f = qL/N$). The height of the masonry wall is L = 6 m (19.7 ft), and the thickness is h = 200 mm (7.9 in.). The mechanical properties are ε_{cu} = 0.005, E = 125.9 N/mm^2 (2.900 ksi) and v = 0.17. Moreover, the concentrated lateral load *Q* the distributed lateral load *q* and the self weight *W* are assumed to be proportional to vertical load, and are represented by normalized variables *qL*2/2*Ph*, *QL/Ph*, *W/P*, and *e/h*. Figure 12

shows the axial load vs. lateral deflection (P-Δ) curves for various values of the parameter $100\varepsilon cr\ /\varepsilon_{cu}$. The case of a masonry wall with no tensile strength, which has been studied by many researchers, corresponds to $100\varepsilon cr\ /\varepsilon_{cu} = 0$, whereas the maximum value for the tensile capacity parameter, i.e., $100\varepsilon cr\ /\varepsilon_{cu} = 2$, represents a practical upper bound for contemporary masonry materials.

Cracking strength is seen to have a remarkable impact on the shape and smoothness of the stability curves, but it does not have much influence on the values for ultimate tip deflection, i.e., when load capacity vanishes ($P = 0$). However, tensile strength does have an effect on tip deflection values corresponding to the critical (peak) axial load (Figure 12). The peak value for vertical load (i.e., the critical axial load P_{cr}) was taken for each of the P-Δ curves that were generated for a specific tensile strength ($100\varepsilon_{cr}\ /\varepsilon_{cu}$). The resulting relationship is shown in Figure 13, which produces the dramatic influence in critical axial load capacity P_{cr} with increasing tensile strength, $100\varepsilon_{cr}\ /\varepsilon_{cu}$.

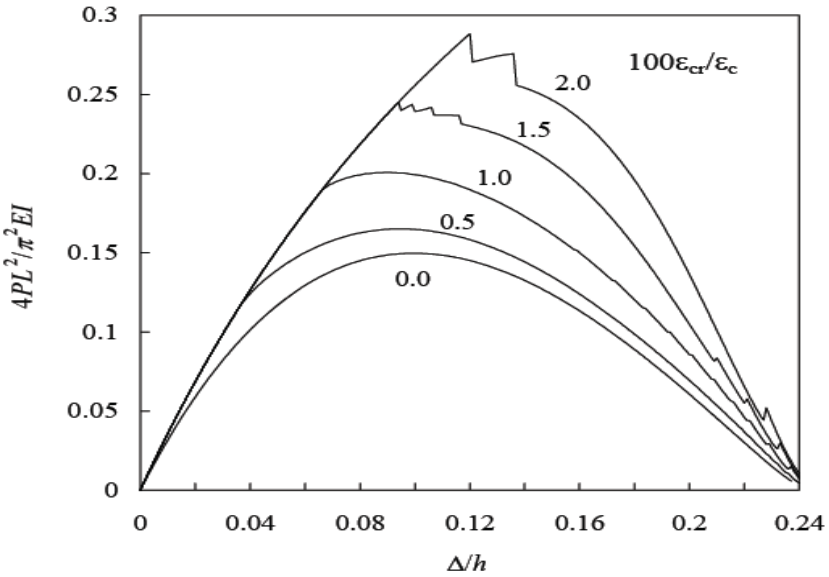

Figure 12: Influence of tensile strength on load deflection behavior (Schultz et al, 2009).

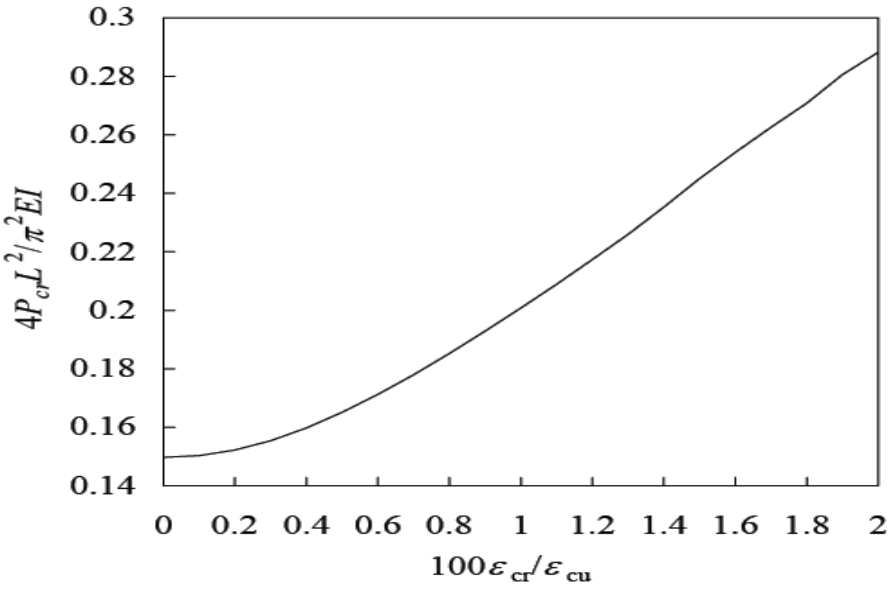

Figure 13: Influence of tensile strength on axial critical load (Schultz et al, 2009).

The same wall configuration was analyzed for increasing eccentricity, *e*, of vertical load *P* but with no lateral loading (i.e., $Q = q = 0$). Critical axial load, as function of eccentricity, is shown in Figure 14, which demonstrates the importance of this parameter on buckling capacity. As *e*/*h* increases from 0 to 0.5, buckling capacity for eccentrically compressed walls decreases by a factor of 5. However, current US code provisions assume that the buckling capacity of eccentrically compressed masonry walls vanishes as eccentricity *e* approaches one-half of the wall thickness *h*.

In the many research the buckling capacities of masonry walls were computed, but only for the case of no tensile strength (i.e., $100\varepsilon_{cr}/\varepsilon_{cu} = 0$). Even modest tensile capacities in masonry give rise to finite buckling strengths, even for cases where $e/h > 0.5$, as noted by the horizontally asymptotic behavior of the curves shown in Figure 14. The P_{cr} vs. $\varepsilon_{cr}/\varepsilon_{cu}$ curves shown in Figure 14 indicate that increases in buckling capacity with tensile strength are substantial only for walls with large eccentricity (i.e., $e/h>0.2$).

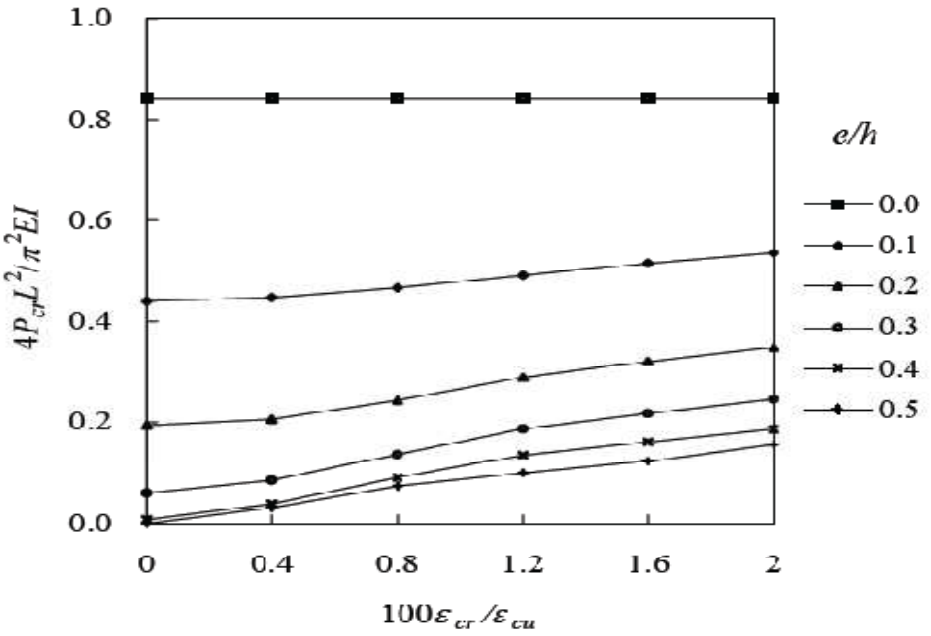

Figure 14: Influence of tensile strength on the buckling capacity of eccentrically loaded wall (Schultz et al, 2009).

2.8 Analytical and Numerical Approaches

Yokel (1971) developed an analytical formula to determine the critical load of prismatic elements that, because of a very low tensile strength, have cracked sections. The study was based on a prismatic rectangular section, consisting of an elastic material, with a linear relationship between stress and strain and did not develop resistance to traction (Figure 15, left). The loading conditions considered by Yokel (1971) consisted of a load P acting direction parallel to the axis of the piece, applied with an eccentricity value $t/2 > e \geq t/6$. The piece considered hinged at both ends, so that the rotation was not restricted (Figure 15, right). The balance in any section requires that the reaction is equal to the applied load. The resulting stress distribution of a section is shown in the Figure 16.

Figure 16 (a) shows the case where the load P acts at an eccentricity equal to kern eccentricity (e=t/). In the case the compressive stresses at one face (the tension face) of the

cross section is zero. At the other face the maximum compressive stress occurs. The value of the maximum stress produced is:

$$\sigma_0 = \frac{2P}{bt}$$

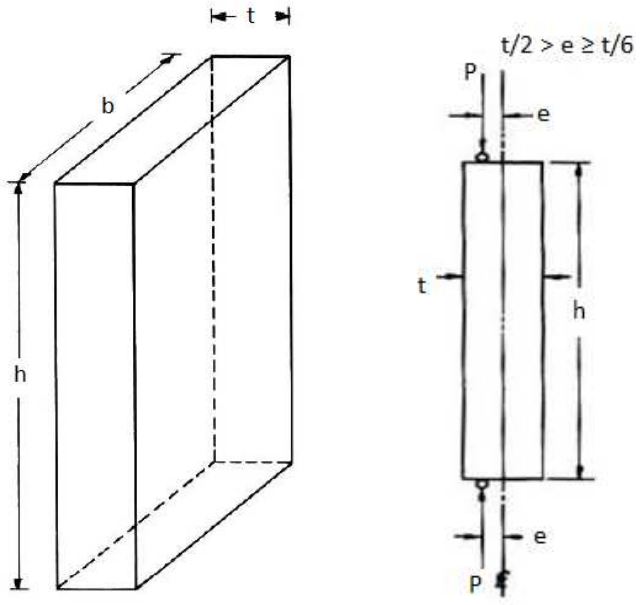

Figure 15: The dimension of wall (left) and loading condition (right).

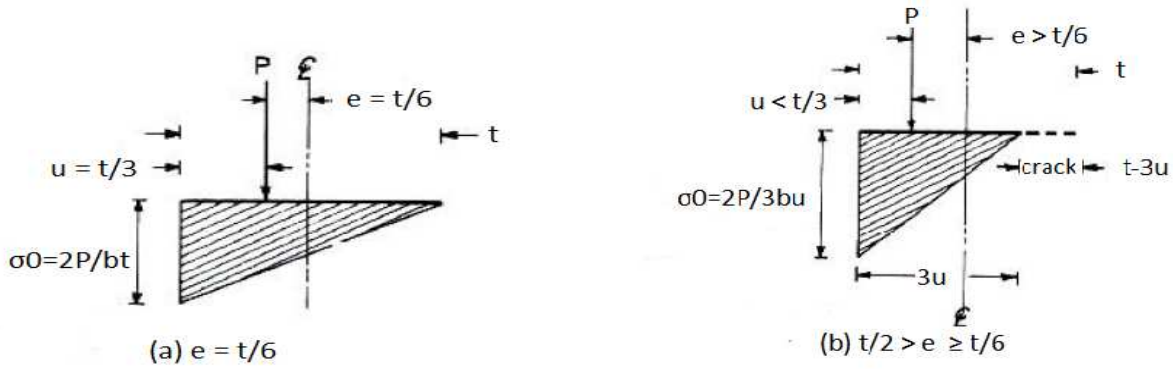

Figure 16: Resulting stress distribution (a) corresponds to an eccentricity t/6 (b) corresponds to an eccentricity greater than t/6.

In the figure 16 (b) the load P acts at a higher eccentricity t/6, i.e. the load is applied outside the kern of the section. The maximum stress at compression face of the cross section is:

$$\sigma_0 = \frac{2P}{3bu} \tag{18}$$

Where, u is the distance between the line of application of P and compression face of section the cross section, P is the compressive force applied to member and b is the width of member. On the other hand, a tensile crack appears at the tension side of the cross section, as the material has no tensile strength. The uncracked part of the cross section has a triangular stress distribution similar to that shown in figure 16 (a), where σ = 0 at the origin of crack. The uncracked thickness of the section is 3u and depth of cracks is therefore t-3u. The expression 18 is valid for all cases in which the values of eccentricity are t/2 > e ≥ t/6. Stress distribution within the entire wall is shown in Figure 17.

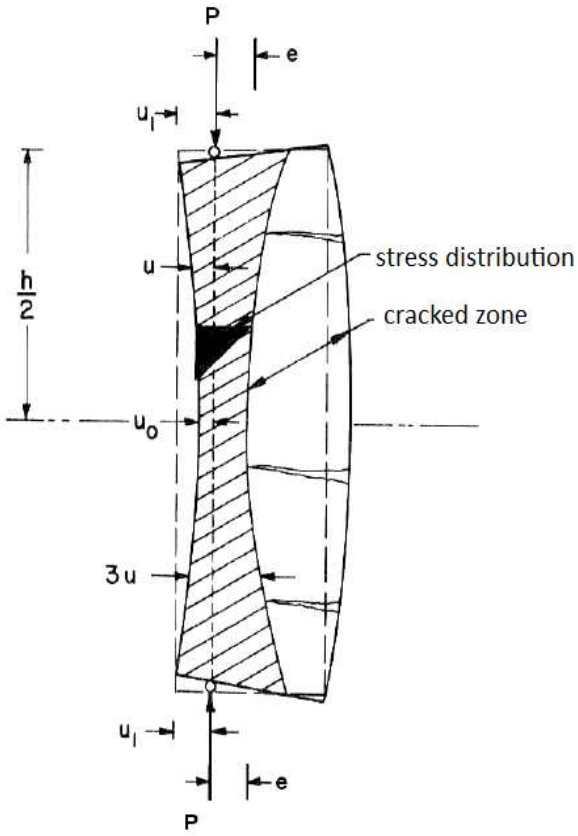

Figure 17: Stress distribution in the units of the wall.

The rectangle obtained by broken lines shows the undeflected shape of the member. The deflected shape is shown by the heavy out line. The shaded area within the deflected member

shows the un-cracked zone which supports the load. The stress distribution at one particular cross section is shown by the heavy-shaded triangle.

Distance, u between the compression face of the member and the line of action of force P varies along the height of the member because of member deflection. The maximum distance u_1 occurs at the two member ends. The minimum distance u_0 occurs at mid-height. The maximum compressive stress in the member occurs at mid-height is:

$$\sigma_{max} = \frac{2P}{3bu_0} \tag{19}$$

Figure 18 shows the deflection curve of the compression face of the member, together with the coordinate system used. The x axis is parallel to the action line of P and is tangential to the deflection curve at the origin. At each point, $y = u - u_0$ and at $x = h/2$, $y = u_1 - u_0$.

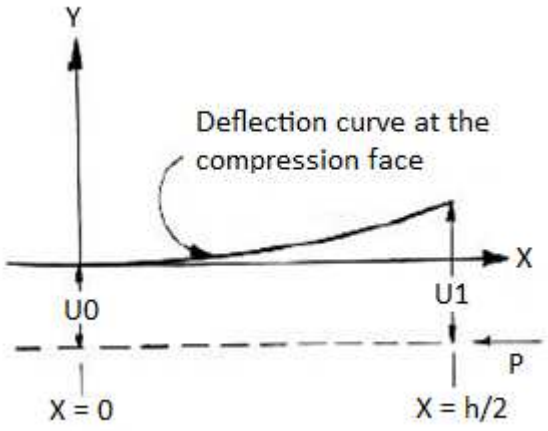

Figure 18: Deflection curve of compression face.

By this approach, finally the equivalent critical load is computed from an equivalent moment of inertia and based on an equivalent thickness of $3u_1$ is:

$$P_{ec} = \frac{9}{4}\frac{Ebu_1{}^3}{h^2} \tag{20}$$

Where,

P_{ec} equivalent critical load;

u_1 distance between line of action of compressive load and compression face of member at member support.

Note that, P_{ec} becomes the Euler load, when the section is loaded at the edge of the kern ($3u_1 = t$) i.e. the load is applied at an eccentricity equal to t/6.

Yokel concluded that the elastic instability is given for the value of good criticism:

$$P_{cr} = 0.285 P_{ec} \tag{21}$$

Where, P_{cr} is the critical load of member.

Substituting the value of P_{ec}in the expression and obtained:

$$P_{cr} = 0.64 \frac{E b {u_1}^3}{h^2} \tag{22}$$

The author observed the expressions obtained by comparing with the results of a pilot scale test conducted by the Institute of Structural Clay Products. The test included slenderness ratio of 6.6 to 46.1 and the eccentricities t/6 to t/3.

In this comparison the author obtained the following conclusions:

- The masonry tested developed a tensile strength of around 2% - 3% of compressive strength. This change translates into greater capabilities than those obtained by author's formulation. These differences will be greater for situations where failure occurs at relatively low stress (high ratio of slenderness and eccentricity).
- The stress - strain curve for bricks is not exactly linear. The tangent modulus of elasticity at failure tends to be about 70% of initial value. If deflections are predicted on the basis of modulus of elasticity at low stress levels, deflections at high stress levels would probably be greater than the predicted deflections. This effect is more pronounced for reasons of slenderness and low eccentricity.
- The brick units themselves have greater strength and stiffness than the mortar beds connecting the units. This discontinuity stress distribution causes a much more complex than the idealized distribution assumed by the author for the solution. The author did not evaluate the effect of these discontinuities on strength and stiffness.

A numerical model for the analysis of structural members under eccentric compression is presented by Vassilev et al. (2009). The equilibrium is formulated in the deformed state and takes account of the effect of deflections on the bearing capacity. The assumed parabolic stress-strain function allows a realistic modeling of the composite material behavior in compression and bending. Due to the physical and structural nonlinearities, the bending

stiffness becomes under loading a function of the stress state, thus leading to variable coefficients of the governing differential equation.

The system solution is obtained within an iterative numeric procedure, based on the discretisation of the structure into finite segments and the piecewise linearization of its parameters. The piecewise integration of the equilibrium differential equation leads to a formulation in terms of the transfer matrix method. The ultimate state is marked either by equilibrium bifurcation and loss of stability or collapse due to material failure. The performance of structural members under eccentric compression is usually assessed through the equilibrium conditions of models like the one on Figure 19. The bearing capacity is ensured as long as the resistance can equal the compressive and bending action of the external load. At ultimate level the capacity is exhausted either due to material failure or excessive increase of deflections leading to loss of stability.

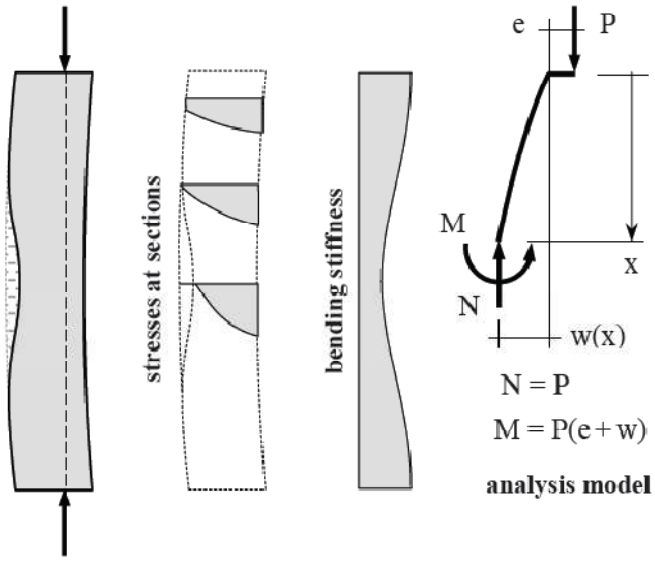

Figure 19: Masonry wall under eccentric compression (Vassilev et al. 2009).

If the bending stiffness B and the compressive force N remain constant over the height, then the problem has an explicit solution, based on the familiar differential equation:

$$Bw'' + P(w + e) = 0 \tag{23}$$

The basic steps of the iterative procedure are presented in Figure 20. An update of the stepped stiffness function serves as starting point for each iteration. The first step of the

analysis procedure under a prescribed load level is the System Solution which is based on the transfer matrix method.

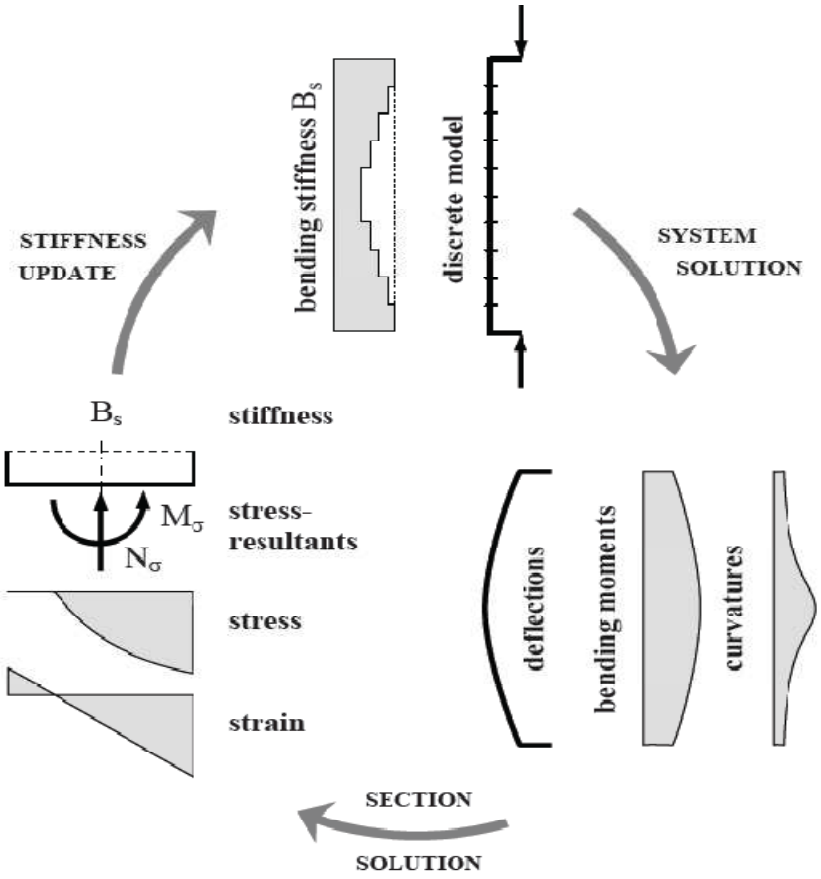

Figure 20: Iterative scheme of the evaluation procedure (Vassilev et al. 2009).

The expression for the compressive resultant becomes thus in the case of rectangular sections:

$$N_\sigma = \frac{b}{K} \int_{\varepsilon_0 - Kt/2}^{\varepsilon_0 + Kt/2} \sigma d\varepsilon = P \tag{24}$$

Where, t, b = width and depth of the section, P = applied load, N_σ = resultant compressive axial force, σ = stress, К = curvature and ε = strain.

The solution of Equation 24 yields the strain at the centroid ε_0 and determines unequivocally – along with the curvature κ – the two relevant values of the current strain state:

$$\varepsilon_{min} = \varepsilon_0 - \frac{Kt}{2} \quad ; \quad \varepsilon_{max} = \varepsilon_0 + \frac{Kt}{2} \tag{25}$$

And finally, the formula for the updated value of the bending stiffness prior to the next iteration:

$$B_s = \frac{b}{K^3} \int_{\varepsilon_{min}}^{\varepsilon_{max}} \sigma \varepsilon d\varepsilon - \frac{\varepsilon_0}{K^2} N_\sigma \tag{26}$$

The results obtained in this numerical study presented below illustrate the potential of the approach. Figure 21 shows the two characteristic modes of failure independent of the load eccentricity. It varies in magnitude, but remains equal at both ends. The slenderness ratio is h/t = 10.

In the case of the figures on the left, the load acts with the small eccentricity e = t/8. The cracking is primarily a consequence of the eccentricity amplification, induced by the second-order deflections. The crack propagation is confined to the central part, while the boundary regions remain undamaged. The bearing capacity is reduced to Φ = 0.597 where Φ is the bearing reduction factor. The ultimate state is associated with material failure at the critical central section, at the stage when the maximum stress equals the material strength.

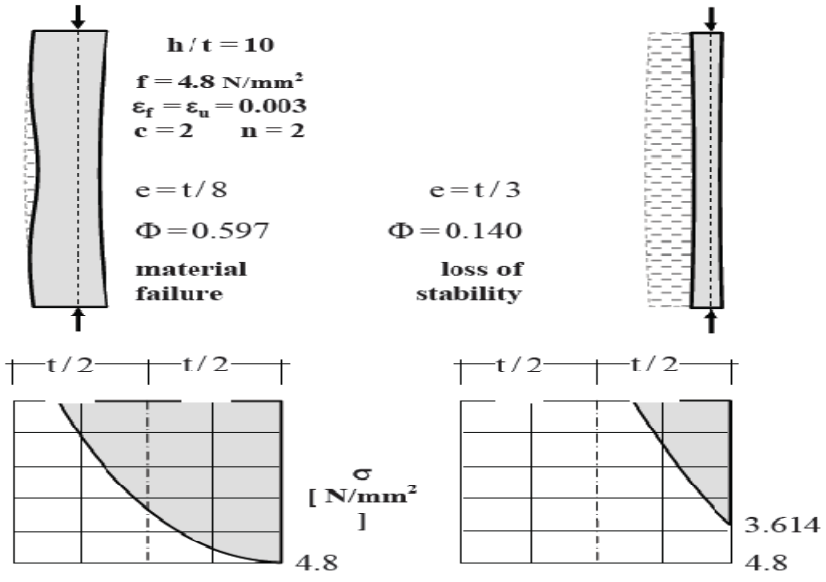

Figure 21: Deflection and damage at ultimate limit state (Vassilev et al. 2009).

In the case on the figures on the right, the larger eccentricity of e = t/3 leads a priori to cracking all over the height. The effective width of the interior sections is further reduced due

to the second-order effects. At ultimate it is barely 1/3 of the thickness at the critical section. The material strength is not reached as the system fails at Φ = 0.140 due to loss of stability. The plot in Figure 22 gives the calculated capacity versus the load eccentricity as well as the results of two series of tests with the eccentricity ratios e/t = 1/3 and e/t = 0.4 respectively. A good agreement between prediction and experiment can be registered in both cases. The numerical simulation indicates material failure as the cause for collapse in the case of the smaller eccentricity and loss of stability for the larger one.

The dashed lines on Figure 22 serve as reference by the evaluation of the results. They represent the material section capacity, based on two common simplified theories: stress-block and linear stress distribution. The prediction lies within the two limits as long as the eccentricity remains relatively small and material failure prevails. The capacity progressively drops below with the increasing eccentricity, when instability becomes dominating.

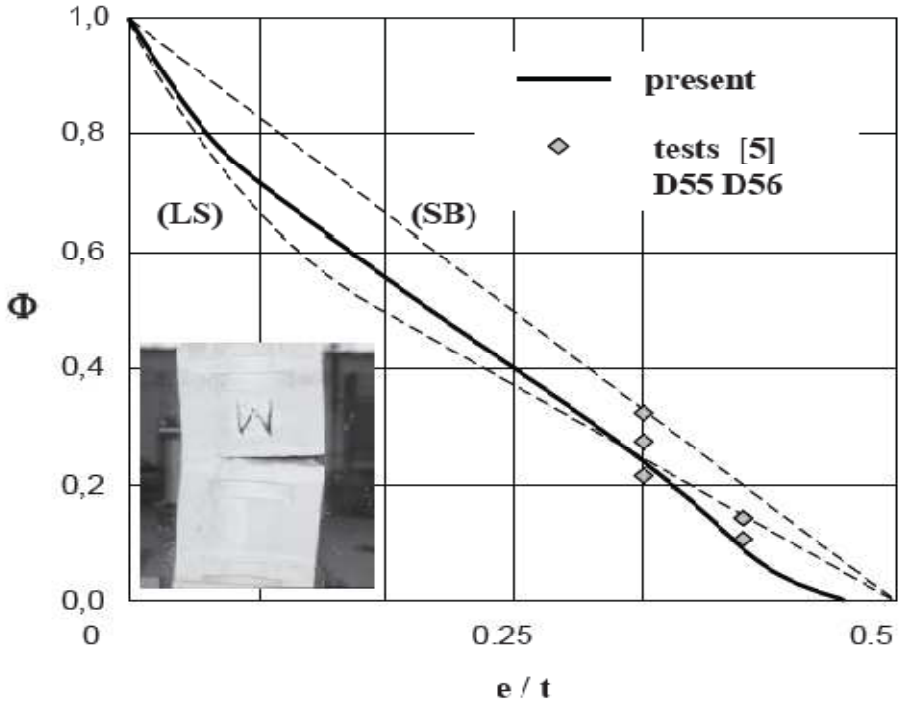

Figure 22: Capacity reduction factor versus load eccentricity; material section capacity (SB) based on stress block theory and (LS)-based on stress distribution (Vassilev et al. 2009).

2.9 Review of Experimental Test of Masonry Walls under Concentric and Eccentric Loading

In this section a review of previous experimental tests in order to study the bearing capacity of masonry walls under the combined effect of slenderness and eccentricity the load has been discussed. Specifically, the experimental tests carried out by Kirtschig and Anstotz(1991), Watstein and Allen (1971) and Hasan and Hendry (1976) has described. The review of these studies will focus on these experimental techniques, objectives, results and conclusions.

2.9.1 Kirtschig and Anstotz (1991)

The influence of slenderness ratio and eccentricity of the load on the load bearing capacity of the masonry is subjected to different treatments in the regulations of each country. The main objective of the experimental tests developed by Kirtschig and Anstotz (1991) was to verify this overestimation by comparing load bearing capacity values with theoretically derived results. The experimental development proposed an empirical formula for the calculation of capacity reduction factors for any eccentricity and slenderness ration under vertical load by using:

$$\alpha = \frac{E}{4f_{ma}} \tag{27}$$

The masonry units considered for the test were calcium silicate and lightweight aggregate concrete with average compressive strength of the units 20.9 MPa and 4.1 MPa respectively. For the specimens mortar with a compressive strength of about 5 MPa was used. The length of the walls was about 1 m and a thickness of 11.5 cm.

In order to introduce the study with different slenderness ratio, walls were made of different heights. These heights were 63.5 cm, 125 cm, 212 cm and 312 cm, which translates into approximately slenderness ratio(calculated as ratio between height and thickness) of 5.6, 11.1, 18.8 and 27.7. A total of 64 walls were tested (32 for each type of wall). The test arrangement of the walls in this way that free rotation on top and bottom was possible (shown in figure 23). The results obtained in the experimental test are shown in Tables 2 and 3 and represented graphically in Figures 24 and 25.

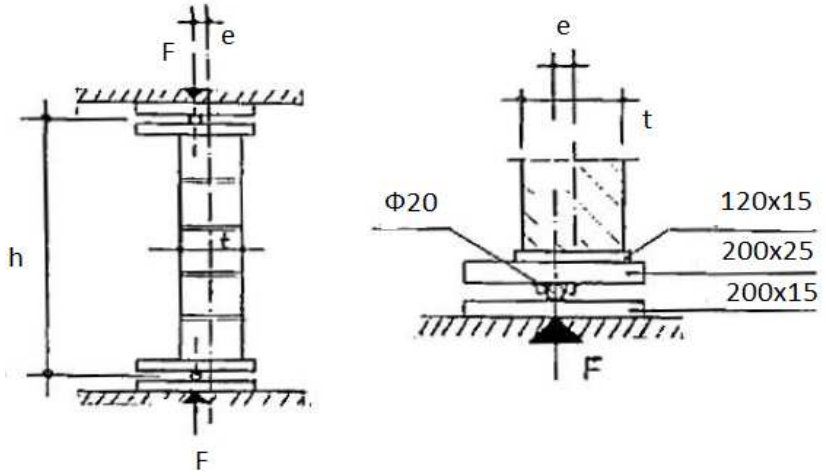

Figure 23: Arrangement of walls for testing (Kirtschig and Anstotz, 1991).

Table 2: Test results in the case of calcium silicate units (Kirtschig and Anstotz, 1991).

Slenderness ratio (h/t)	Failure load (KN) (1-means individual and 2-means mean results)			
	e =0	e = t/8	e = t/4	e = t/3
5.6	1450 (1) 1350 (1)	1050 950	685 585	328 382
	1400 (2)	1000	635	355
11.1	1225 1270	900 860	100 465	170 144
	1248	880	433	157
18.8	1170 1060	460 600	214 204	138 118
	1115	530	209	128
27.7	710 615	240 270	80 84	35 32
	663	255	82	34

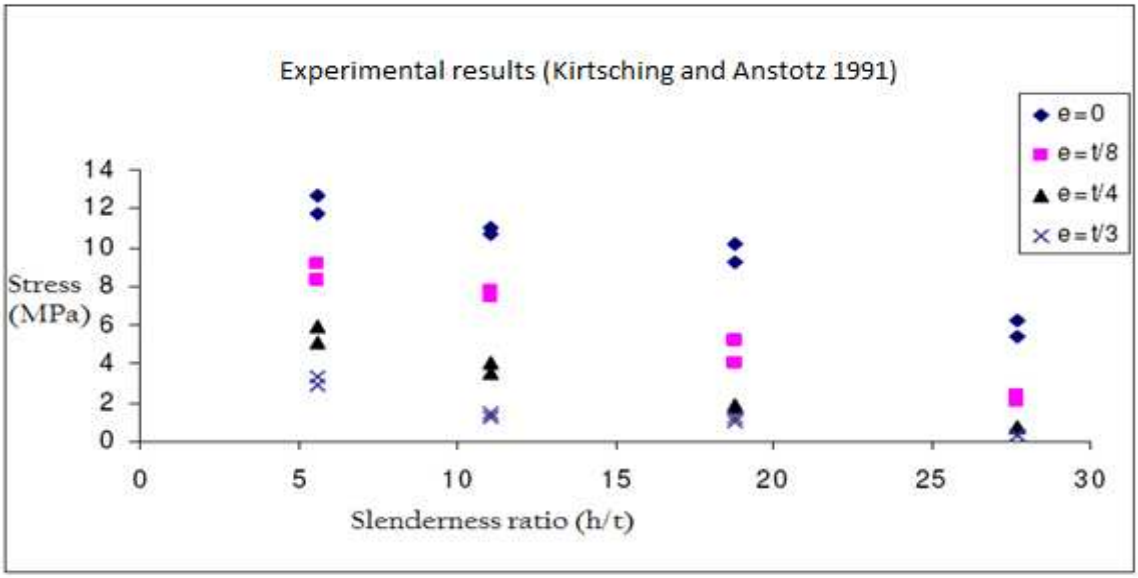

Figure 24: Test results in the case of calcium silicate units (Kirtschig and Anstotz, 1991).

Table 3: Test results in the case of lightweight concrete units (Kirtschig and Anstotz, 1991).

Slenderness ratio (h/t)	Failure load (KN) (1-means individual and 2-means mean results)			
	e =0	e = t/8	e = t/4	e = t/3
5.6	395 (1) 368 (1)	280 310	185 175	138 130
	382 (2)	295	180	134
11.1	390 332	265 280	132 150	80 78
	361	273	141	79
18.8	302 350	208 162	90 96	60 51
	326	185	93	56
27.7	248 210	116 110	64 60	36 29
	229	113	62	33

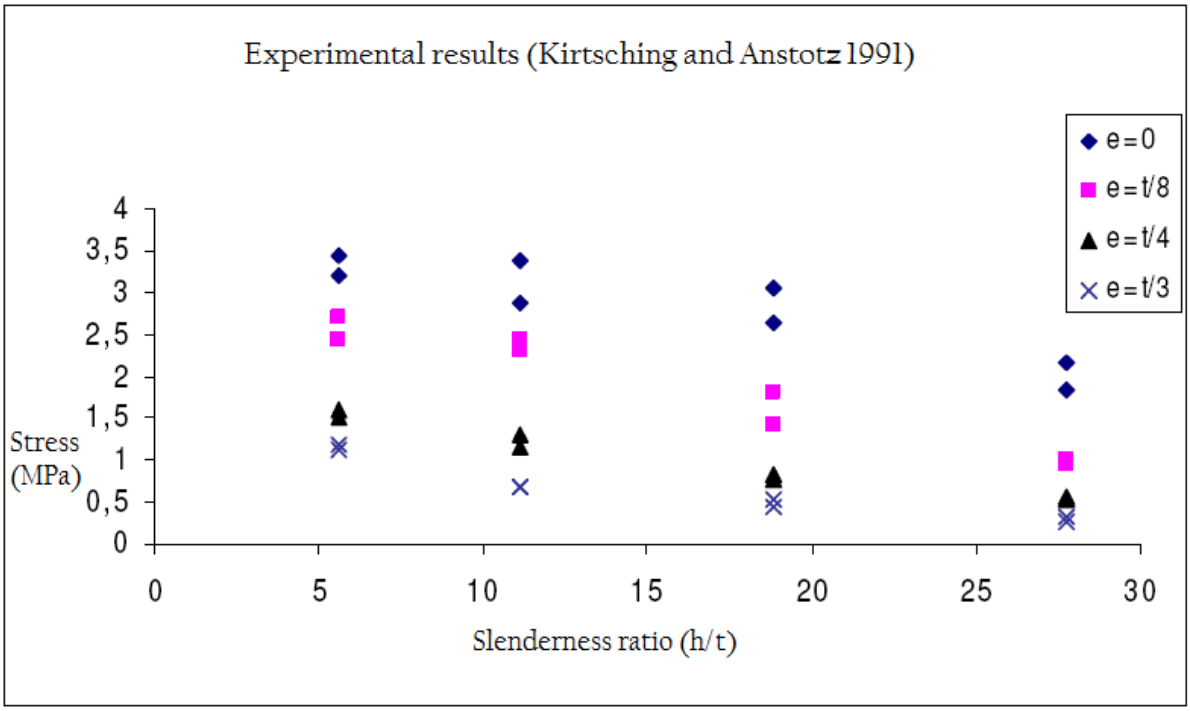

Figure 25: Test results in the case of lightweight concrete units (Kirtschig and Anstotz, 1991).

The comparison established by Kirtschig and Anstotz (1991) shows a greater proximity between the experimental and theoretical values, which led them to assert that development is a good approach for determining the bearing capacity of the masonry face action vertical loads with the advantage of being a relatively simple expression management.

2.9.2 Watstein and Allen (1970)

The main factor of limiting the strength of brick masonry imposed by the relatively low tensile bond strengths developed between the masonry units and conventional Portland cement mortars. According to the authors, the mechanism of failure due to geometric instability of the masonry works suggests that increasing of bond tensile strength of masonry will significantly affect not only the transverse strength of the masonry but also its compressive and shearing strengths. The typical mode of failure in compression is neither crushing nor shear, but tensile splitting of the materials as a result of axial loading. The walls were tested as hinged-hinged compression members, centrally supported at the bottom. The arrangement of testing is shown in the Figure 26. The applied load eccentricity were 0, t/6

and t/3. Six type brick were used in the test of compressive prism to investigate the effect of brick compressive strength on the compressive strength of masonry. The mortar was prepared from type I Portland cement, hydrated lime and sand mixed with marble dust as additive and organic modifier saran polymer.

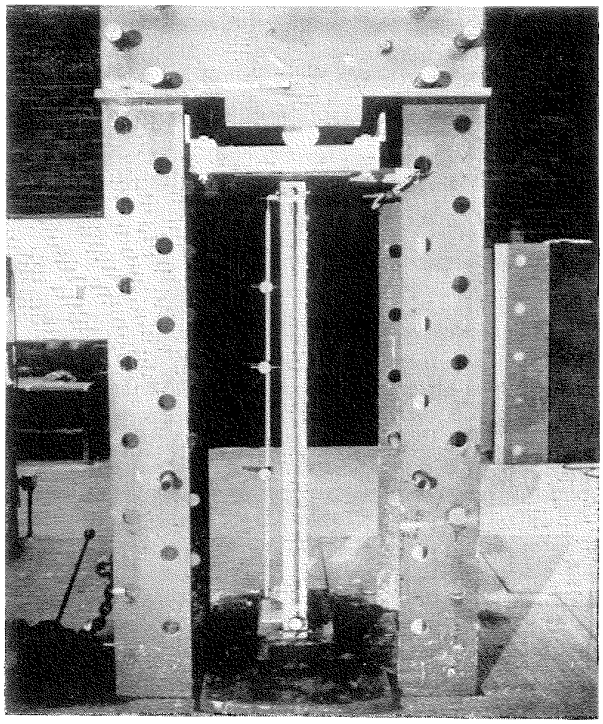

Figure 26: View of an eccentrically loaded wall in testing machine (Watstein and Allen, 1971).

The effect, slenderness ratio and the eccentricity of applied load, was studied for walls built with high bond mortar ranging in height from 37 inch to 144 inch with effective slenderness ratio 12.4, 22.8, 32 and 42.5. The capacity obtained for the walls with mortar of high adhesion according to slenderness ratio and comparing these capacity values with walls of conventional mortar walls are reflected in Figures 27 and 28.

Figure 27: Capacity of walls obtained with mortar of high strength for different slenderness and load eccentricity (Watstein and Allen, 1971).

Comparing the strength obtained for the effective slenderness ratio 22.8 shows that the capacity of walls with high bond mortar is was 1.09, 1.25 and 1.33 times of the capacity of conventional type mortar walls for the eccentricity ratio of 0, 1/6 and 1/3 respectively. From the results it is clear that performance of high bond mortar walls compared to conventional mortar increases with eccentricity of load application. This is because a higher eccentricity applied the greater the influence of tensile strength developed in the joints.

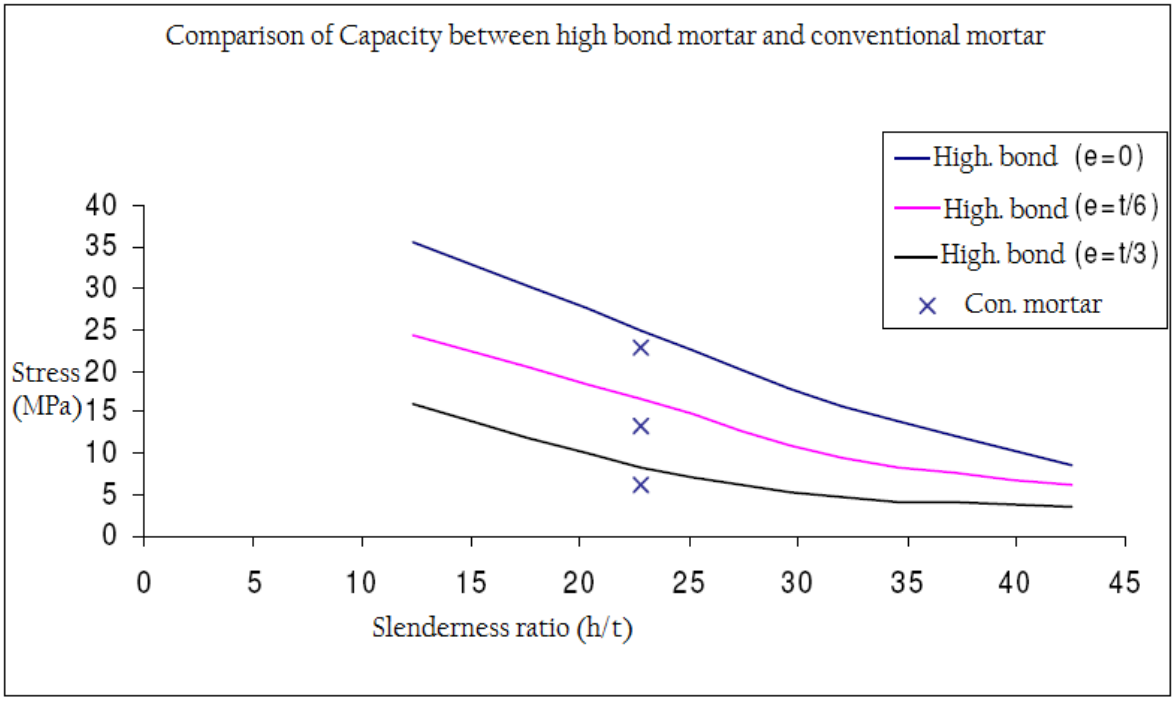

Figure 28: Relationship between the average compressive strength of the walls and the value of its slenderness ratio for different load eccentricity (Watstein and Allen, 1971).

The compressive strength of walls built with mortar high adhesion of slenderness ratio 22.8 was 25% greater than the resistance of walls made of conventional mortar for eccentricity equal to one sixth the thickness of the wall. For the eccentricity equal to one third the thickness of the wall, compressive strength of high bond mortar walls was 33% greater than the strength of walls with conventional mortar. In these data reflected the influence of the tensile strength of the wall is greater in the case of the greater eccentricity of load application because the lateral deflections given for the same load value increases with eccentricity.

2.9.3 Hasan and Hendry (1976)

The effect of slenderness ratio and eccentricity on the compressive strength of wall was investigated by Hasan and Hendry (1976). The main objective of this study was to determine whether reduction factors prescribed in various codes are conservatives. One third scale

model has been tested with axial and eccentric loading and with various end conditions. The arrangement for rotation measurement is shown in the Figure 29. The results were compared with various national codes. Twenty five specimens were tested for various slenderness ratio 6, 12, 18 and 25 with different end conditions (flat ended, reinforced concrete slab and hinged) and load eccentricity of 0, t/6 and t/3.

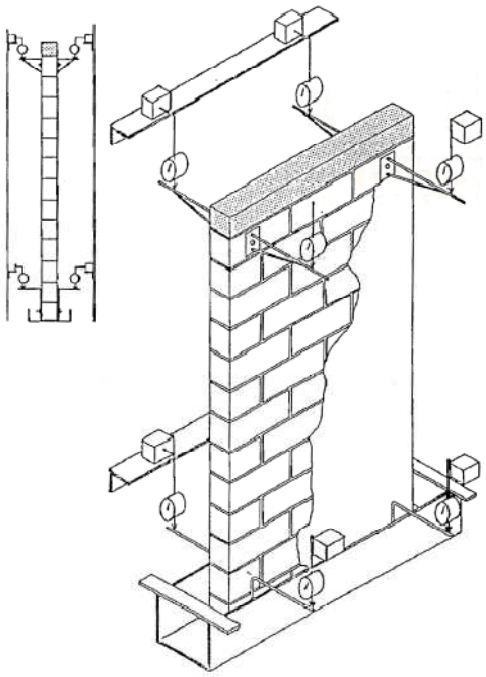

Figure 29: Test setting for measurement of rotation at the supports (Hasan and Hendry, 1976).

One third scale solid bricks were used with variable strength. For calculation purpose the strength of brick unit was taken as f_b = 28 MPa. Dry Leighton buzzard sand with rapid hardening Portland cement was used for all tests. The water cement ratio for mortar varied from 0.8 to 0.95. The results of the test carried out by the author's reflected in the Figure 30.
In all walls except hinge supported series, the first hairline crack appeared between 50-60% of failure load and enlarged with further increase of load. The general mode of failure of the walls was vertical splitting accompanied by crushing and splitting of various courses of bricks. However, in walls of slenderness ratio 25 and all walls of vertical load eccentricity t/3

group failure occurred at mortar brick interface due to breakdown of bond between the mortar and the brick at the time of maximum deflection.

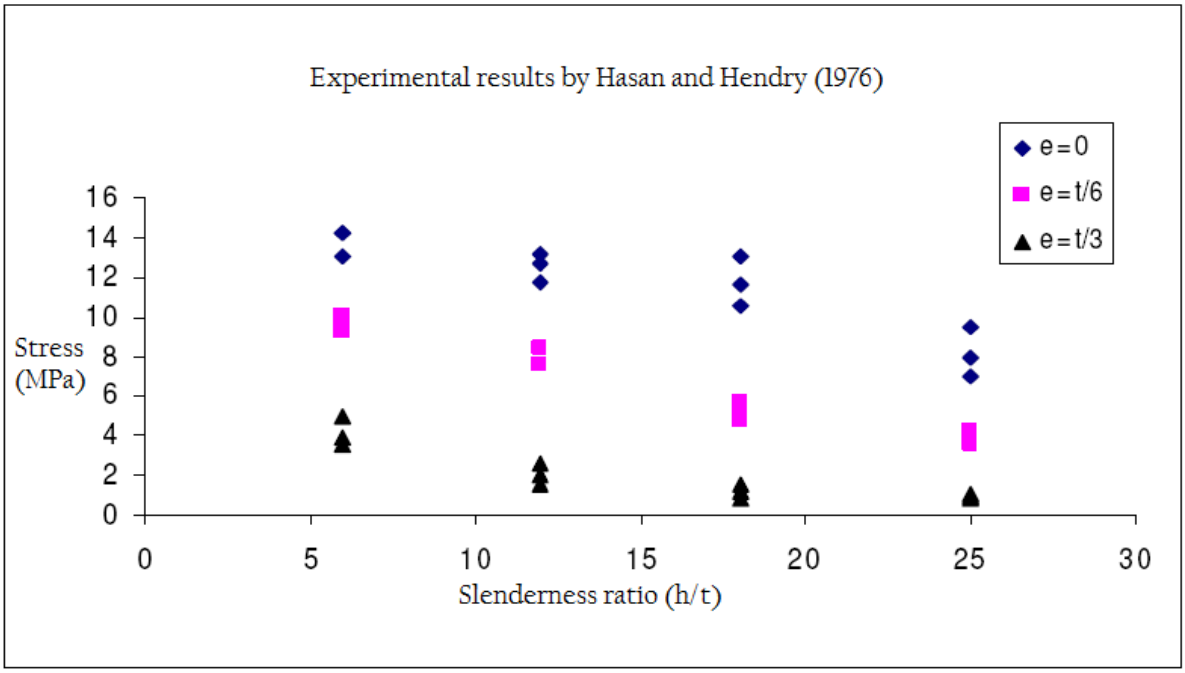

Figure 30: Relation between the capacity of walls and slenderness ratio with various eccentricity (Hasan and Hendry, 1976).

When comparing the reduction factor calculated by the author's found that except the walls with slenderness ratio 25, the reduction factor calculated according to SCP1 is about 10% lower in the series of hinge supported walls with eccentricity 0. In the case of walls series eccentrically loaded t/6, the reduction factor obtained is practically same as that obtained by SCP1. However, the value of reduction factor for wall series eccentrically loaded at t/3 is 25% higher than SCP1. It is noteworthy that the maximum value of the slenderness of the walls tested by the authors is 25.0, while the results of SCP1 provide up to 46.1 slenderness ratio.

In the opinion of the authors, test walls with slenderness greater than 30 are more a matter of academic rather than practical interest. The results of Haller (1969) are approximately 18% lower than those obtained by the authors for the series walls with 0 eccentricities. In the case of walls of applied load with an eccentricity equal to one sixth of wall thickness, the results of Haller are lower than those obtained by the authors.

3. MODELING MASONRY

3.1 Micro- modeling Approach

Masonry is a material which exhibits distinct directional properties due to the mortar joints which act as planes of weakness. In general, the approach towards its numerical representation can focus on the micro-modeling of the individual components, viz. unit (brick, block, etc.) and mortar, or the macro-modeling of masonry as a composite. Depending upon the level of accuracy and the simplicity desired, it is possible to use the following micro-modeling strategies, see Figure 31.

In the case of detailed micro-modeling, units and mortar in the joints are represented by continuum elements whereas the unit-mortar interface is represented by discontinuous elements. On the other hand simplified micro-modeling expanded units are represented by continuum elements whereas the behavior of the mortar joints and unit-mortar interface is lumped in discontinuous elements.

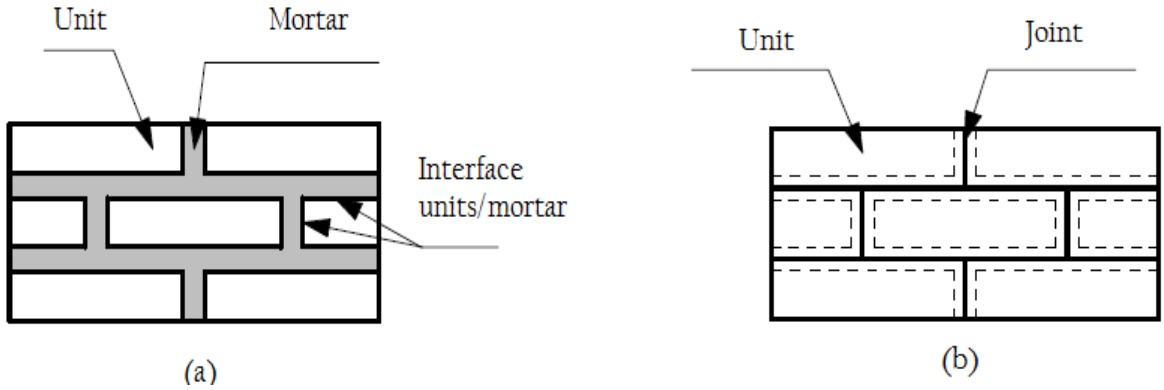

Figure 31: Micro-modeling approach for masonry structures (a) detailed micro-modeling (b) simplified micro-modeling (Lourenco, 1996).

In the detailed micro-modeling approach, Young's modulus, Poisson's ratio and, optionally, inelastic properties of both unit and mortar are taken into account. The interface represents a potential crack/slip plane with initial dummy stiffness to avoid interpenetration of the continuum. This enables the combined action of unit, mortar and interface to be studied under

significant concentration. In the simplified micro-model approach, each joint, consisting of mortar and the two unit-mortar interfaces, is lumped into an “average” interface while the units are expanded in order to keep the geometry unchanged. Masonry is thus considered as a set of elastic blocks bonded by potential fracture/slip lines at the joints. Accuracy is lost since Poisson’s effect of the mortar is not included.

Micro-modeling studies are necessary to give a better understanding about the local behavior of masonry structures. This type of modeling applies notably to structural details, but also to modern building systems like those of concrete or calcium-silicate blocks, where window and door openings often result in piers that are only a few block units in length. These piers are likely to determine the behavior of the entire wall and individual modeling of the blocks and joints is then to be preferred.

Accurate micro-modeling of masonry structures requires a thorough experimental description of the material. However, the properties of masonry are influenced by a large number of factors, such as material properties of the units and mortar, arrangement of bed and head joints, anisotropy of units, dimension of units, joint width, quality of workmanship, degree of curing, environment and age. Due to this diversity, only recently the masonry research community began to show interest in sophisticated numerical models as an opposition to the prevailing tradition of rules-of-thumb or empirical formulae. Moreover, obtaining experimental data, which is reliable and useful for numerical models, has been hindered by the lack of communication between analysts and experimentalists. The use of different testing methods, test parameters and materials preclude comparisons and conclusions between most experimental results. It is also current practice to report and measure only strength values and to disregard deformation characteristics (Lourenco, 1996).

3.2 Softening Behavior of Masonry

Softening is a gradual decrease of mechanical resistance under a continuous increase of deformation forced upon a material specimen or structure. It is a salient feature of quasi-brittle materials like clay brick, mortar, ceramics, rock or concrete, which fail due to a process of progressive internal crack growth. Such mechanical behavior is commonly attributed to the heterogeneity of the material, due to the presence of different phases and

material defects, like flaws and voids. Even prior to loading, mortar contains micro-cracks due to the shrinkage during curing and the presence of the aggregate. For tensile failure this phenomenon has been well identified, Hordijk (1991). For shear failure, a softening process is also observed as degradation of the cohesion in Coulomb friction models. For compressive failure, softening behavior is highly dependent upon the boundary conditions in the experiments and the size of the specimen, Van Mier (1984) and Vonk (1992). Experimental concrete data provided by Vonk (1992) indicated that the behavior in uniaxial compression is governed by both local and continuum fracturing processes. Figure 32 shows characteristic stress-displacement diagrams for quasi-brittle materials in uniaxial tension and compression. In the present study, it is assumed that the inelastic behavior both in tension and compression can be described by the integral of the σ-δ diagram. These quantities, denoted respectively as fracture energy G_f and compressive fracture energy G_c are assumed to be material properties.

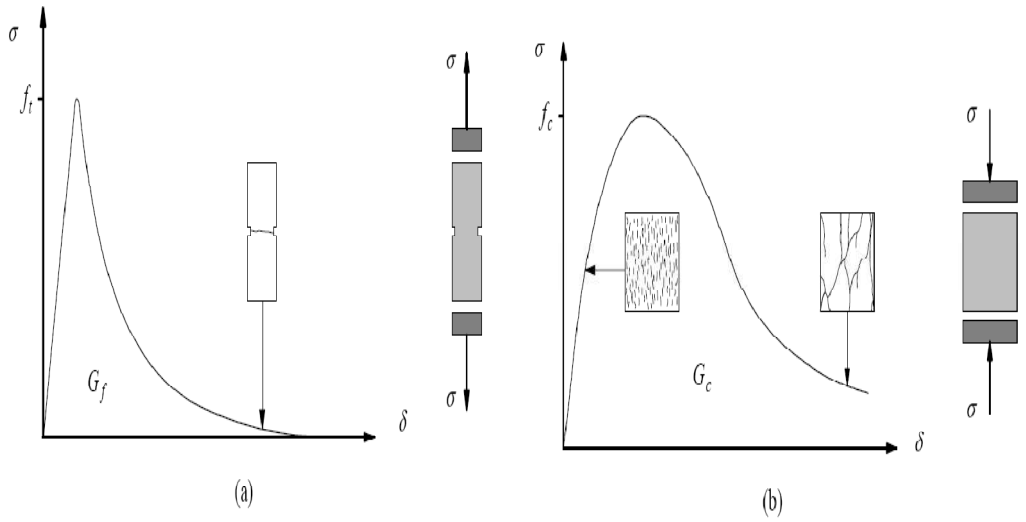

Figure 32: Typical behavior of quasi-brittle materials under uniaxial loading and definition of fracture energy: (a) tensile loading; (b) compressive loading.

3.3 Characteristics of Unit Mortar Interface

The adhesion between the unit and mortar is often the weakest link in masonry works. The nonlinear response of the joints, which is then controlled by the unit-mortar interface, is one of the most relevant features of masonry behavior. Two different phenomena occur in the

unit-mortar interface, one associated with tensile failure (mode I) and the other associated with shear failure (mode II).

For the case of tensile failure (mode-I) Van der Pluijm (1992) carried out deformation controlled tests in small masonry specimens of solid clay and calcium-silicate units. These tests resulted in an exponential tension softening curve with a mode I fracture energy G_f^I ranging from 0.005 to 0.02 (Nmm/mm^2) for a tensile bond strength ranging from 0.3 to 0.9 (MPa), according to the unit-mortar combination. This fracture energy is defined as the amount of energy to create a unitary area of a crack along the unit-mortar interface. A close observation of the cracked specimens revealed that the bond area was smaller than the cross sectional area of the specimen

On the other hand, Van der Pluijm (1993) presents the most complete characterization of the masonry shear behavior, for solid clay and calcium-silicate units. The test set-up permits to keep a constant normal confining pressure upon shearing. Confining (compressive) stresses were applied with three different levels: 0.1, 0.5 and 1.0 (MPa). The test apparatus did not allow for application of tensile stresses and even for low confining stresses extremely brittle results are found with potential instability of the test set-up. Noteworthy, for several specimens with higher confining stresses shearing of the unit-mortar interface was accompanied by diagonal cracking in the unit.

3.4 Multisurface Interface Model Proposed by Lourenco and Rots (1997)

Micro-models are considered as the best tool available to understand the behavior of masonry. The benefit of using such an approach is that all the different failure mechanisms can be considered. In a simplified micro-modeling strategy, interface elements are used as potential crack, slip or crushing planes. A multisurface interface model, which includes a tension cut-off for mode I failure, a Coulomb friction envelope for mode II failure and a cap mode for compressive failure, is developed in modern plasticity concepts. In addition, interface elements are considered to model potential cracks in the units. The assumption that all the inelastic phenomena occur in the interface elements leads to a robust type of modeling, capable of following the complete load path of a structure until total degradation of stiffness. In addition, interface elements are considered to model potential cracks in the units. The

parameter necessary to define the model are derived from carefully displacement control micro-experiments. The main difference between the present strategy and the research carried out by Lourenco and Rots lies in the assumption that all the inelastic phenomena occur in the interface elements. This assumption leads to a robust type of modeling, capable of following the complete load path of a structure until total degradation of stiffness.

An accurate micro-model for masonry must include the basic types of failure mechanisms that characterize the masonry material, (a) cracking of the joints, (b) sliding along the bed or head joints at low values of normal stress, (c) cracking of the units in direct tension, (d) diagonal tensile cracking of the units at values of normal stress sufficient to develop friction in the joints and (e) Splitting of units in tension as a result of mortar dilatancy at high values of normal stress , as illustrated in Figure 33. It is clear from the described phenomena that (a,b) are joint mechanisms, (c) is a units mechanism and (d,e) are combined mechanisms involving units and joints. The question remains of how to consider all phenomena in the model. The approach followed here is to concentrate all the damage in the relatively weak joints and, if necessary, in potential pure tensile cracks in the units placed vertically in the middle of each unit, see Figure 34. These potential cracks in the units are able to reproduce a jump from one head joint to the other (immediately below or above), which is a typical masonry characteristic. The joint interface yield criterion has then to include all the mechanisms referred above except uniaxial tensile cracking of the unit.

Inclusion of the first two mechanisms (tensile and shear failure of the joint) has been pursued before, e.g. Page (1978) and Rots *et al.* (1994), but the compressive cap model here set forth is novel. By limiting the compressive/shear stress combinations, diagonal tensile cracking of the units and masonry crushing, failure mechanisms (d,e) in Figure 33, can be incorporated in the model. It is noted that the composite interface model developed next is used at a micro-level.

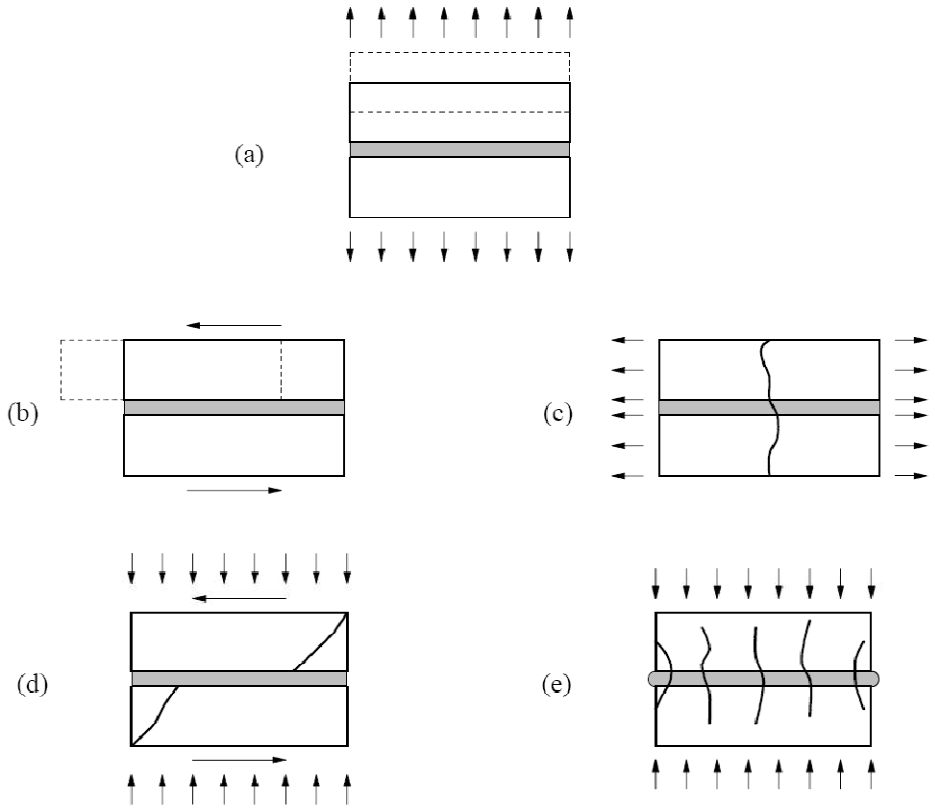

Figure 33: Masonry failure mechanisms: (a) joint tensile cracking; (b) joint slipping; (c) unit direct tensile cracking; (d) unit diagonal tensile cracking; (e) masonry crushing.

An interface allows discontinuities in the displacement field and its behavior is described in terms of a relation between the traction t and relative displacement u across the interface. In the multisurface interface model for the masonry proposed by Lourenco and Rots, the quantity of traction and displacement is denoted as generalized stress σ and generalized strain, ε. In this case the elastic constitutive relation between stresses and strain is given by:

$$\sigma = D\varepsilon \tag{28}$$

For 2D configuration $D = diag\{k_n, k_s\}, \sigma = (\sigma, \tau)^{\tau}, and\ \varepsilon = (u_n, u_s)$

Where, n and s is the normal and shear components respectively. The terms in the elastic stiffness matrix can be obtained from the properties of both masonry components and thickness of the joint as:

$$k_n = \frac{E_u E_m}{t_m(E_u - E_m)};\ \ k_s = \frac{G_u G_m}{t_m(G_u - G_m)} \tag{29}$$

Where, E_u and E_m = Young's moduli; G_u and G_m = Shear moduli and t_m = thickness of the joint.

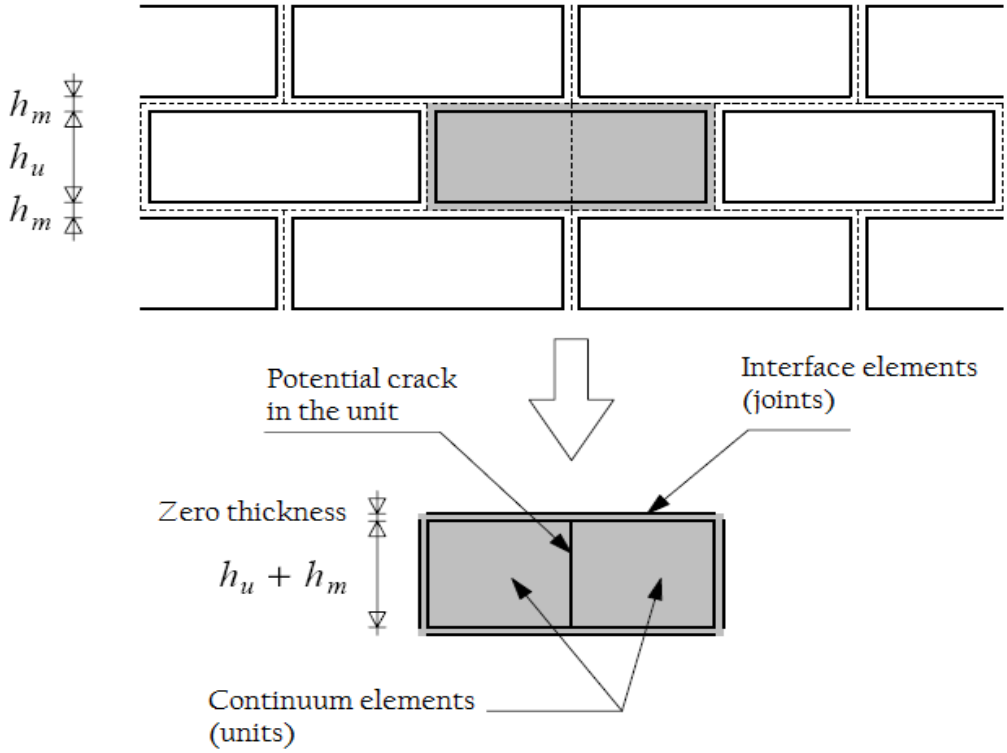

Figure 34: Proposed modeling strategy. Units (u), which are expanded in both directions by the mortar thickness, are modeled with continuum elements. Mortar joints (m) and potential cracks in the units are modeled with zero-thickness interface elements.

The interface model includes a compressive cap where the complete inelastic behavior of masonry in compression is lumped. This is a phenomenological representation of masonry crushing because the failure process in compression explained by the microstructure of units and mortar and the interaction between them. In the model the failure mechanism represented in such way that the global stress strain diagram is captured.

The model was justified by Lobato et al. and found that the model is efficiently able to reproduce the experimental results. For this reason, the proposed micro-model was selected by the author to simulate the wall for buckling failure.

3.5 Formulation of Multisurface Interface Model

The elastic domain is bounded by a composite yield surface that includes tension, shear and compression failure with softening shown in the Figure 35. Cap models originated in the field of soil mechanics. The introduction of a spherical cap for the Drucker-Prager model was firstly made by Drucker *et al.* (1957) for the purpose of describing plastic compaction and to enhance the behavior in hydrostatic compression. Since then, the name "cap model" has been adopted for a broad set of models which include a compressive cap, e.g the well-known Cam-clay model of Roscoe and Burland (1968) and the material model for granular soils proposed by DiMaggio and Sandler (1971). Recently the numerical algorithm has been revised by Simo *et al.* (1988a) with the use of unconditionally stable closest point projection return mappings, tangent operators consistent with the integration algorithm and proper handling of the corners. Cap models have been, in general, limited to associated plasticity and hardening of the cap while the other yield surfaces remained in ideal plasticity.

For the application envisaged here the behavior found experimentally leads to a more complex model. Masonry joints have extremely low dilatancy and the model must be formulated in the context of non-associated plasticity. Also softening behavior should be included for all modes of the composite yield surface. The model presented in this study is of general application but the formulation is shown in the characteristic interface (σ, τ)-space. The rate independent interface model is defined by a convex composite yield criterion which consists of a tension cut-off, the Coulomb friction model and an elliptical cap.

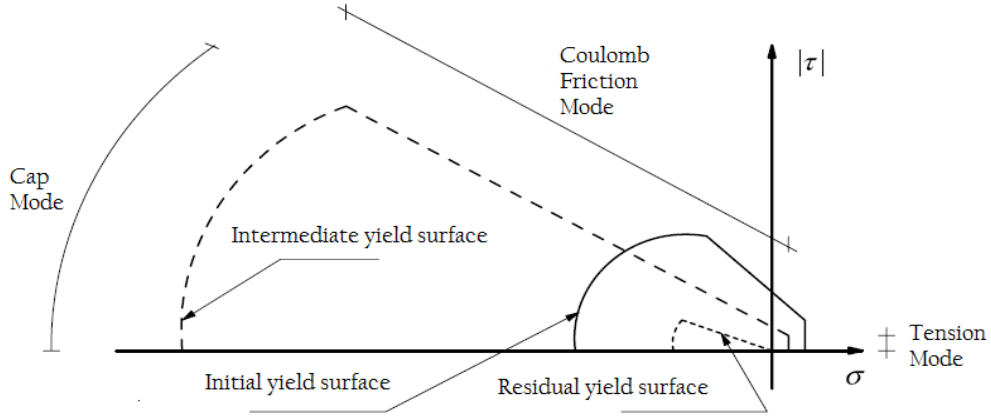

Figure 35: Proposed interfaces cap model.

4. EXPERIMENTAL STUDY

This chapter deals with the description of the testing program carried out in Structural Technology Laboratory of the Technical University of Catalonia (UPC) which was the basis of numerical simulation of this research. The following is the characterization of materials used for the manufacture of the walls and a description of the manufacturing process, with emphasis on those details because it is a 1:4 scale study. Finally, a description is given on the equipments used to perform the test and data acquisition in the Laboratory of Structural Technology (Valladares, 2010).

4.1 General

Thirty six walls were tested with slenderness ratio (calculated as h / t) 6, 12, 18 and 25 and values of eccentricity of load was e = 0, e =t/6 and e = t/3. A summary of the number and type of the test specimens and test program is shown in Table 6.

Table 6: Summary of number and type of test specimens.

Wall series	Slenderness ratio	Height (cm)	Eccentricity of load	Support condition	Observation
W-0-6	6	21	0	Hinge-hinge	Slenderness ratio calculated as H/t
W-0-12	12	42	0		
W-0-18	18	63	0		
W-0-25	25	87.5	0		
W-1/6-6	6	21	t/6	Hinge-hinge	Slenderness ratio calculated as H/t
W-1/6-12	12	42	t/6		
W-1/6-18	18	63	t/6		
W-1/6-25	25	87.5	t/6		
W-1/3-6	6	21	t/3	Hinge-hinge	Slenderness ratio calculated as H/t
W-1/3-12	12	42	t/3		
W-1/3-18	18	63	t/3		
W-1/3-25	25	87.5	t/3		

The walls were constructed as single leaf with scale of 1:4. The width was of 297 mm and thickness of 35 mm. In order to introduce different slenderness ratio, walls were built with heights of 210 mm, 420 mm, 630 mm and 875 mm. The thickness of the vertical and horizontal joints was approximately 2.5 mm. Figure 36 shows the layout of the tested wall.

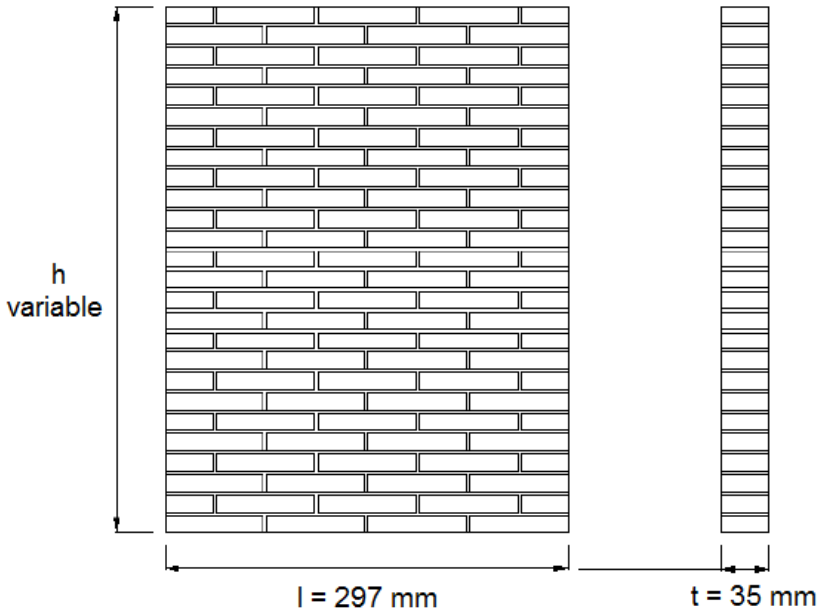

Figure 36: Layout of tested wall.

4.2 Materials

All the materials used in the construction of the test specimens were commercially available and were typical of those commonly used in building construction.

4.2.1 Brick Units

One fourth scale bricks were used for the construction of walls. The dimensions of the bricks (Length x width x thickness) are 72.5 x 35 x 12.5 mm. The manufacturing process can be found in Charry (2010).The following is a description of tests to characterize the pieces. The water absorption capacity was determined according to UNE-EN 772-11 (2001). This test was conducted on 13 pieces. The test pieces were dried in an oven at a temperature constant 105^0 C, until the loss in mass between two subsequent drying processes carried out in 24

hour's interval did not exceed 0.1% of the total mass, time is considered to be reached constant mass and obtained an average value of water absorption is 17.87%. In addition, the average density of the brick was found, 1717.17 kg/m^3, after the drying process. The compressive strength of the brick is f_b = 32.45 MPa.

4.2.2 Mortar

The mortar used for the construction of the masonry walls was an M-8 prepared mortar. In order to adjust the fineness of the mortar for 1:4 scale sieving is made of it, removing all the percentage of material retained by the sieve1 mm aperture, since the presence of larger sizes difficult to maintain size of the joint. Plasticizer is used to improve the workability of the mortar and thus ensure the proper penetration of the mortar in the joints of the walls. To characterize the mortar, flexural and compression strength test of the mortar specimens were carried out. The determination of the flexural strength of mortar specimens was performed according to test method described in the UNE-EN 1015-1011. This rule specifies that the test is performed on prismatic specimens 160 x 40 x 40 mm. The specimens were unmolding at the age of 2 days and air cured in the same conditions as the walls. The test consists of applying a load at three points of these specimens up to failure shows in the Figure 37. The two specimens resulting from this fracture halves were stored for determination of compressive strength. Compressive strength of mortar was determined according to test method in the UNE-EN 1015-1911 (2000). The test was conducted on the two halves found from the flexural strength test and consists of applying a uniaxial loading up to rupture. The test was conducted by IBERTEST press machine shows in the Figure 37.

Figure 37: Flexural strength test of mortar (left) compressive strength test of mortar (right).

The UNE-EN 1015-1911 (2000) proposed the following expression for the determination of bending strength of the mortar:

$$f_{xm} = \frac{Fl}{bd^2} \tag{30}$$

Where, f = flexural strength of the mortar, F = Maximum load applied to the specimen, l = distance between the axis of the support rollers, b = width of specimen and d = thickness of the specimen.

The results obtain from of the flexural and compression test of the mortar are given by the Table 4 and 5.

Table 4: Results of flexural strength test of mortar.

Cured	Specimen	Age (days)		Maximum load (KN)	f_{xm} (MPa)
		unmold	Test		
Air	1	2	28	1.15	2.70
	2	2	28	1.51	3.54
	3	2	28	1.24	2.91

Table 5: Results of compressive strength test of mortar.

Cured	Specimen	Half	Age (days)		Maximum load (KN)	f_m (MPa)	f_m (ave.) (MPa)
			unmold	Test			
Air	1	A	2	28	11.76	7.35	6.96
		B			10.52	6.58	
	2	A	2	28	12.49	7.81	7.95
		B			12.95	8.09	
	3	A	2	28	10.81	6.76	6.96
		B			11.47	7.17	

From the test result it is found that the average value of flexural strength is 3.05 MPa and the average compressive strength of the mortar is 7.29 MPa which was taken as the value for the further calculation.

4.3 Description and Fabrication of the Prism Specimens

Through tests on small uniaxial specimen of bricks and mortar as a particular configuration is possible to determine some parameters of interest in the study of behavior of the masonry. The behavior of the mortar joints is rarely studied in tests on small samples of two or three pieces. The state of stresses introduced into the mortar joints is highly heterogeneous, often difficult to interpret the results. By the test of masonry prisms it is possible to determine the compressive strength of the masonry. Due to its small size, these prisms cannot consider fully representative and therefore the results obtain from the test are usually considered as reference values.

The uniaxial compressive strength and Young's modulus test was performed according to the procedure specified by the UNE-EN 1052-1 (1999). To determine the uniaxial compression and Young's modulus of elasticity five specimens of 147.5 mm x 147.5 mm (height of 10 rows and width of 2 pieces) considered as Figure 38.

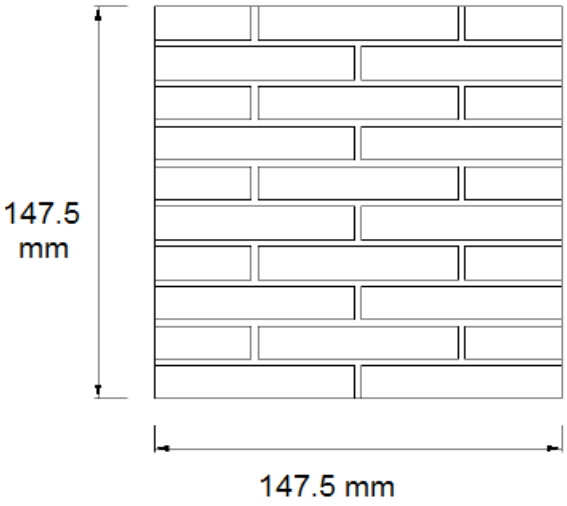

Figure 38: Layout of the prism specimen used for compressive strength and Young's modulus test.

The specimens were subjected to uniaxial compression in the direction perpendicular to the bed joints up to the rupture. In addition, during determination of compressive stress, the specimens were instrumented to measure the deformation experienced by two vertical extensometers in order to obtain Young's modulus of the masonry. The trial was conducted in INSTRON press machine shown in the Figure 39.

Figure 39: Prism specimen under test.

According to the norm mentioned above, the Young's modulus of elasticity is calculated by using following expression:

$$E_i = \frac{F_{i,max}}{3e_i A_i} \tag{31}$$

Where, E = Young's modulus of the specimen, $F_{i,max}$ = maximum load applied, A_i = cross section of the specimen, and e_i = deformation of the specimen.

The results obtained from the compressive strength and Young's modulus test of prism specimens are shown in the Table 6.

Table 6: Results of compressive strength and Young's modulus test of prism.

Specimen	$F_{max}\ (KN)$	Compressive stress (MPa)	Young's modulus (MPa)
1	77.42	14.7	3378
2	68.88	13.1	3445
3	68.26	13.0	4615
4	78.89	15.0	3038
5	79.65	15.2	2816

The average value of the compressive strength and Young's modulus obtained from the test are 14.2 MPa and 3458 MPa respectively.

4.4 Construction of the Wall Specimens

First, it was considered that the building of walls similar to that done scale, i.e. placing the pieces one by one, was not feasible in this case. The main difficulty of this process was to control the width of the joint and slow process of implementation. The methods proposed to overcome these difficulties by using horizontal sheets of wood for construction process, which was considered more simple, fast and effective. The following is a brief description of this process. Figure 40 (left) shows the construction process of the wall specimens for the test. In a first step, the wood was covered as a basis with laminated paper. This material consists of a thin plastic adhesive sheet pasted on paper is so that the paper to be placed on

the timber, but that was fixed by adhesive tape, leaving paper face outwards. Then the pieces were fixed by gluing them to wood by Loctite 454. The paper covered the wooden base ensured a perfect fit of parts, since the cyanoacrylate does not work effectively on other surfaces such as plastic which ensure to maintain the joint thickness of the wall. When it was obtained the number of course needed to reach the height of the walls that defined as a wall template consisting of units without mortar joints. Once generated the various configurations, stored until of grouting by mortar. Figure 40 (right) shows two of those templates.

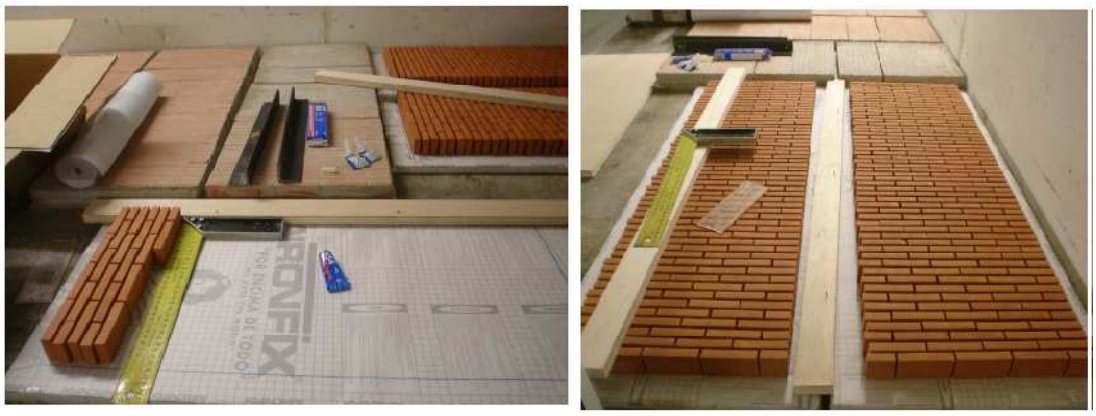

Figure 40: Fixing process of units (left) and stored the walls after fixing units (right).

To avoid the shrinkage cracking, all units and base wood remained submerged in water for 2 hours prior to the discharge of mortar after this left to air for 30 minutes for drain properly. The next step was to place a perimeter molding that used to pour the mortar into the joints. The mortar is subjected to confinement-induced weight of the wall.

Once molding, it proceeded to pour the mortar previously made in a mixer of 50 liters. As specified in other sections, in the manufacture of mortar was used plasticizer to ensure consistency of the mortar joints fully penetrated. The template was then placed on a table shaker for dumping of mortar that performed as layers. Each layer was vibrated in order to ensure the penetration of mortar into the entire joints and to eliminate air bubbles. After the casting process, the walls were covered with plastic and stored. Figure 41(left) is shows the wall after being filled.

Figure 41: Wall after pouring of mortar (left) and wall after cleaning its surface (right).

Approximately 24 hours after discharge of mortar, proceeded to clean the surface by removing the excess mortar as well as the introduction of the above compression cited by threaded rods, shows Figure 41(right). The walls were left standing for trial at minimum age of 28 days, performing curing and covered with burlap and polyethylene.

4.5 Instrumentation for Walls Test

This section lists the various equipment and materials used for test in the Structural Technology Laboratory of UPC. The press INSTRON machine shows in the Figure 42 (left), used to apply vertical load on the wall and the prism for determining compressive strength and Young's modulus. The maximum load capacity of this machine is 1000 KN.

IBERTEST loading equipment used for flexural tests and uniaxial compression in the mortar specimens. It has load capacity of 10 KN to 200 KN. Extensometer (LVDT's) was used to measure the vertical and horizontal displacements of the wall under vertical load. Also during the compression test a laser scanner used for determining the horizontal displacement at the midpoint of the wall shown in the Figure 42 (right).

Figure 42: Press INSTRON machine for compression and Young's modulus test (left) and Laser scanner for measurement of displacement (right).

4.6 Compression Test on Walls

To study the effect of slenderness and eccentricity on the compressive strength of the walls thirty six specimens were tested for slenderness ratio 6, 12, 18 and 25 with different load eccentricity such as 0, t/6 and t/3. All the specimens are tested in the 1000 KN compression machine by incrementally applying the load. The procedure was first apply an axial preload, record the deformations then re-zeros all gauge reading. From this point, the load is increased and deformation readings are recorded for each increment. For the application of load correctly to the location of eccentricity, a small support neoprene provided on the ends of the wall so that the distance of neoprene from the axis of the wall equal to the value of eccentricity studied. This support neoprene was coincided with the axis of load application, ensuring the proper realization of the eccentricity (Figure 43). The end conditions at the top and bottom of the wall was hinge supported. Two horizontal strain gauges with a laser scanner used to measure horizontal deformation and vertical deformations.

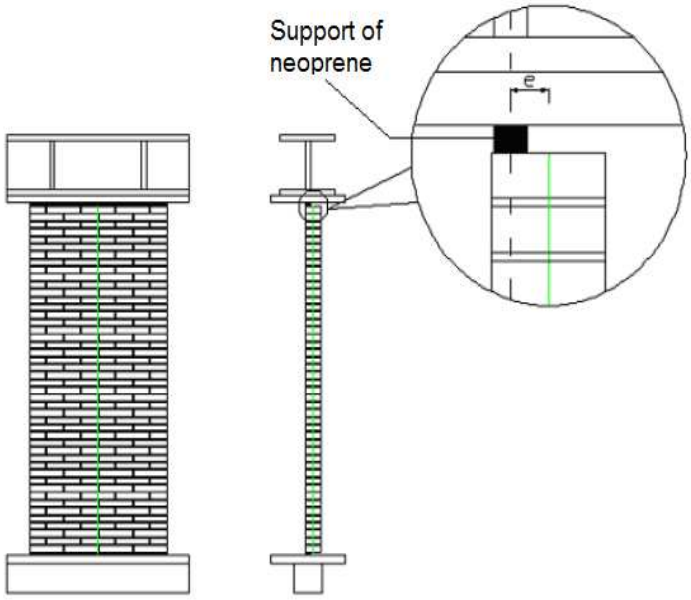

Figure 43: Details of application of load at correct eccentricity.

The machine performed in control movement so that the method allows better control of post-peak behavior. To study in detail the process of loading and modes of failure of the walls tested were recorded by using a high speed camera. Figure 44 shows an image from an ongoing test.

Figure 44: Final configuration of wall test.

4.7 Test Results

The results obtained in tests carried out on the walls for different configurations are summarized in Table 7 and Figure 45.

Table 7: Test results for different configurations of wall.

Wall	Slenderness ratio	Compressive stress (MPa)		
		e = 0	e = t/6	e = t/3
W6-1	6	14.09	8.74	3.77
W6-2	6	11.70	10.54	4.51
W6-3	6	11.74	8.85	6.26
W12-1	12	12.21	7.49	2.46
W12-2	12	11.50	9.41	2.25
W12-3	12	10.51	7.43	2.12
W18-1	18	10.21	4.41	1.52
W18-2	18	9.38	4.60	0.84
W18-2	18	9.77	4.53	1.24
W25-1	25	9.38	3.89	1.35
W25-2	25	7.24	3.01	1.49
W25-3	25	6.67	2.64	0.96

As expected, the result clearly shows that the compressive strength of the wall decreases with the increase of slenderness ratio and eccentricity of load application, obtaining lower resistance the higher are these. The experimental result shows a significant dispersion. However, such dispersion is to be common in experimental work and of similar magnitude to those obtained by other authors in their studies.

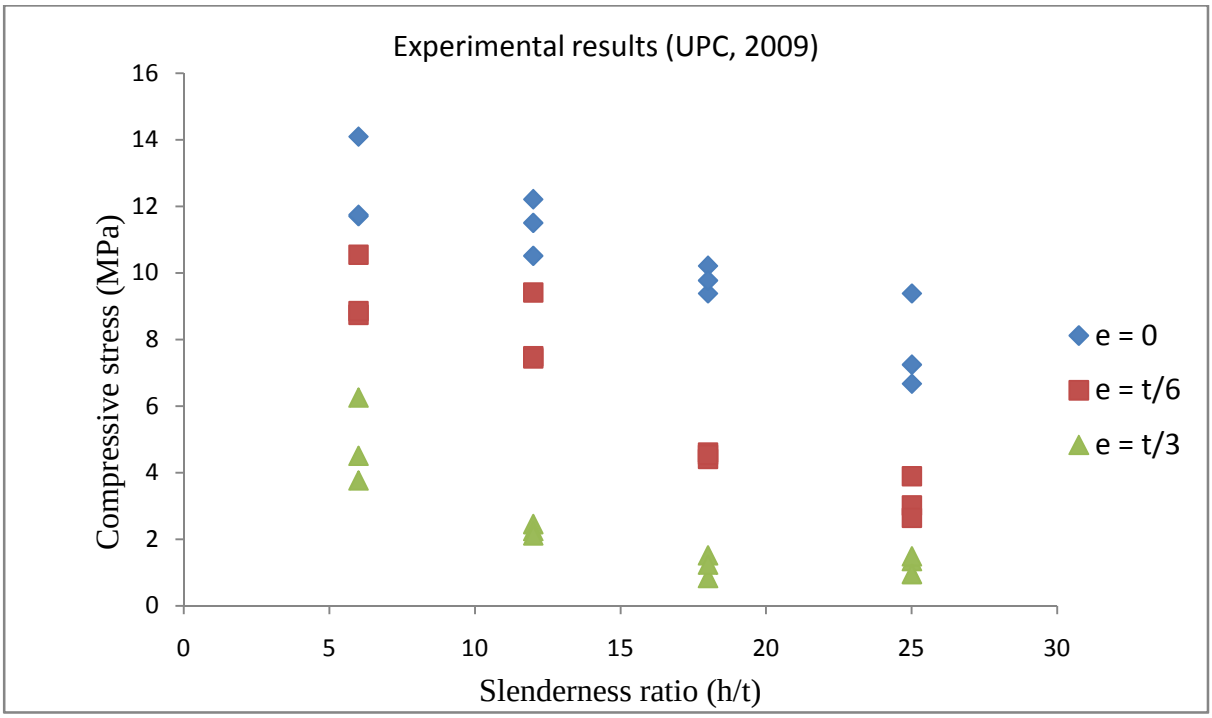

Figure 45: Relation between compressive strength and slenderness ratio with different eccentricity obtained from the test.

4.7.1 Mode of Failure

In the case of slenderness ratio 6, formation of vertical cracks is observed initially and then splitting up to the failure by crushing of the material. This occurred for all eccentricities and wall failed without experience any buckling. For the slenderness ratio 12, the influence of buckling is observed from the beginning. The wall shows significant chipping at the centre before failure by buckling. However, for loads applied eccentrically, failure was observed clearly due to buckling without presence of splitting. The following figures show the failure mode of some cases.

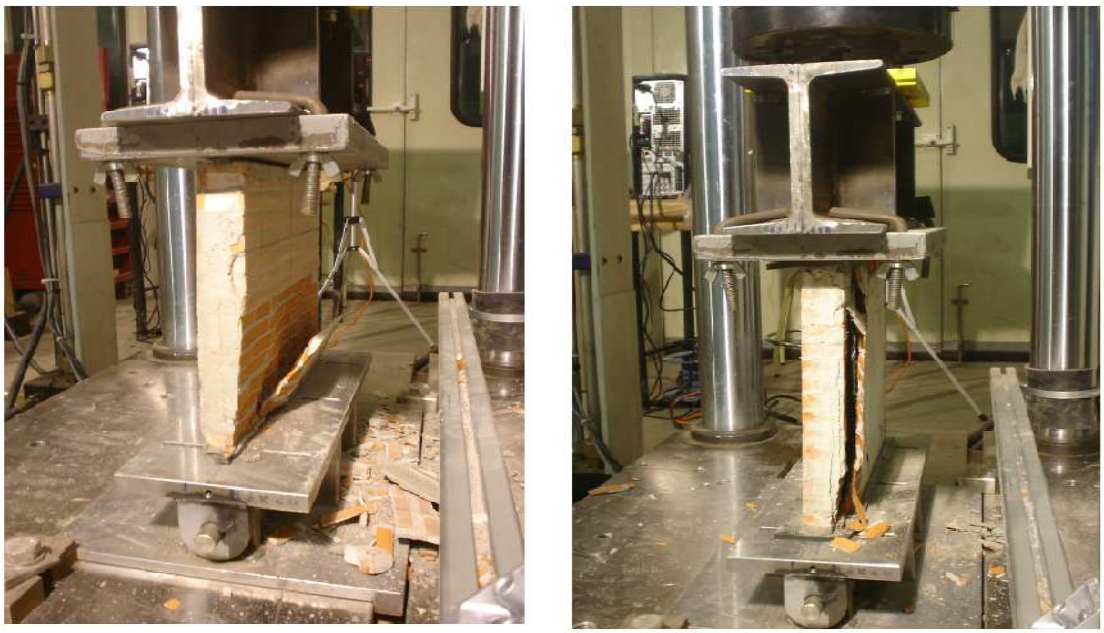

Figure 46: Failure of wall by splitting and crushing of material (Slenderness 6, eccentricity e=t/6).

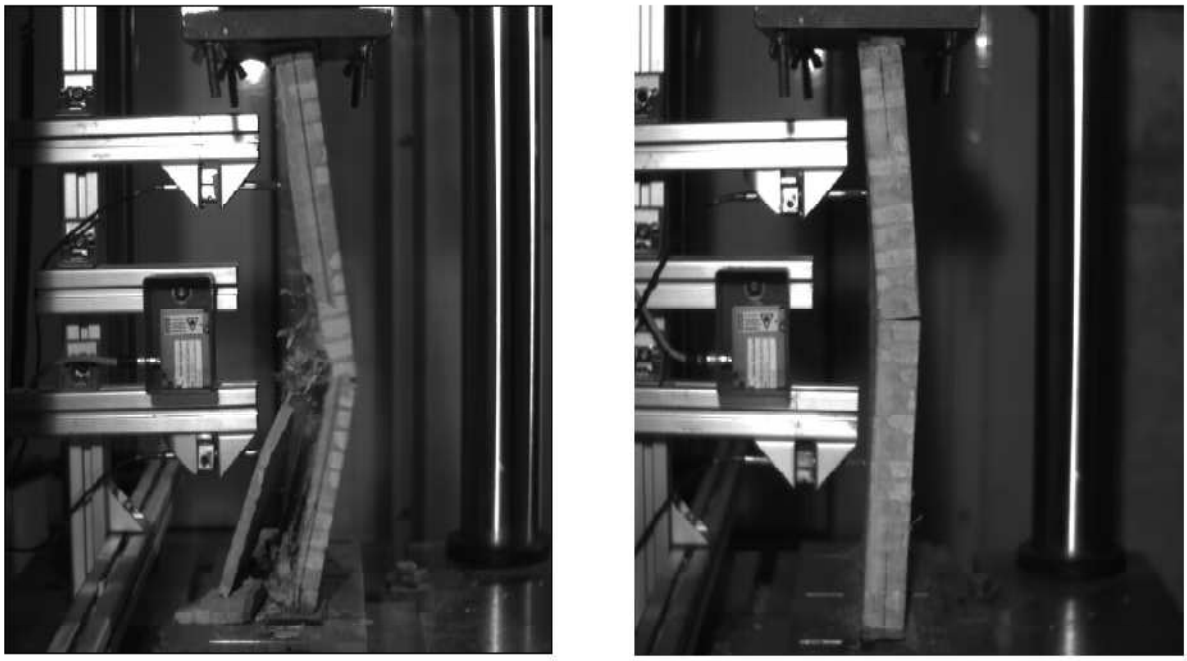

Figure 47: Failure of wall by combination of splitting and buckling for slenderness ratio 12, eccentricity e = 0 (left) only buckling for eccentricity e = t/3 (right).

In general, for all the walls of slenderness ratio 18 and 25, failure occurred due to the buckling. The sudden and explosive break of adhesion between the units and mortar occurred at the point of maximum deflection. The followings figures show the failure mode of some cases.

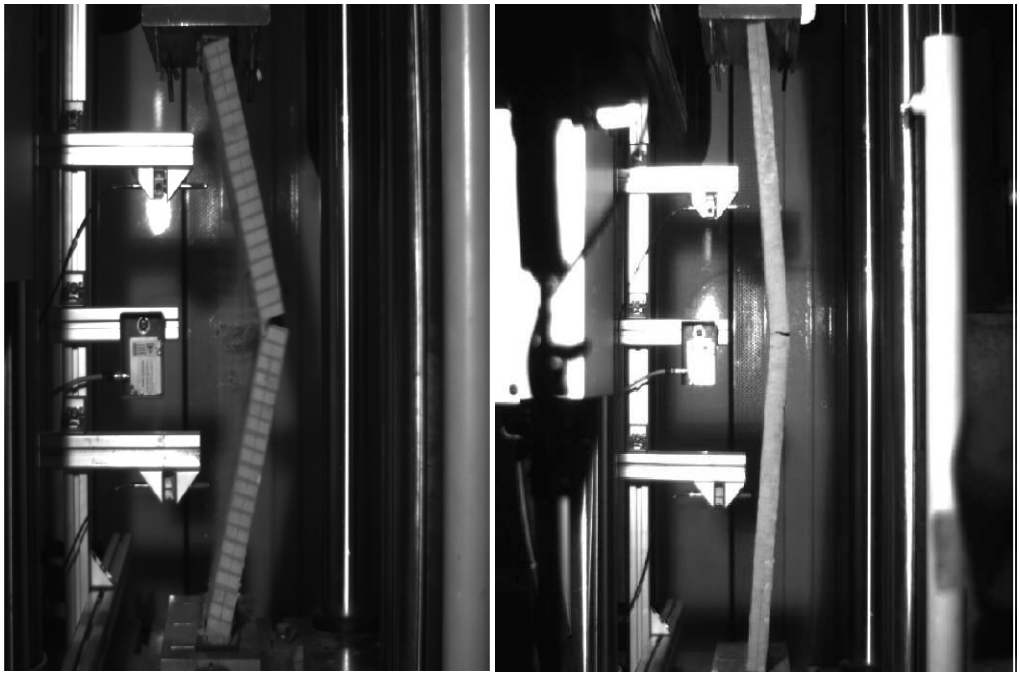

Figure 48: Typical mode of failure of walls of slenderness ratio 18 eccentricity e = 0 (left) and slenderness ratio 25 eccentricity e = 0 (right).

4.8 Conclusions

The effect of slenderness ratio and load eccentricity on the ultimate compressive strength of the wall is shown in the Figure 45. From this plot the allowable working stress in compression can be calculated for walls of various slenderness ratio and eccentricity by means of a suitable column formula. During the experimental works, one of the main concerns was, to application of vertical load at proper eccentric location because it was very difficult to maintain lower value of eccentricity practically. The reduction in capacity attributable to slenderness ratio and load eccentricity effects was also evident in the results of

tests on scale size brick wall specimens. From the above study it is also clear that with the increases of the slenderness ratio and application of load eccentricity the ultimate load capacity of the wall decreased and failure occurred due to buckling.

5. NUMERICAL SIMULATION

5.1 Introduction

The micro-modeling strategy, is considered at present as one of the most accurate tools available to model the behavior of masonry structures, and has been adopted in the present research in order to carry out the needed numerical simulations. Micro-modeling allows, in particular, an appropriate simulation of the buckling response taking into account joint tensile cracking in combination with masonry crushing in compression. In this study, the predictions on the ultimate capacity of walls obtained by means of micro-modeling approach and compared with experimental results obtained from the experimental study in UPC. Moreover, results obtained from current masonry standards are also considered and compared with the experimental and numerical results. Conclusions are drawn on the ability of both the numerical models and standards' formulations to accurately predict the experimental result.

5.2 Adopted Modeling Strategy

The numerical simulation presented is performed with the well-known micro-model proposed by Lourenco & Rots (1997) requires more specific software oriented to masonry analysis. For all cases, micro-models assume 2D plain-stress and a hinged-hinged configuration. The hinges are modeled by means of stiff triangular objects placed at the bottom and at top of the wall, whose end vertex is allowed to freely rotate. In addition, a minimum eccentricity of 1mm is always applied in order to account for possible irregularities of the wall geometry of the load positioning. Basically, the model assigns an elastic behavior to the units whereas masonry inelastic behavior is transferred to the joints. This analysis was performed with DIANA software. The integration schemes used are 2x2 points Gauss integration for the continuum elements and 3 points Lobato integration for the interface elements.

5.3 Model Description

5.3.1 Geometry and Meshing

In the numerical simulation, the units were modelled by using plain-stress continuum 8-node elements and for the mortar joints adopted 6-node zero-thickness line interface elements. In addition, hinges are modeled by means of stiff triangular objects. Each unit was modelled with 12 x 3 elements. The geometry and meshing of the wall for slenderness ratio 6 and eccentricity 0, t/6 and t/3 are shown in the Figure 49 and 50 respectively.

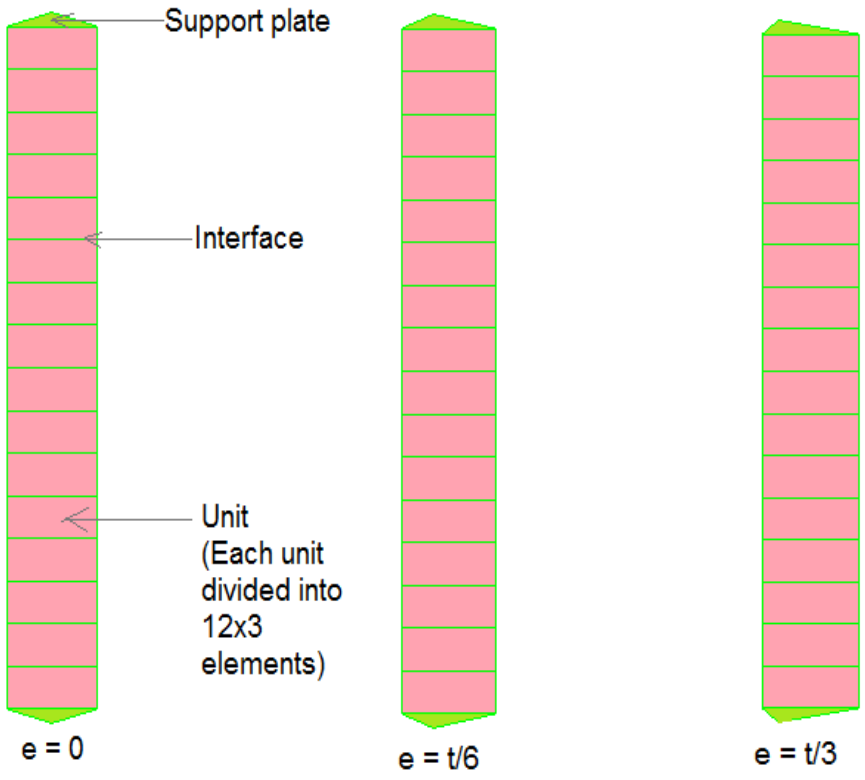

Figure 49: Geometry of walls for slenderness ratio 6 with different load eccentricity.

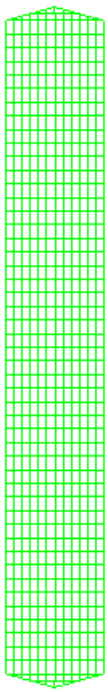

Figure 50: Meshing of the wall of slenderness 6 and eccentricity e = 0.

5.3.2 Material Properties

The material parameters used for the numerical simulation are shown in the Table 8. Some parameters such as $G^I{}_f$ and C_s have been taken directly from the previous research The fracture energy for mode I, $G^I{}_f$ have been taken from the test carried out by Van der Pluijm (1992) and for the parameter of shape of elliptical cap C_s a value of 9 has been adopted from Lourenco (1996). The interface elastic stiffness values were calculated from thickness of the joint h_j, the Young's moduli of unit and joint E_u and E_j, respectively, and the shear moduli of unit and joint G_u and G_j, respectively as CUR (1994):

$$k_n = \frac{E_u E_j}{h_j(E_u - E_j)} \; ; \; k_t = \frac{G_u G_j}{h_j(G_u - G_j)} \tag{32}$$

The different strength values f_t, c and f_m have been obtained from the experimental study carried out in UPC (2009). The compressive fracture energy G_{fc} and equivalent relative displacement k_p calculated according to Model Code 90 and Eurocode 6, respectively by using followings formula (Lourenco, 1996):

$$G_{fc} = 15 + 0.43f_m - 0.0036{f_m}^2;\ \ k_p = \left\{0.002 - f_m\left(\frac{1}{E_u} + \frac{1}{k_n(h_u + h_j)}\right)\right\} f_m \qquad (33)$$

Table 8: Material parameters adopted for numerical analysis.

Components	Parameter	Symbol	Units	Values
Brick	Elastic modulus	E_b	N/mm^2	4800
	Poison ratio	ν	-	0.15
	Tensile strength	f_{tb}	N/mm^2	3.95
Joint	Normal stiffness	k_n	N/mm^2	2800
	Shear stiffness	k_t	N/mm^2	1900
	Bond tensile strength	f_t	N/mm^2	0.554
	Mode – I fracture energy	${G^I}_f$	Nmm/mm^2	0.02
	Cohesion	c	-	0.45
	Mode – II fracture energy	${G^{II}}_f$	Nmm/mm^2	0.175
	Angle of internal friction	$tan\varphi$	-	0.812
	Angle of dilatancy	$tan\Psi$	-	0.009
	Compressive strength of masonry	f_m	N/mm^2	14.20
	Compressive fracture energy	G_{fc}	Nmm/mm^2	20.38

5.3.3 Boundary Condition and Loading

For all cases, micro-models of wall considered hinged-hinged configuration. The hinges are modeled by means of stiff triangular objects placed at the bottom and at top of the wall, whose end vertex is allowed to freely rotate. The vertical load was applied concentrically and eccentrically as unit deformation. The boundary condition and loading configuration is shown in the Figure 51.

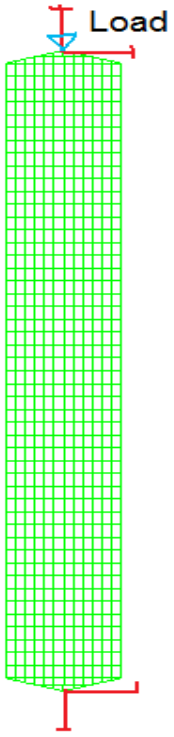

Figure 51: Boundary and loading configuration of wall.

5.4 Validation of Model

The micro-models were validated next by a comparison with experimental results obtained from UPC (2009). Usually, experiments on load bearing walls have been adopted by the masonry community as the most common axial load test and the tensile capacity of masonry has been neglected. As a result, the clear understanding of the buckling characteristics of masonry load bearing walls under concentric and eccentric vertical load was absent. In this study, special attention is given to the load bearing wall tests carried out in the UPC (2009), because most of the parameters necessary to characterize the material model are available from micro-experiments. The main concern of this work was, to demonstrate the ability of the model to capture the behavior observed in the experiments and close quantitative reproduction of the experimental results. The large number and variability of the material parameters necessary to characterize the developed model permits to adopt a set of parameters suitable to closely fit the experimental capacity slenderness ratio diagrams. For the numerical analyses, units are represented by plane stress continuum elements (8-noded)

while line interface elements (6-noded) are adopted for the joints. Each unit is modeled with 12 × 3 elements. For the joints, the composite interface model described in this study is adopted.

5.5 Results of Numerical Simulation

The comparison between the experimental collapse load and collapse load obtained from the micro- model is presented in the Figure 52, 53 and 54.

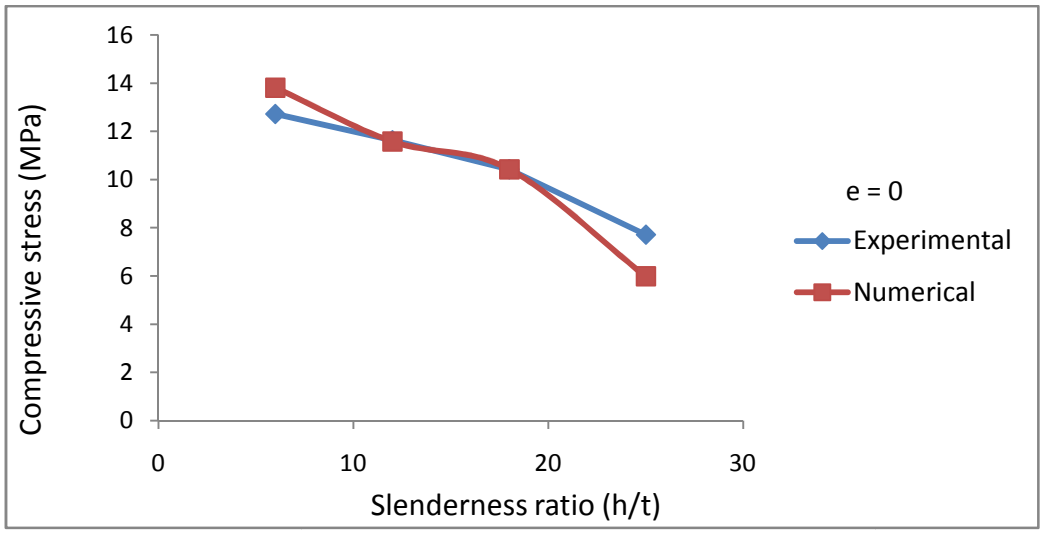

Figure 52: Ultimate compressive strength vs. slenderness ratio for e = 0.

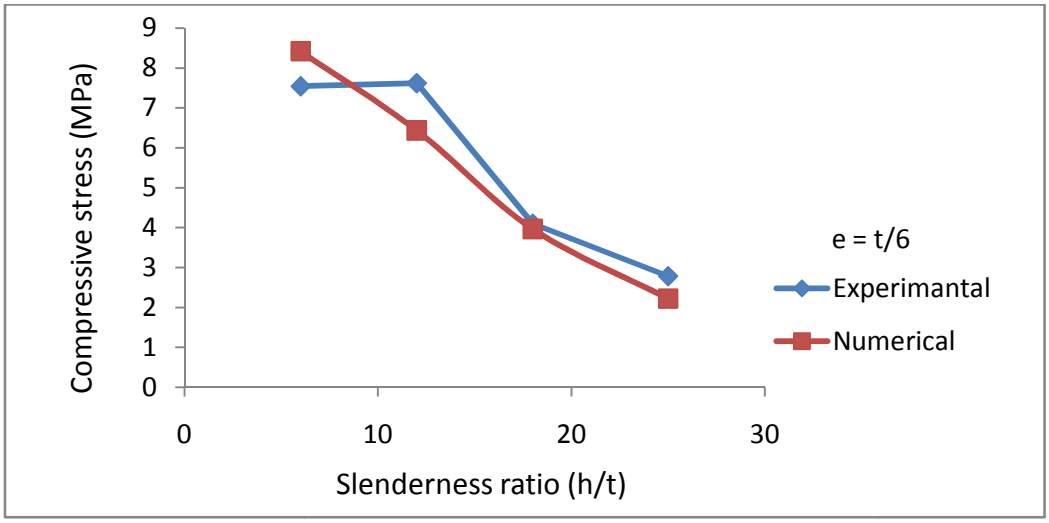

Figure 53: Ultimate compressive strength vs. slenderness ratio for e = t/6.

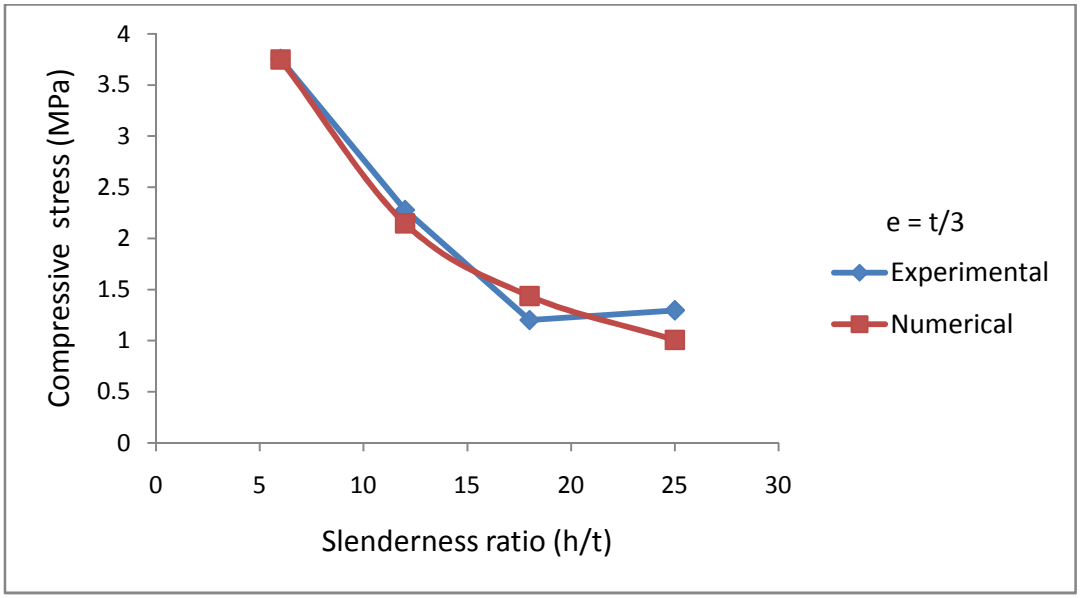

Figure 54: Ultimate compressive strength vs. slenderness ratio for e = t/3.

The above figure shows that the experimental behavior is satisfactorily reproduced and the collapse load estimated within a 15 % range of the experimental values. The micro-modeling approach is being able to provide a very satisfactory estimation of the experimental capacity of the walls particularly, for the case with e = 0. The average errors are 7.85%, 12.6% and 11.93% for the eccentricity of 0, t/6 and t/3 respectively. For all cases, one tendency is clear that with the increasing of slenderness ratio and application of load eccentricity the capacity of the wall decreased.

The distribution of vertical stresses in the wall and their deformed shape is shown in the Figure below 55, 56, 57 and 58. Most of the cases, the failure occurs due to the crushing of the compressed zone and tensile cracking of the joints for the higher slenderness ratio and eccentricity due to the buckling effect. The mentioned figure shows contour of compressive stress distribution along the height of the wall. For all the cases, the intensity of red color indicates the intensity of increasing compressive stress and for all cases unit of stress is (MPa).

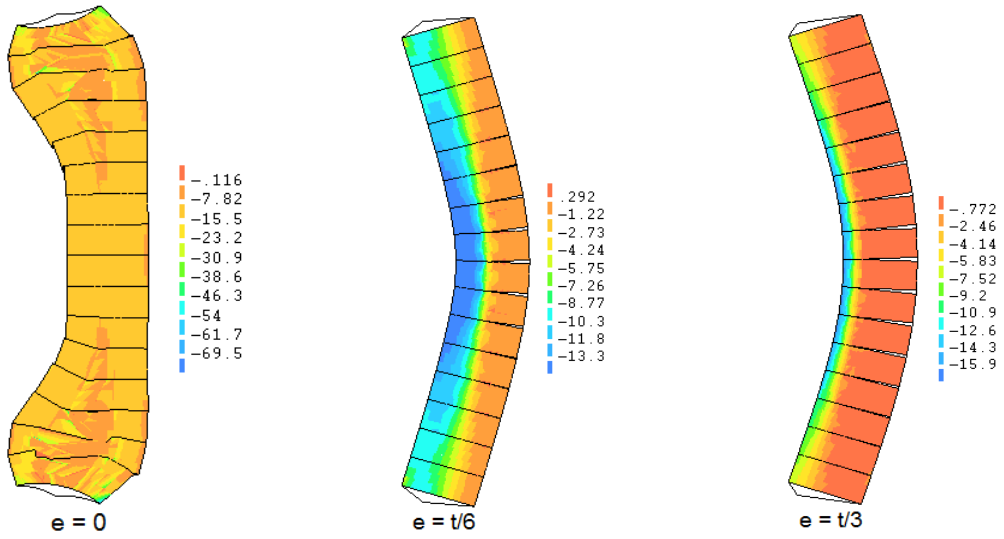

Figure 55: Stress distribution and deformed shape of wall for slenderness ratio 6.

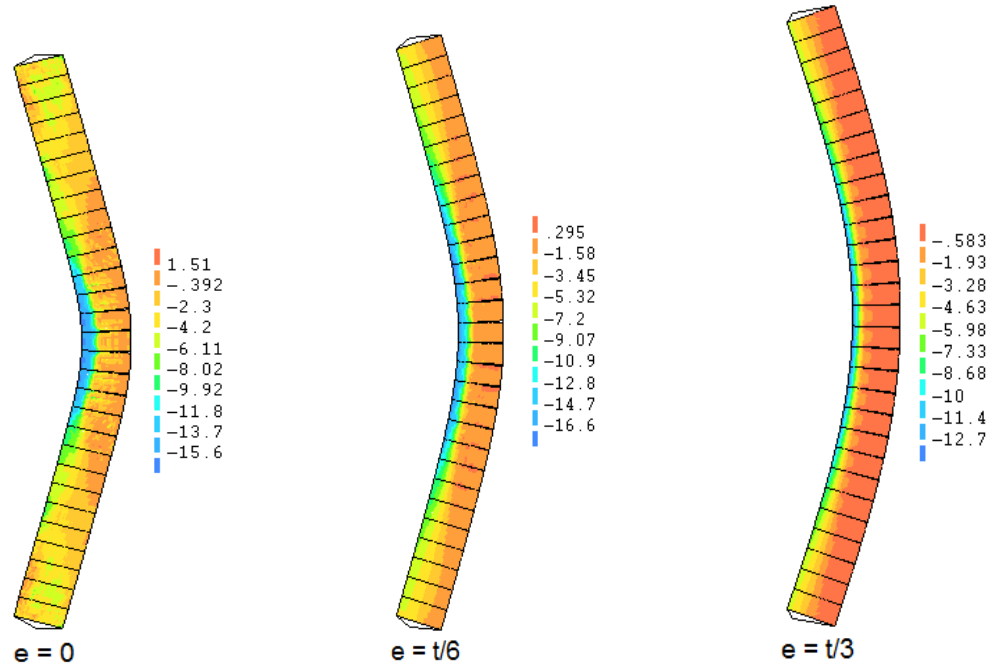

Figure 56: Stress distribution and deformed shape of wall for slenderness ratio 12.

In the case of slenderness ratio 6 and eccentricity 0 (Figure 55), the intensity of compressive stress concentrated near the end and the wall failed due to crushing of material while for other cases of same slenderness ratio with the increasing of load eccentricity, compressive stresses are concentrated near the middle, cracking occurs and walls were failed due to combined crushing and buckling.

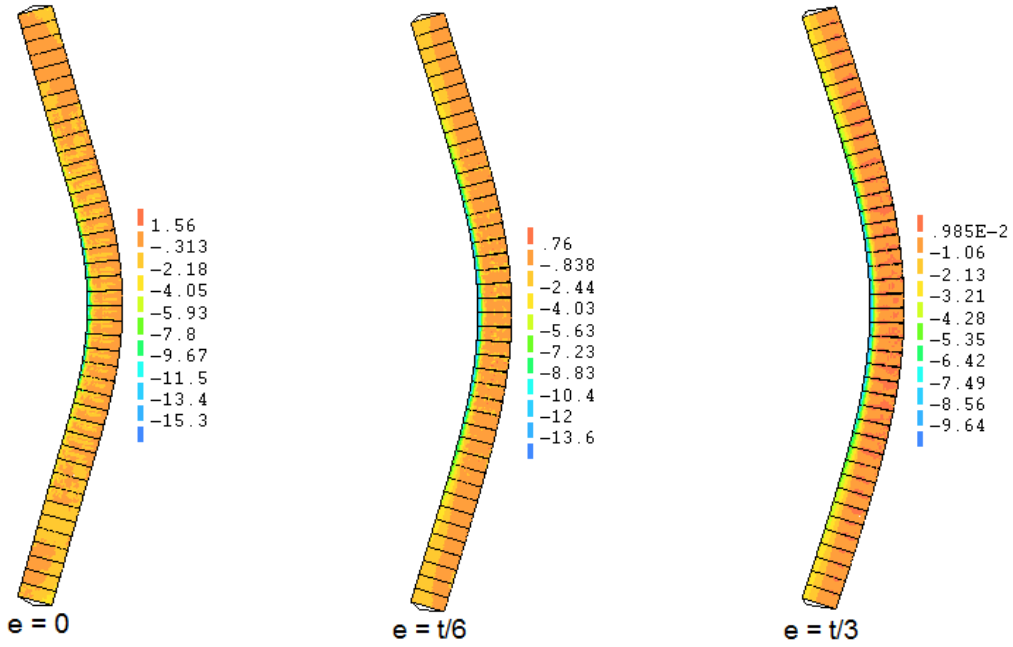

Figure 57: Stress distribution and deformed shape of wall for slenderness ratio 18.

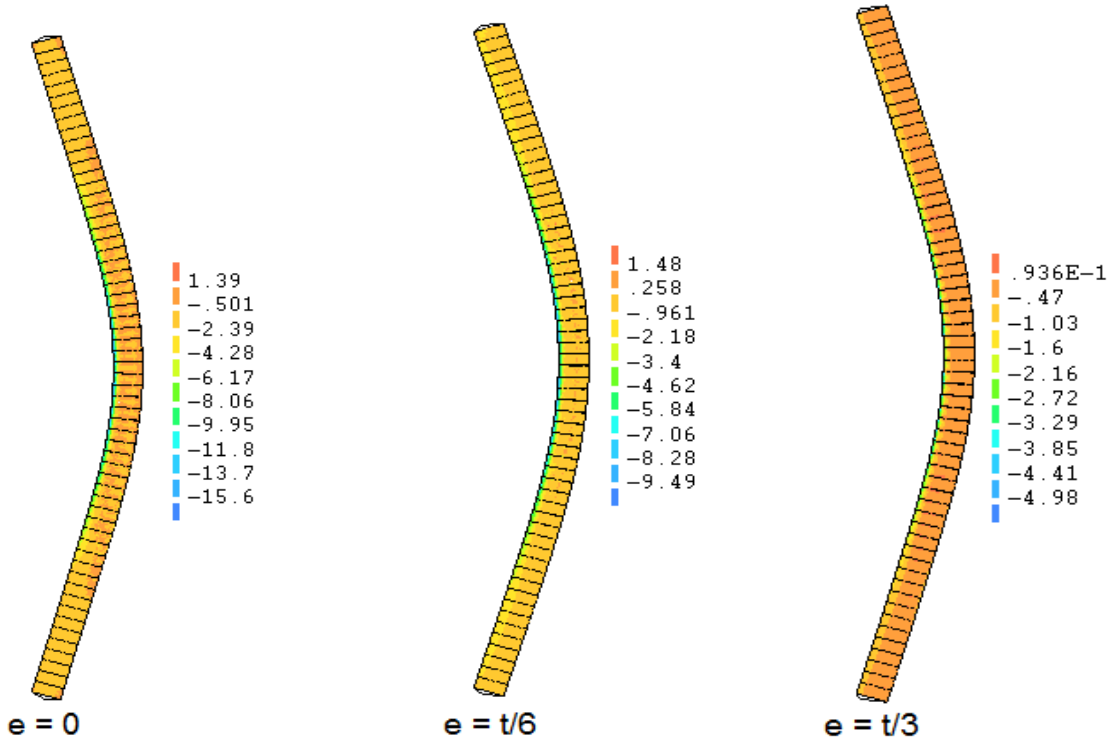

Figure 58: Stress distribution and deformed shape of wall for slenderness ratio 25.

In the Figure 57 and 58, similarly, shows the compressive stress distribution for slenderness ratio 18 and 25. For all cases, a common tendency observed that with the increasing load eccentricity the intensity of compressive stress at the middle increase and failure of walls dominated by buckling.

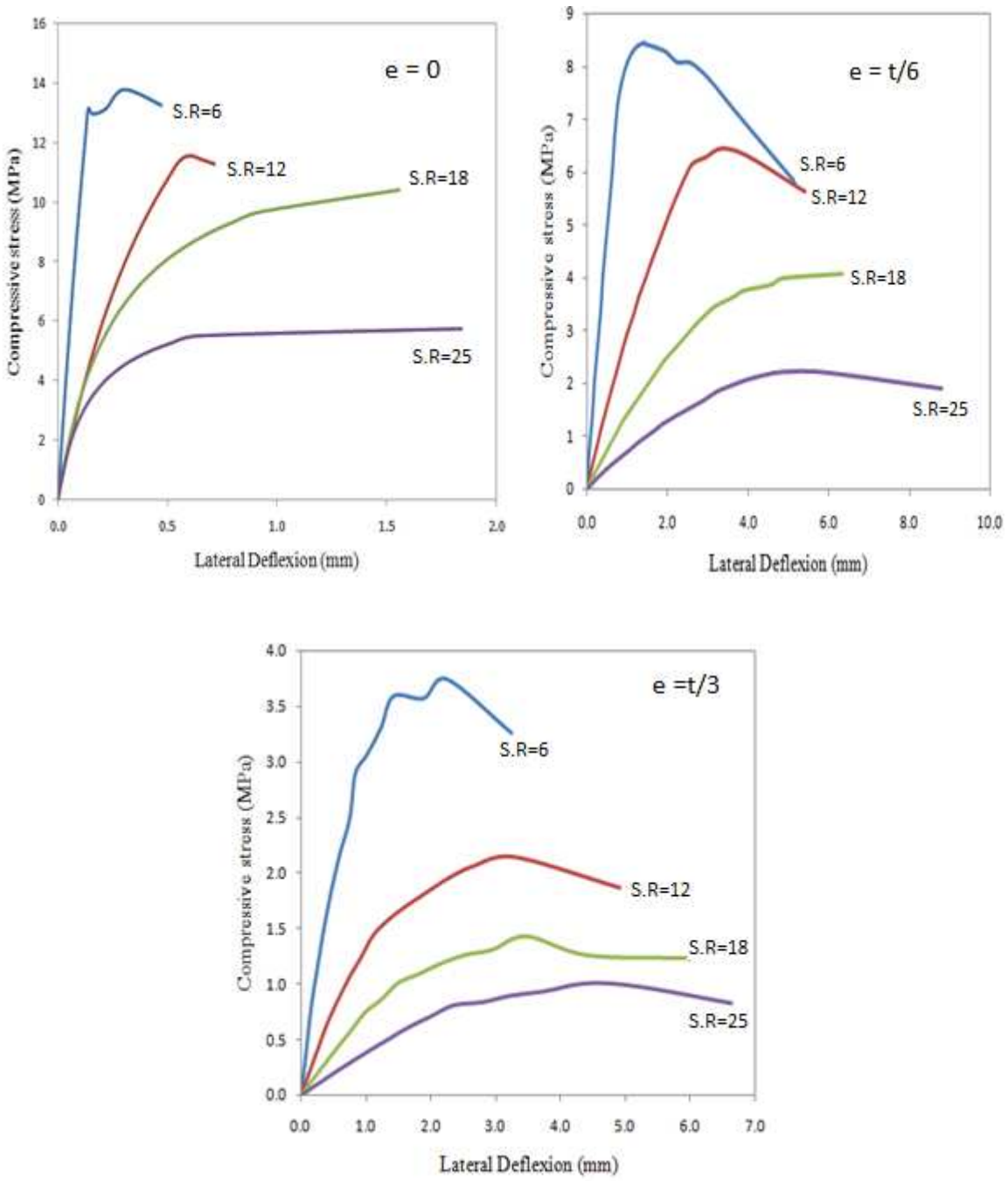

Figure 59: Load-deflection diagram for different slenderness ratio and eccentricity.

Figure 59 shows load-deflection curve for different slenderness ratio and load eccentricity. It is clear from the above figures that with the increasing of slenderness ratio ultimate capacity of wall decreasing and lateral deflection increasing. In the case of eccentricity 0, the maximum deflection obtained 1.84 mm for slenderness ratio 25 while the wall of slenderness ratio 6 produced minimum (0.47 mm) of lateral deflection.

The maximum deflection 8.79 mm and 6.63 mm found from slenderness ratio 25 for eccentricity t/6 and t/3 respectively, however, minimum deflection for both cases occurs for slenderness ratio 6.

5.6 Discussion

A set of experimental tests on the buckling failure of masonry walls has been numerically simulated by means of simplified micro-modeling approach. The micro-model described the nonlinear response of masonry in compression in an indirect way by localizing it to the units. In all cases, the non-linear response in tension is localized to the joints. The simplified micro-models afford a satisfactory prediction of the ultimate load of walls taking into account the buckling behavior. Simulations carried out by the micro-model provide the best fits for the test results with an acceptable error. It must be noted that some difference with respect to the experimental results is unavoidable because of the influence of possible non-reported accidental eccentricities.

6. PARAMETRIC ANALYSIS

6.1 Parameter Lists and Parameter Investigation

This section describes a list of parameters important to characterize the buckling behavior of masonry load bearing wall under concentric and eccentric vertical loading. The list below includes these factors and other factors that influence the buckling behavior and ultimate capacity of wall:

- Wall length;
- Material property (compressive stress of units and masonry, modulus of elasticity of unit, tensile strength of mortar, fracture energy, etc.);
- Wall continuity;
- Loading conditions (location of load application, point load, uniformly distributed load, etc.);
- Boundary conditions;
- Cross-sectional dimensions of wall;
- Type of bonding;
- Wall slenderness ratio;
- Residual stress pattern and magnitude;
- Magnitude and shape of the initial imperfections.

Some of factors presented here are outside of the scope of this study. Parameter outside the scope of this investigation includes residual stress and magnitude, magnitude and shape of the initial imperfection. Continuity of wall is partially considered through boundary condition and length of the wall. The point of application of vertical load and slenderness ratio of wall has a significant effect on the capacity and buckling behavior of the wall. For this parametric study vertical load is applied with different eccentricity and different boundary conditions such as hinge-hinge, hinge-fixed and fixed-fixed configurations. Four variables are investigated in the parametric study, namely, wall slenderness, loading conditions, boundary conditions and effect of tensile strength.

6.2 Methodology

6.2.1 Walls Slenderness Ratio

The slenderness ratio affects its susceptibility to buckling behavior of masonry load bearing walls under vertical loading. According to HASAN and HENDRY (1976), test walls with slenderness greater than 30 are more a matter of academic rather than practical interest. To investigate ultimate bearing capacity and buckling behavior of masonry wall under vertical load, walls of slenderness ratio 6, 12, 18 and 25 selected. The slenderness ratio was calculated as the ratio of height to thickness (h/t) of the wall.

6.2.2 Load Type and Eccentricity

Different loading conditions provide different combination of vertical capacity and distribution of vertical stress at various sections of the wall. This influences the buckling behavior as well as failure mechanism. Two loading conditions are considered in this study, namely, concentric and eccentric uniformly distributed loading. The goal of investigating different loading scenarios is to determine how these load cases influence the behavior of masonry load bearing wall.

6.2.3 Boundary Conditions

Considering a wall, there are many possible combinations of boundary conditions are hinge-hinge; hinge-fixed, fixed-fixed, free fixed, free-hinge, etc. A simple hinge boundary condition prevents the wall from translating in all directions, but allows rotation about weak and strong axis. For lateral buckling, it is assumed that rotation about the longitudinal axis restrained but warping is free at both ends. This model was used in this study. Fixed boundary conditions that prevents the end of the wall from rotating about its longitudinal axis and prevents warping. Different boundary conditions results in different collapse load and buckling behavior. It is important that the design methods applicability to variety boundary conditions can be verified.

6.3 Parametric Study Results

6.3.1 Change in Boundary Conditions

In this study an investigation was carried out to better understanding the effect of boundary conditions on the strength and buckling behavior of masonry load bearing walls by using hinge-hinge, hinge-fixed and fixed-fixed configurations. The results of collapse load for different end conditions are shown in the Figure 60, 61 and 62.

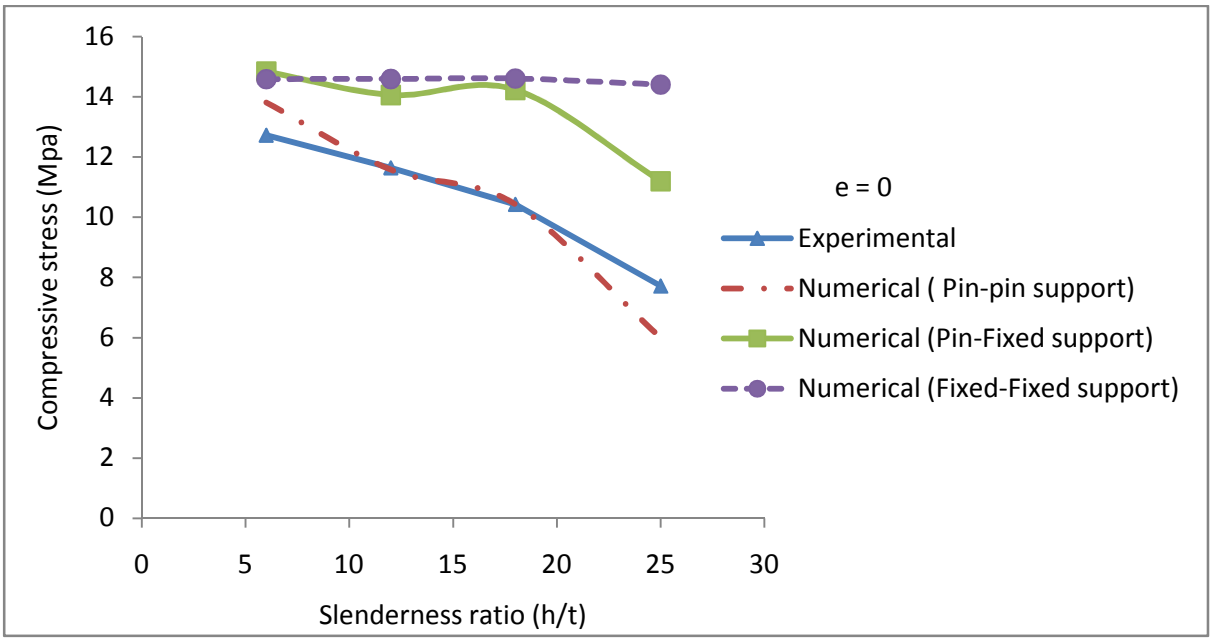

Figure 60: Capacity of wall for different boundary conditions at load eccentricity = 0.

The above figure shows that due to the change of end condition from hinge-hinge to fixed-fixed, the ultimate capacity of wall increases significantly. This increment has small value for lower slenderness ratio and rate of increment increased with the increasing of slenderness ratio. In the case of slenderness ratio 25, when the support changes from hinge-hinge to hinge-fixed and fixed-fixed, the ultimate load capacity of wall increase more than two times and very close to three times respectively and for slenderness ratio 18 capacity increase around 1.5 times of hinge-hinge support.

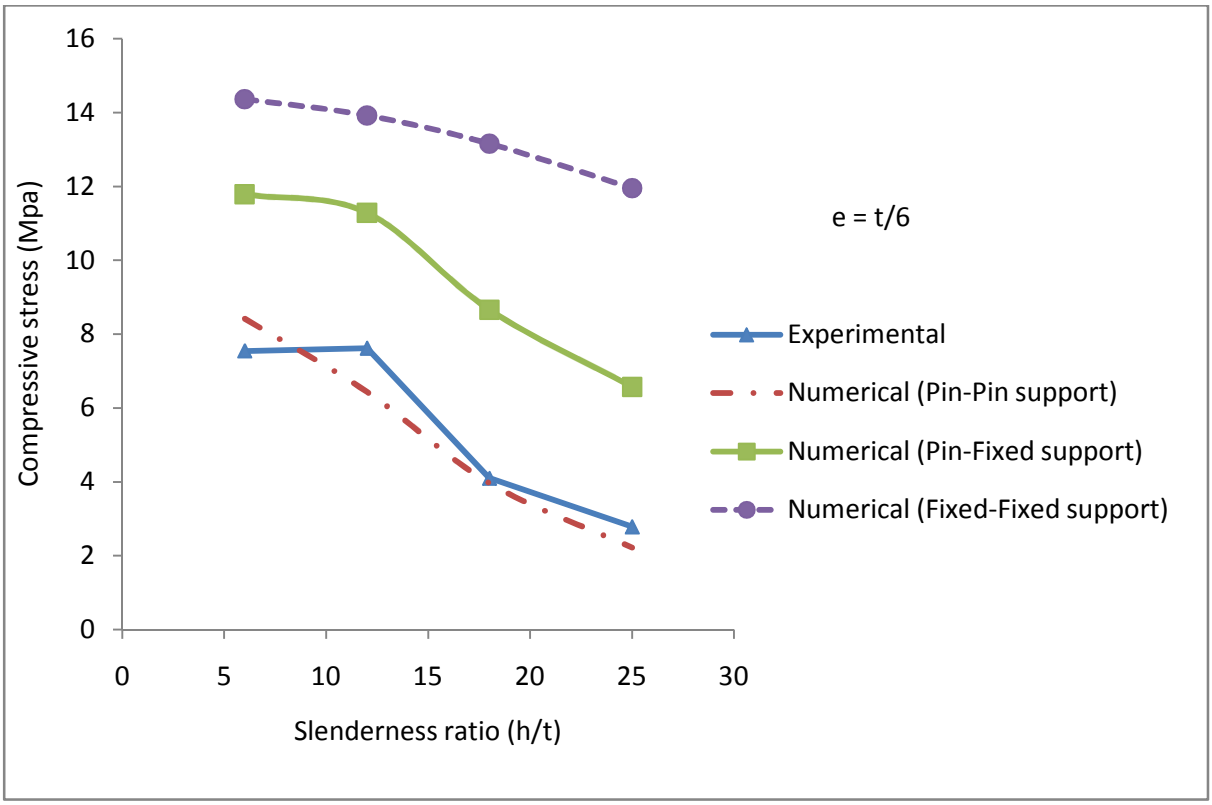

Figure 61: Capacity of wall for different boundary conditions at load eccentricity = t/6.

In the Figure 61, the capacity of the wall increases significantly for both cases of hinge-fixed and fixed-fixed support, however, the higher increment obtained for fixed-fixed support. Also found the similar tendency of higher increment rate for higher slenderness ratio. The ultimate capacity for slenderness ratio 25 increased three times and five times for hinge-fixed and fixed-fixed supports respectively and about two times and around four times respectively when consider slenderness ratio 18. For the other slenderness ratio the capacity increases within the ranges between 1.2 to 2 times of hinge-hinge support.

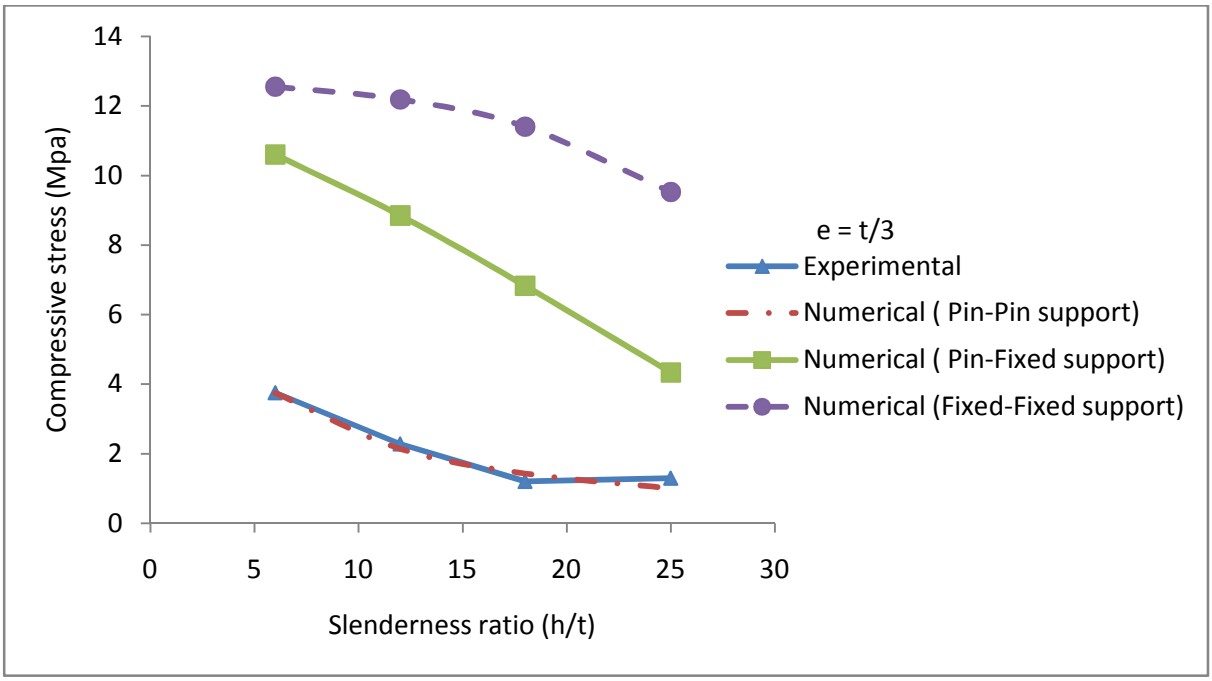

Figure 62: Capacity of wall for different boundary conditions at load eccentricity = t/3.

Figure 62 clearly shows that the collapse load of walls for all slenderness ratio increases with the change of support conditions. For the case of eccentricity t/3, the increment of capacity is higher than the other two eccentricities. The ultimate load increased around ten times for fixed-fixed support in cases of both slenderness ratio 25 and 18 respectively, while for hinge-fixed support about four times in cases of both slenderness ratio 25 and 18 respectively. On the other hand, the collapse load increased 4 to 6 times for slenderness ratio 6 and 12 with hinge-fixed and fixed-fixed end conditions respectively.

To describe buckling characteristics, load – deflection diagram for hinge-hinge and fixed-fixed boundary conditions are shown in the Figure 63. The figure shows that the ultimate load capacity of the wall as well as the lateral deflection has higher values for fixed-fixed support condition compared to hinge-hinge support. The lateral deflection and load capacity increased with the increasing of slenderness ratio for both support and eccentricity except e = 0.

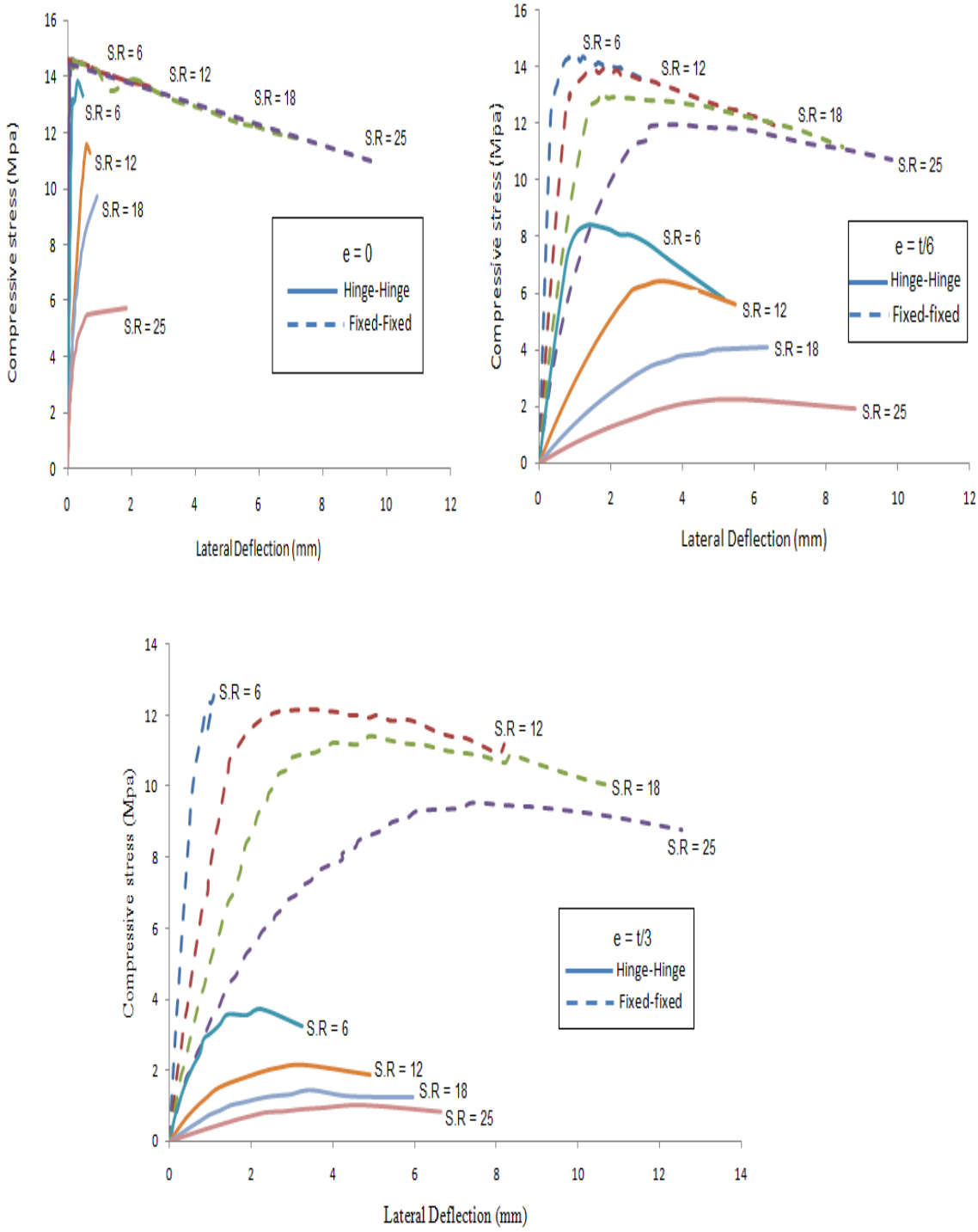

Figure 63: Comparison of load-deflection curve for hinge-hinge and fixed-fixed boundary conditions.

In Figure 64, shows that most of the cases, the lateral deflection values increased with slenderness ratio for hinge-fixed support than hinge-hinge support except slenderness ratio 6.

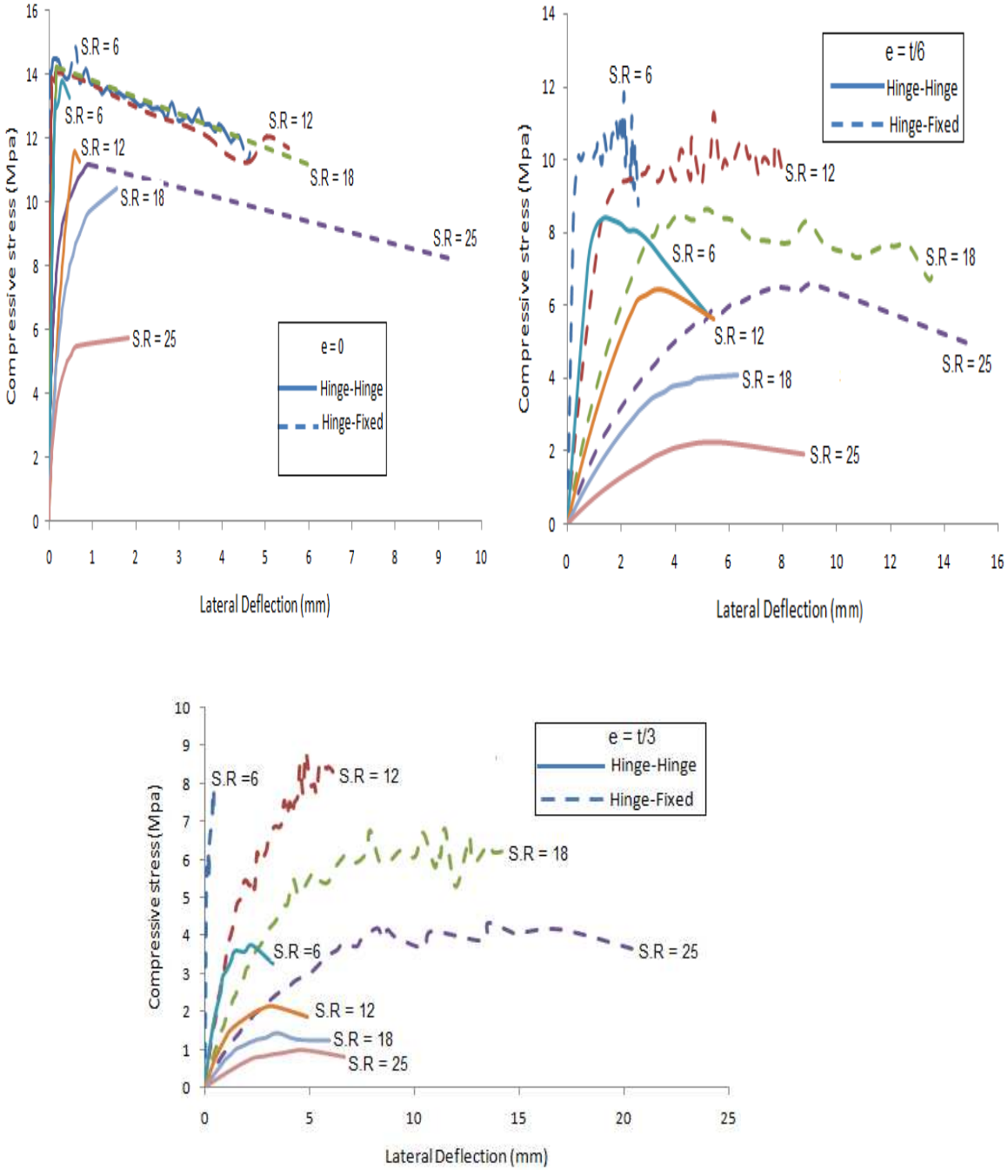

Figure 64: Comparison of load-deflection curve for hinge-hinge and hinge-fixed boundary conditions.

6.3.2 Study of Sensibility of the Tensile Strength

For better understanding the effect of tensile strength of masonry on the collapse load and buckling behavior, the parametric analysis was carried out by using tensile strength f_t of 0.001, 0.284, 0.568, 0.852, 1.136 and 1.42 MPa which was 1%, 2%, 4%, 6%, 8% and 10% of masonry prism compressive strength respectively. The analysis was performed for the boundary conditions of hinge-hinge, hinge-fixed and fixed-fixed. The results obtained from this analysis are shown in the following Figures.

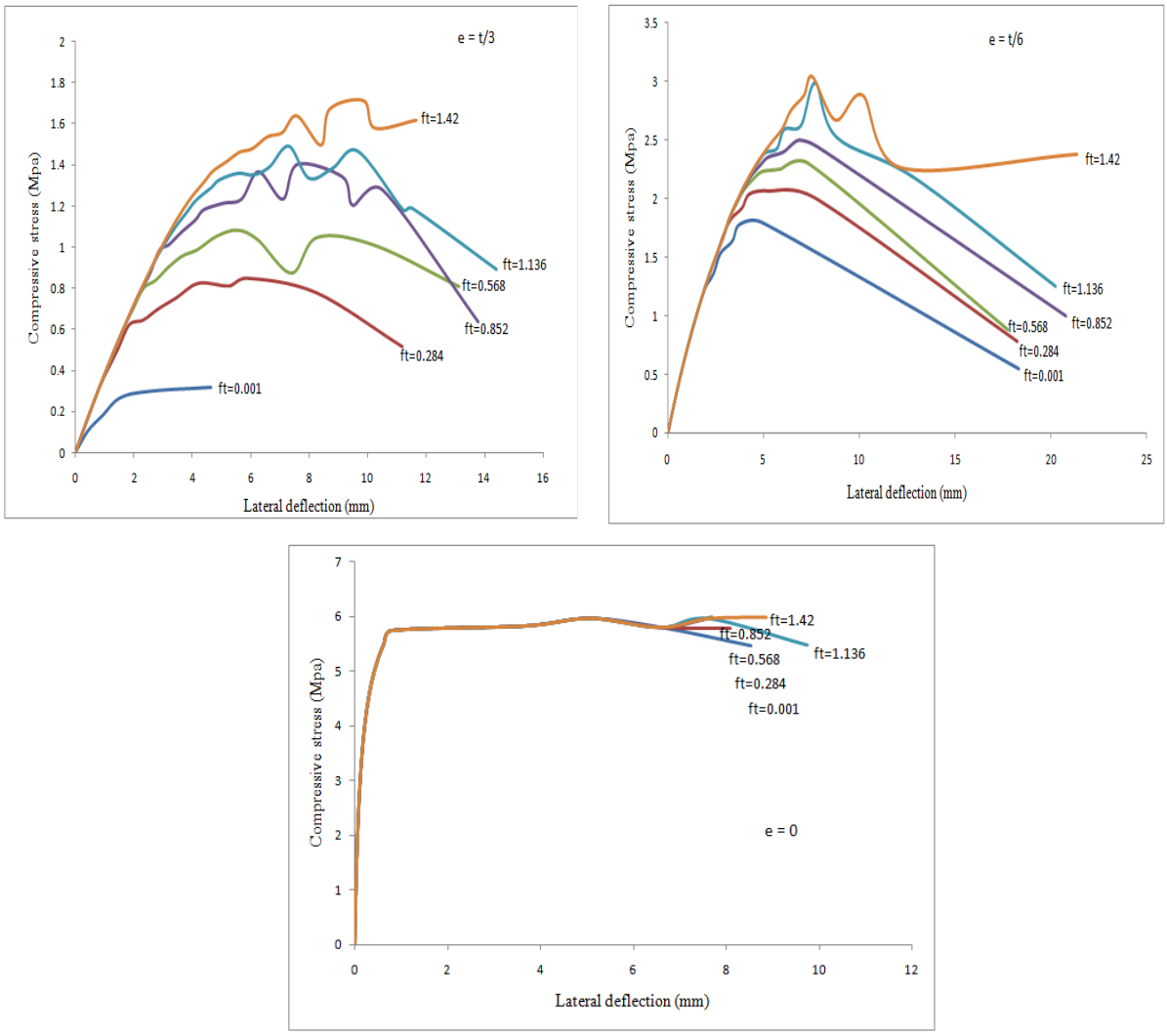

Figure 65: Load-deflection curve (hinge-hinge support) of different tensile strength for slenderness ratio 25.

The Figure 65 shows that if the tensile strength varies from 0.001 to 1.42 MPa, the compressive stress of masonry increased from 0.31 to 1.49 MPa, 1.79 to 2.98 MPa and 5.96 to 5.98 MPa for the eccentricity t/3, t/6 and 0, respectively. The influence of tensile strength on ultimate capacity of masonry wall is very high in the case of higher load eccentricity and the influence decreases with the decreasing of load eccentricity.

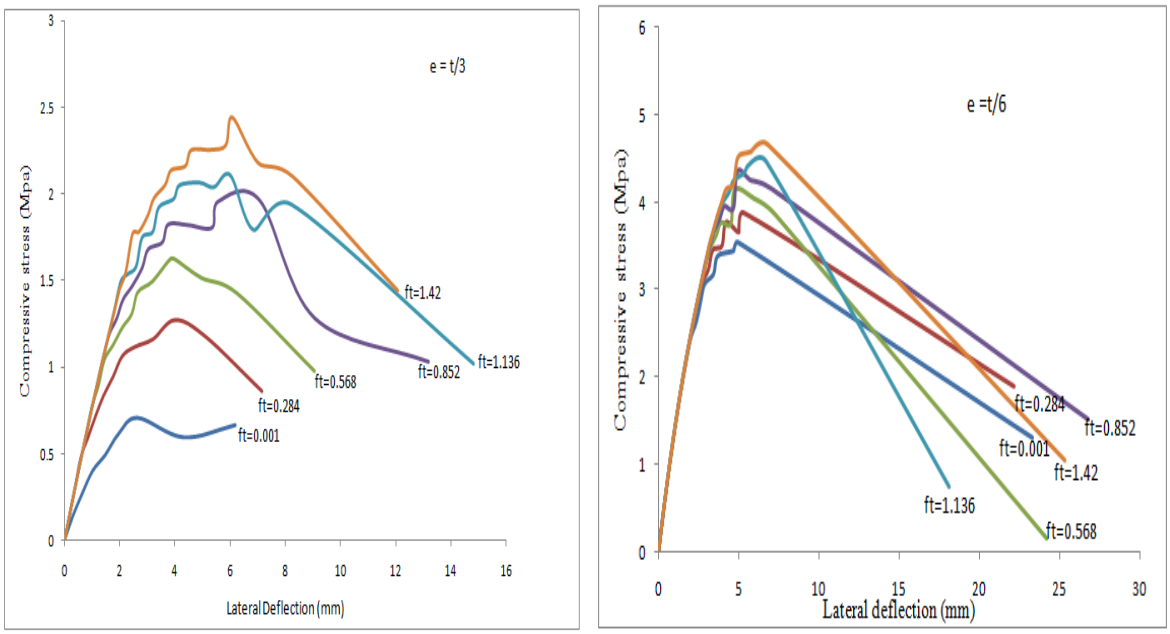

Figure 66: Load-deflection curve (hinge-hinge support) of different tensile strength for slenderness ratio 18.

In case hinge-hinge support, Figure 66 and 67 (left) shows that the tensile strength has low effect on compressive strength for low eccentricity. The ultimate load increased 0.93 MPa and 1.40 MPa when the tensile strength of masonry varies from 1% to 10% of masonry prism compressive strength for eccentricity of load t/6 and t/3, respectively while the no effect of tensile strength on capacity in the case of eccentricity equal to zero.

Figure 67 (right) shows that when tensile strength changes from 0.001 to 1.42 MPa the failure load changes from 1.23 to 3.28 MPa with irregular variation of lateral deflection.

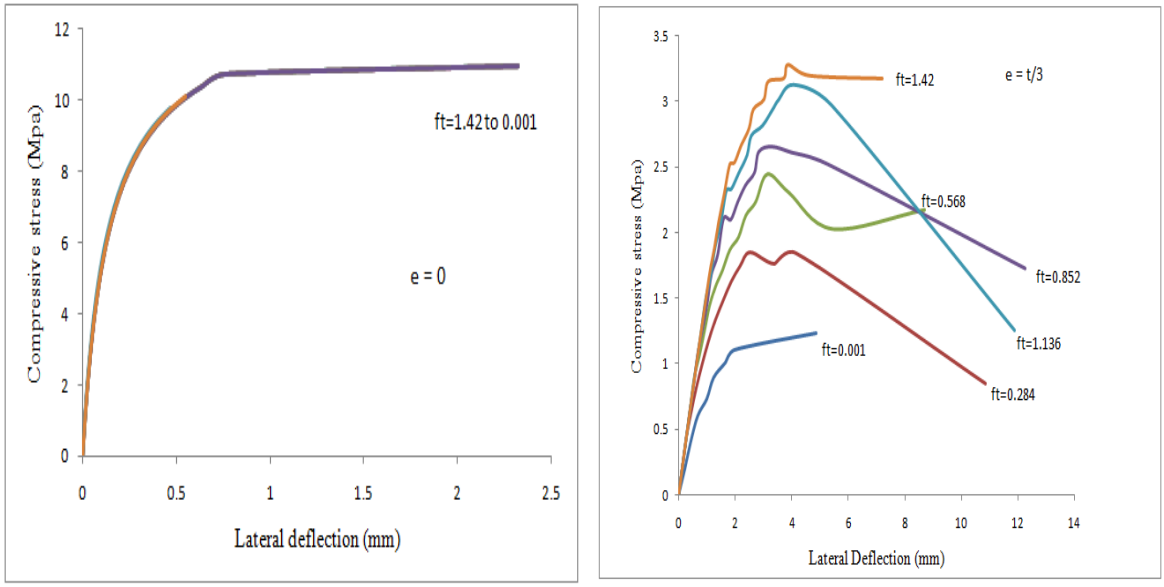

Figure 67: Load-deflection curve (hinge-hinge support) of different tensile strength for slenderness ratio 18 (left) and 12(right).

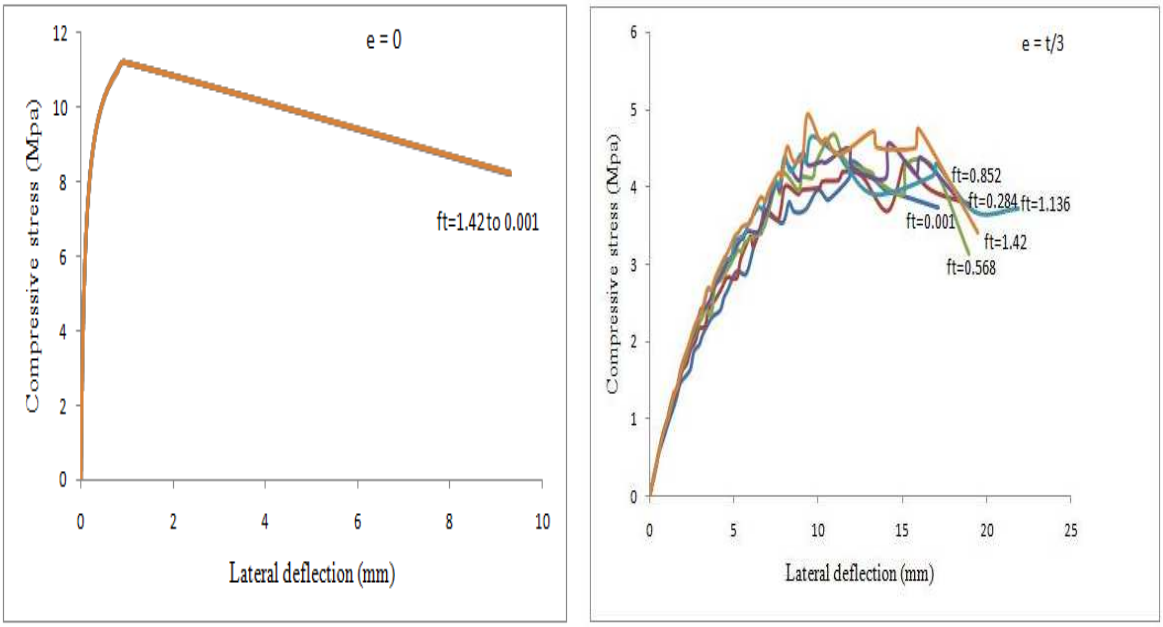

Figure 68: Load-deflection curve (hinge-fixed support) of different tensile strength for slenderness ratio 25.

The Figure 68 shows that due to the increasing of tensile strength of 1% to 10% of compressive strength masonry the ultimate load capacity of the wall increases 4.32 MPa to 4.93 MPa for eccentricity t/3 while the influence of tensile strength on capacity of wall is nothing in the case of null eccentricity.

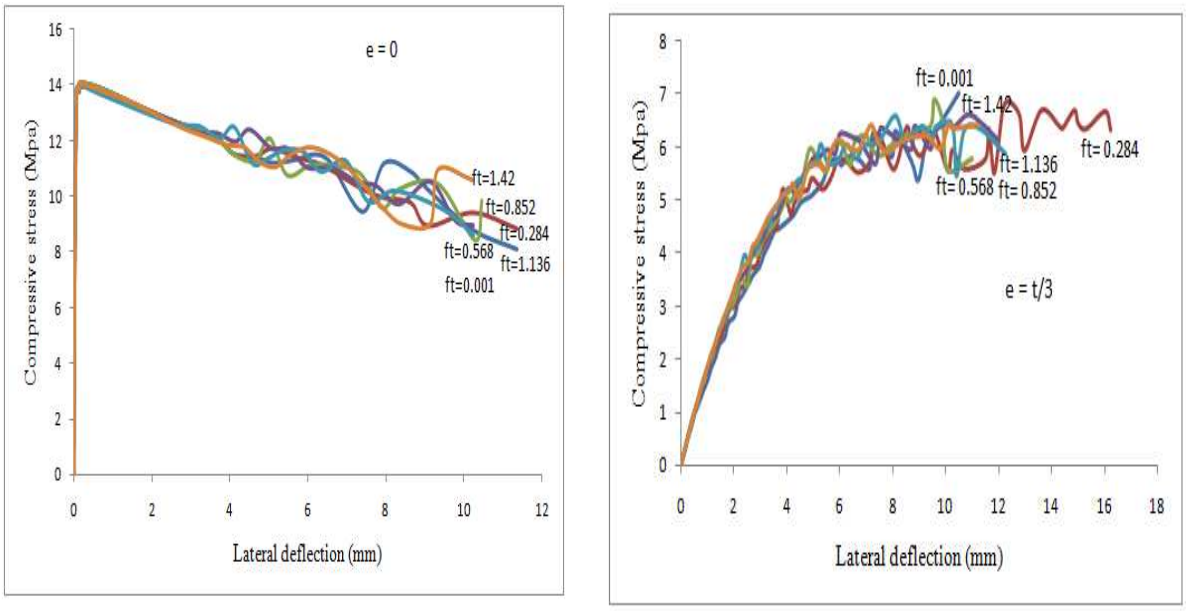

Figure 69: Load-deflection curve (hinge-fixed support) of different tensile strength for slenderness ratio 12 (left) and 18 (right).

In the case of hinge-fixed end condition shows in the Figure 69 (left), there is no effect of tensile strength on failure load in case of null eccentricity while a very small influence is found for eccentricity t/3 in Figure 69 (right). For increasing of tensile strength 1.41 MPa ultimate loads capacity increased 0.57 MPa.

Figure 70 shows the effect of tensile strength of masonry on ultimate bearing capacity for fixed-fixed support condition. From the figure it is clear that there is negligible influence of tensile strength on failure load for all cases of eccentricity. Only little variations are observed of lateral deflection for eccentricity t/3.

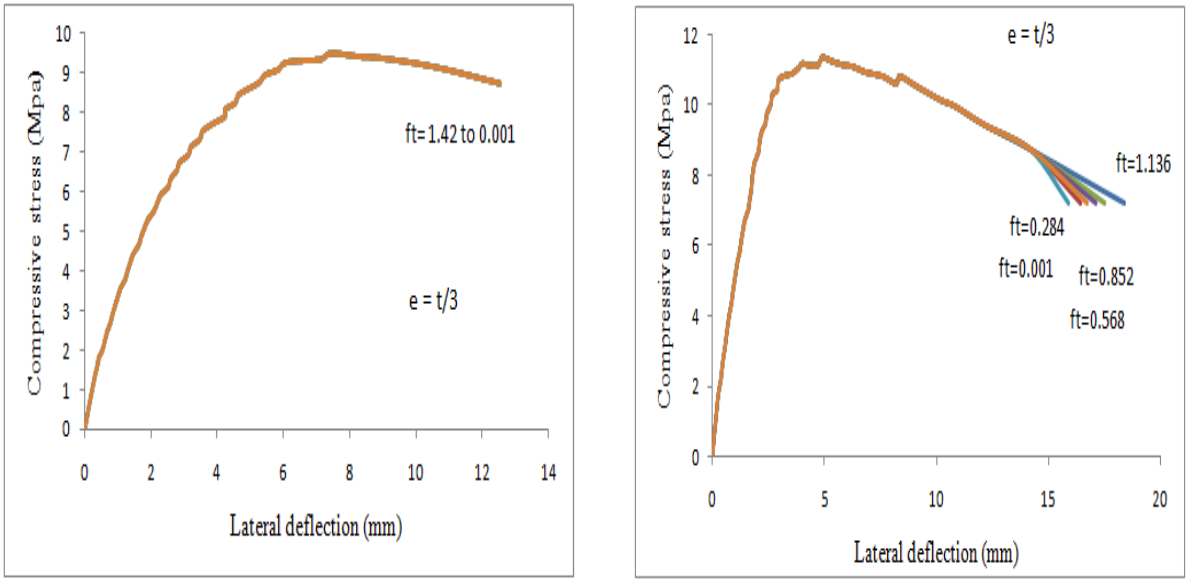

Figure 70: Load-deflection curve (fixed-fixed support) of different tensile strength for slenderness ratio 25 (left) and 18 (right).

6.4 Discussion

The effects of boundary condition and tensile strength on the failure load and buckling characteristics of masonry load bearing walls have been investigated by numerical parametric simulation. In the case of fixed support, the load capacity increased 2 to 6 times higher than hinge support depending on slenderness ratio and eccentricity. The capacity of wall for hinge-fixed support lies between the both end hinge and both end fixed support.

In the case of hinge-hinge support with high eccentricity, the influence of tensile strength is higher than the other support conditions. Most of the cases, negligible effect was found for null eccentricity. The influence of tensile strength follow a common tendency from higher to lower values when the support condition and load eccentricity moves from hinge to fixed and higher to lower eccentricity respectively. These results make sense, however, further experimental tests and detail numerical simulation, to characterize the effect of end support conditions and tensile strength on buckling failure together with different slenderness ratio and load eccentricity, is recommended by the author.

7. APPLICATION OF CODE PROVISIONS

7.1 EUROCODE 6 (EC 6)

According to EUROCODE 6, the resistance of a masonry wall subjected to vertical load depends on the geometry of the wall, the eccentricities of the load and constituent material properties. This development allowed the following assumptions:

- After each cross-section deformation remains plane and normal to the deformed axis (Bernoulli-Navier hypothesis);
- The resistance of the wall in tension perpendicular to the bed joints is zero.

The general stress-strain diagram for masonry is shown in Figure 71.

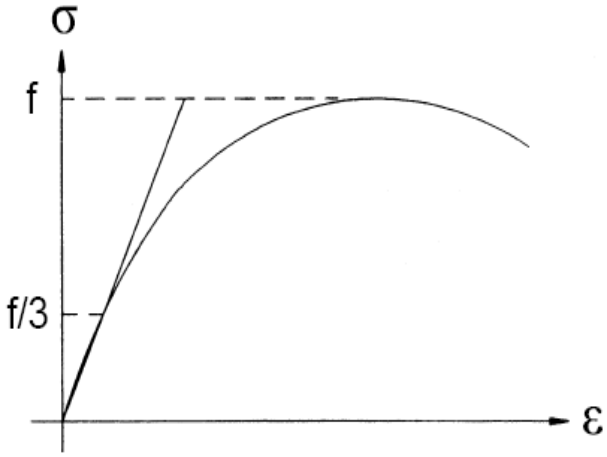

Figure 71: General shape of stress-strain relationship of masonry.

7.1.1 Determination of Vertical Load Resistance

The vertical load resistance of a single leaf wall per unit length, N_{RD}, can be calculated as:

$$N_{RD} = \frac{\Phi_{i,m} t f_k}{\gamma_M} \tag{34}$$

Where,

$\Phi_{i,m}$ is the capacity reduction factor Φ_i (top or bottom of wall) or Φ_m (in the middle one fifth of the height of wall), allowing for the effects of slenderness and eccentricity of loading;

f_k is the characteristic compressive strength of masonry according to paragraph 3.6.2 of EC 6, if the cross-sectional area A is less than 1 m^2, this property is multiplied by the factor (0.7 + 3A);

γ_M is the partial safety factor for the material, under paragraph 2.3.3.2 of EC 6;

t is the thickness of the wall, taking into account the depth of recesses in joints greater than 5 mm.

7.1.2 Determination of Reduction Factor for Slenderness ratio and Eccentricity

- At the top or bottom of the wall.

$$\Phi_i = 1 - \frac{2e_i}{t} \tag{35}$$

Where,

e_i is the eccentricity at the top or the bottom of the wall;

$e_i = \frac{M_i}{N_i} + e_{hi} + e_a \geq 0.05t$

M_i is the design bending moment at the top or the bottom of the wall resulting from the eccentricity of the floor load at the support, according to 4.4.7 (Figure 4.1) of EC 6;

N_i is the design vertical load at the top or bottom of the wall;

e_{hi} is the eccentricity at the top or bottom of the wall, if any, resulting from horizontal loads (for example, wind);

$e_a = \frac{h_{ef}}{450}$; is the accidental eccentricity and

t is the thickness of the wall.

- In the middle one fifth of the wall height.

$$\Phi_m = A_1 e^{\left(-\frac{u^2}{2}\right)} \tag{36}$$

Where,

A_1 Numerical factor, $A_1 = 1 - 2\frac{e_{mk}}{t}$

u Numerical factor, $u = \frac{\left(\frac{h_{ef}}{t_{ef}} - 2\right)}{23 - 37\frac{e_{mk}}{t}}$

h_{ef} is the effective height, obtained from 4.4.4 of EC 6 for the appropriate restraint or stiffening condition;

t is the thickness of the wall;

t_{ef} effective thickness of the wall in accordance with paragraph 4.4.5 of the EC 6;

e base of natural logarithms, approximately, e = 2.71828;

e_{mk} is the eccentricity within the middle one fifth of the wall height;

$$e_{mk} = e_m + e_k \geq 0.05t$$

with $e_m = \frac{M_m}{N_m} + e_{hm} \pm e_a$

e_m is the eccentricity due to loads;

M_m is the greatest moment within the middle one fifth of the height of the wall resulting from the moments at the top and bottom of the wall (see Figure 72);

N_m is the design vertical load within the middle one fifth of the height of the wall;

e_{hm} is the eccentricity at mid-height resulting from horizontal loads (for example, wind);

e_k is the eccentricity due to creep;

$$e_k = 0.002\Phi_\infty \frac{h_{ef}}{t_{ef}}\sqrt{te_m}$$

Φ_∞ is the final creep coefficient from Table 3.8 of EC 6.

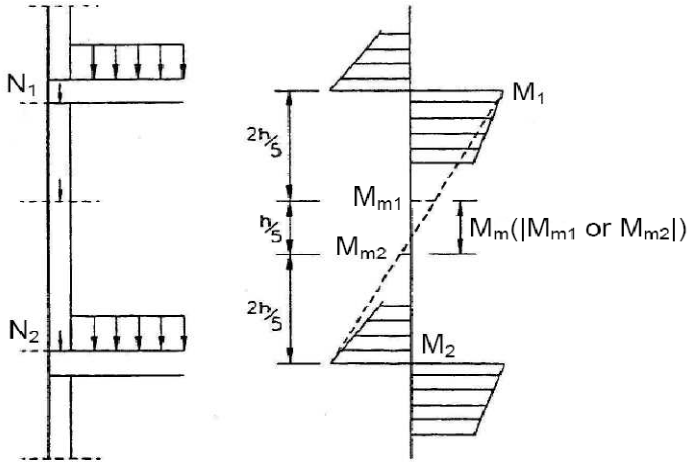

Figure 72: Moments from calculation of eccentricities according to EC 6.

Figure 73 shows the values of Φ_m depending on the slenderness for different values of eccentricity of expression 36. This chart is entered with the value h/t and the eccentricity and extracts the value of Φ_m.

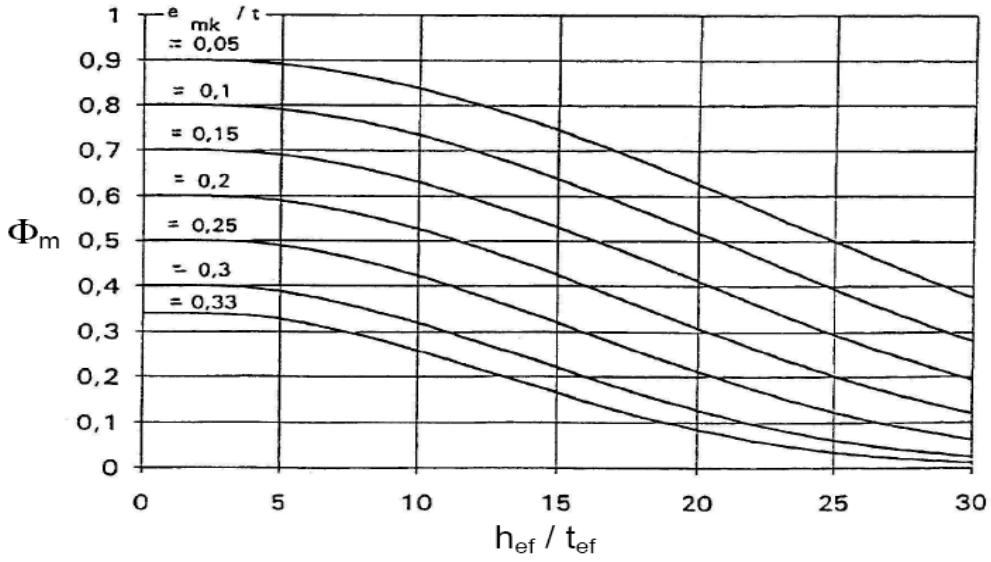

Figure 73: Graph showing values of Φ_m against slenderness ratio for different eccentricities.

This development has taken a modulus of the elasticity of masonry as a thousand times the compressive resistance property of masonry ($E = 1000 f_k$).

7.2 ACI-530

ACI 530-05 code was reported by Masonry Standards Joint Committee (MSJC), the design of unreinforced masonry has included a limit on the allowable axial compression force that may be applied. The limit is that the maximum allowable compressive force P is not exceed one fourth of the buckling load P_e as defined in the code.

The maximum compressive force is limited to:

$$P \leq \frac{P_e}{4} \tag{37}$$

Where,

$$P_e = \pi^2 \frac{E_m I}{h^2} \left(1 - 0.577 \frac{e}{r}\right)^3 \tag{38}$$

In which,

E_m modulus of elasticity;

I uncracked moment of inertia of the section;

e eccentricity of the compressive force P;

r radius of gyration of the uncracked unit section;

h unbraced height of the member under load.

As the member deflects and bends under the action of eccentrically applied force, flexural tension cracking occur wherever the bending stress due to moment exceed the axial compression stress.

The buckling equations for members subjected to compressive force are shown below:

$$P_e = \pi^2 \frac{E_m I}{h^2} \left(1 - 2\frac{e}{t}\right)^3 \tag{39}$$

For a solid rectangular cross-section, the radius of gyration is approximately equal to 0.289t. For members having an slenderness ratio less than 99 and greater than 99, the allowable compression stress under axial load F_a is given from the following equation 40 and 41.respectively:

$$F_a = \left(\frac{1}{4}\right) f_m \left(\frac{h}{140rh}\right)^2 \tag{40}$$

$$F_a = \left(\frac{1}{4}\right) f_m \left(\frac{70r}{h}\right)^2 \tag{41}$$

Where,

f_m specified compressive strength of masonry;

t thickness of the wall.

7.3 Comparison of Collapse Loads

A comparison between the experimental results obtained from UPC (2009), the results calculated with standards ACI-530 and EUROCODE 6 (EC 6) and the proposed numerical micro-models is presented. The results are shown in Figure 74, 75 and 76. As can be observed, the method proposed in EC 6 underestimates substantially the bearing capacity of the walls. The other standard considered, ACI-530, also underestimates the strength of walls in all cases.

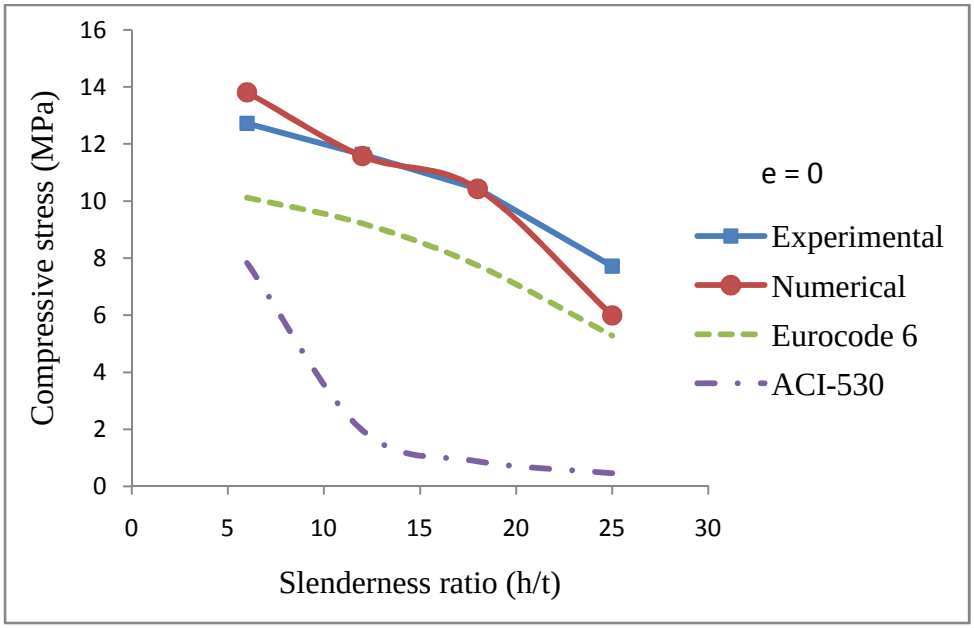

Figure 74: Comparison of compressive stress for different slenderness ratio and eccentricity.

In fact, ACI-530 is the most conservative method to predict the collapse load for all cases, especially; the underestimation is increases with the increase of eccentricity. There is a general tendency that ACI-530 underestimates the bearing capacity of high slenderness ratio more for all cases of both concentric and eccentric load.

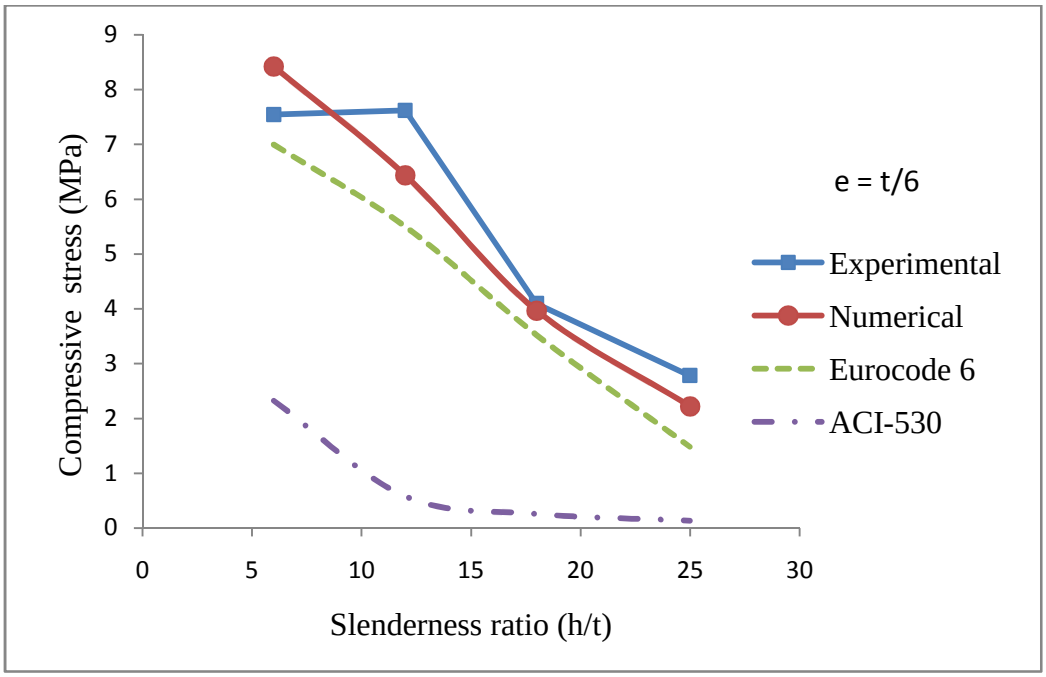

Figure 75: Comparison of compressive stress for different slenderness ratio and eccentricity.

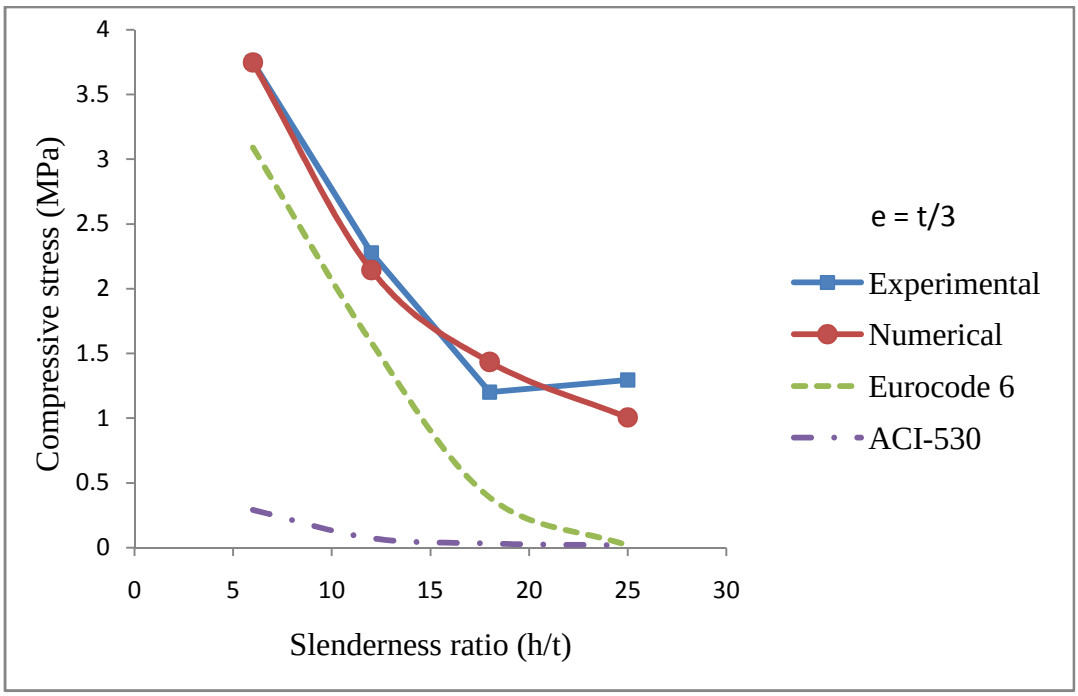

Figure 76: Comparison of compressive stress for different slenderness ratio and eccentricity.

ACI-530 code produce average error of 76.86%, 87.62% and 96.26% compared to experimental results for the cases of load eccentricity 0, t/6 and t/3 respectively. For overall cases this ACI-530 code shows average error 86.92%.

EC 6 underestimates the strength of the walls in all cases, although it is able to reproduce the general tendency. The standard provides more satisfactory estimations for the lower eccentricity and lower slenderness ratio specifically, for the eccentricity t/6 which provides average error of 23.94%. Moreover, EC 6 is the most conservative method to predict the collapse load of the higher eccentrically loaded walls (e=t/3) with an average error of 53.6% while it produce overall average error of 34% when compared with experimental results.

The best fit occurs in the EC 6 (7.29%) and ACI-530 (38.47%) for the eccentricity t/6 and 0 respectively, with slenderness ratio 6 for both, while the standards produce maximum error of 98.70% and 98.77% for eccentricity t/3 and slenderness ratio 25.

On the other hand, both standards are underestimates the collapse load of wall when compared to numerical micro-models. ACI-530 provides most conservative results with average error of 87.19%, while EC 6 estimates collapse load by 31.30% of average error.

7.4 Recommendation

From the comparison of collapse load according to the EUROCODE 6 and ACI-530 with the experimental and numerical results, it is clear that the standards are produces conservative results. So, it very important to make a revision of formula used to predict collapse load. A revision is recommended for present provisions of determination of the collapse load of wall subjected to vertical loading on the basis of scale and full scale experimental test by considering effects of slenderness ratio and load eccentricity. During the experimental study more concentration should be given on, to maintain appropriate eccentricity of load application. In the case of both standards EC 6 and ACI-530, the formula should be revised by using real material property of masonry such as modulus of elasticity and tensile strength. Further study is recommended to observe the effect of boundary conditions on ultimate capacity and buckling behavior of load bearing masonry wall with different slenderness ratio and load eccentricity.

8. CONCLUSIONS

The diverse combinations of slenderness ratio and load eccentricity used in the experimental program which provided the means for a comprehensive numerical analysis of the masonry wall. In this research a set of experimental tests on the buckling failure of masonry walls has been numerically simulated by means of simplified micro-modeling approach. The micro-model describes the nonlinear response of masonry in compression in an indirect way by localizing it to the blocks to the joints. In all cases, the non-linear response in tension is localized to the joints. In addition, experimental and numerical results have been compared with predictions obtained from two current masonry standards.

The simplified micro-models afford a satisfactory prediction of the ultimate load of walls taking into account the buckling behavior. Simulations carried out by the micro-model provide the best fits for all load eccentricity, (with an average error of 10.79%). It must be noted that some difference with respect to the experimental results is unavoidable because of the influence of possible non-reported accidental eccentricities.

The comparison between experimental and the standards' results shows significant errors of 86.92% and 34.07% for ACI-530 and EC 6, respectively. In particular, this comparison suggests that the both method proposed by EC 6 and ACI-530 tends to conservatively underestimate the strength of walls. The micro-modeling approach has shown its ability to assess the bearing capacity of masonry walls subjected to concentric or eccentric vertical loading. It has been observed that an accurate description of tensile cracking and opening of mortar joints, by means of an appropriate interface element, is essential to obtain reliable results on the bucking failure of walls.

The parametric analysis shows that the end condition has great influence on ultimate capacity and buckling behavior of the masonry wall. If the support conditions change from hinge-hinge to fixed-fixed, the failure load increased with a range between 2 to 6 times depending on the slenderness ratio and load eccentricity. However, when the end condition change from hinge-hinge to hinge-fixed the failure load of masonry wall increased significantly and values lies between both hinge and both fixed condition.

The effects of tensile strength on buckling failure also briefly studied and found that ultimate capacity of wall is highly influenced by tensile strength in the case of hinge support condition

and this effect decreases when the support condition tends to fixed. In addition, the failure load of the higher eccentrically loaded wall is highly influenced by the tensile strength than lower load eccentricity.

9. REFERENCES

PAYNE, D. C., BROOKS, D. S. and DVED, G. (1990) - *The analysis and design of slender brick walls*. Masonry International Journal, 4(2), p. 55-65.

ROMANO, F., GANDUSCIO, S. and ZINGONE, G. (1992) - *Stability of masonry with nonlinear stress-strain relationship.* J.Brit. Mas. Soc., Masonry International, 6(2), p. 69-74.

CERIONI, R., IORI, I. and APAGNOLI, A. (2007) - *Influence of a nonlinear stress-strain relationship on the stability of certain masonry walls.* J. Brit. Mas. Soc., Masonry International, 42, p. 207-211.

KNUTSSON, H. H. (1991) - *Vertical load bearing masonry - The Danish Approach*. J. Brit. Mas. Soc., Masonry International, 5(1), p. 23-26.

KIRTSCHIG, K. and ANSTOTZ, W. (1991) - *Kinckuntersuchungen an mauerwerksproben*. Proceedings of 9th International brick/block masonry Conference, p. 202-209.

WATSTEIN, D. and ALLEN, M. H. (1970) - *Structural performance of clay masonry assemblages built with high-bond organic-modified mortars*. SIBMAC Proceedings, Ed. H.W.H. West and K.H. Speed, p.99-112.

HASAN, S. S. and HENDRY, A.W. (1976) - *Effect of slenderness and eccentricity on the compressive strength of walls*. Proc. 4th International Brick Masonry Conference (Brugge). Paper 4.d3.

VALLADARES, I. N. (2010) - *Estudi experimental de la fallada a vinclament de parets de càrrega de fábrica de maó.* MSc. thesis, Technical University of Catalonia, Barcelona, Spain.

YOKEL, F. Y. (1971) - *Stability and load capacity of members with no tensile strength*. J. Struct. Div. ASCE, 97(7), p. 1913-1926.

MORTON, J. (1990) - *The design of masonry compression members*. Brit. Mas. Soc. Proceedings, 4, p. 106-111.

ROMANO, F., GANDUSCIO, S. and ZINGONE, G. (1993) - *Cracked nonlinear masonry stability under vertical and lateral loads*. J. Struct. Engrg., ASCE, 119(1), p. 69-87.

BRENCICH, A., CORRADI, C. and GAMBAROTTA, L. (2008) - *Eccentrically loaded brickwork.* J. Engrg. Struct., ELSEVIER, 30, p. 3629-3643.

MORTON, J. and HORNE, M. R. (1992) - *The development of stability parameters for the cracked section analysis of solid walls at high eccentricity*. Brit. Mas. Soc., J. Masonry International, 5(3), p. 73-78.

COLVILLE, J. (2001) - *Stability of unreinforced masonry under compressive load*. J. TMS, p. 49-56.

PARLAND, H. (1982) - *Basic principles of the structural mechanics of masonry: A historical review*. Int. J. Mas. Constr., 2(2).

LOURENÇO, P. B. (1996) - *Computational strategies for masonry structures*. PhD thesis, Delft University of Technology, Delft, The Netherlands.

LOURENÇO, P. B. and ROTS, J.G (1997) - *Multisurface interface model for analysis of masonry structures*. Journal of engineering mechanics, 123(7), p. 660-668.

LOURENCO, P. B. (1996) - *A user / programmer guide for the micro-modeling of masonry structures.* TU-DELFT, Report no. 03-21-1-31-35, Delft University of Technology, Delft, The Netherlands.

YOKEL, F. Y. (1971) - *Stability and load capacity of members with no tensile strength*. J. Struct. Div. ASCE, 97(7). p. 1913-1926.

FELIX, I. P. (1999) - *Compressive strength and modulus of elasticity of masonry prisms*. Master of Engineering thesis, Carleton University, Ottawa, Ontario, Canada.

SAHLIN, S. (1978) - *Structural masonry.* Prentice-Hall Inc., New jersey, U. S. A.

SAWKO, F. and TOWLER, F. (1982) - *Numerical analysis of walls and piers with different end conditions.* 6IBMAC. Ed. Laterconsult s.v.l., Rome, Italy.

SCHULTZ, A., BEAN, J., LU, M., STOLARSKI, H. and OJARD, N. (2009) - *Interaction of slenderness and lateral loading in URM*. J. Brit. Mas. Soc., 57(39).

CHAPMAN, J. C. and SLATFORD, J. (1957) - *The elastic buckling of brittle columns.* Inst. Civ. Eng., Vol. 107, No. 6.

PLUIJM, R. VAN DER (1992) - *Material properties of masonry and its components under tension and shear*. *Proc. 6th Canadian Masonry Symposium*, Eds. V.V. Neis, Saskatoon, Saskatchewan, Canada, p. 675-686.

VASSILEV, T., JAGER, W. and PFLUCKE, T. (2009) - *Nonlinear transfer matrix model for the assessment of masonry buckling behavior*. J. Brit. Mas. Soc., 71(24).

PARLAND, H., HEINISUO, M. and KOIVULA, R. (1982) - *On the problem of bending and compression of masonry structures*. Ibid, p. 430-441.

PAGE, A.W. (1978) - *Finite element model for masonry*. *J. Struc. Div.,* ASCE, 104(8**)**, p. 1267-1285.

SCHUBERT, P. and HOFFMANN (1994) - *Compressive strength of mortar in masonry: Significance, influences, test methods, requirements*. *Proc. 10th Int. Brick and Block Masonry Conf.,* Eds. N.G. Shrive and A. Huizer, University of Calgary, Calgary, Alberta, Canada, p. 1335-1344.

HAMID, A. A., ZIAB, G. and NAWAY, O. E. (1987) - *Modulus of elasticity of concrete block masonry*. The 4th North American Masonry Conference, Los Angeles, USA.

SIMO, J.C., JU, J.-W., PISTER, K.S. and TAYLOR, R.L. (1988a) - *Assessment of cap model: Consistent return algorithms and rate-dependent extension*. *J. Engrg. Mech.,* ASCE, 114(2), p. 191-218.

DIMAGGIO, F.L. and SANDLER, I.V. (1971) - *Material model for granular soils*. *J. Engrg. Mech.,* ASCE, 97(3), p. 935-950.

DRUCKER, D.C., GIBSON, R.E. and HENKEL, D.J. (1957) - *Soil mechanics and work hardening theories of plasticity*. *Trans. ASCE,* 122, p. 338-346.

FATTAL, S. G. and CATTANEO, L. E. (1976) - *Structural performance of masonry walls under compression and flexure*. NBS Building Science Series 73, U.S.A.

CUR (1994) - *Structural masonry: an experimental/numerical basis for practical design rules*. Report 171, CUR, Gouda, The Netherlands.

CEN (1995) - *Eurocode 6: Design of masonry structures.* ENV 1996-1-1:1995, CEN, Brussels, Belgium.

STRUCTURAL CLAY PRODUCTS RESEARCH FOUNDATION. (1965) - *Compressive, transverse and racking strength tests of four-inch brick walls*. Research report no. 9, Div. of Struct. clay products Inst., Geneva, Illinois.

ASTM C270-57T (1958) - *Tentative specification for mortar for unit masonry.* West Conshohocken, Pennsylvania.